Role of receptor conformation in retinal interactions with the visual GPCR rhodopsin

By

Christopher Thomas Schafer

A dissertation

Presented to the Department of Biochemistry & Molecular Biology

And the Oregon Health & Science University School of Medicine

in partial fulfillment of the requirements for the degree of

Doctor of Philosophy

June 2016

School of Medicine

Oregon Health & Science University

CERTIFICATE OF APPROVAL

This is to certify that the Ph.D. thesis of

Christopher Thomas Schafer

has been approved

Dr. David Farrens, Mentor/Advisor

Dr. Michael Chapman, Committee Chair

Dr. Ujwal Shinde, Committee Member

Dr. Francis Valiyaveetil, Committee Member

Dr. Matthew Whorton, Committee Member

Dr. Drake Mitchell, Committee Member

Table of Contents

List of Tables ..... **ix**

List of Figures ..... **x**

List of Abbreviations ..... **xiii**

Acknowledgements ..... **xix**

Abstract ..... **xx**

Chapter 1: Introduction **1**

1.1: G protein-coupled receptor signaling 1

1.1.1: Ligand-binding GPCR signaling 1

1.1.1.1: GPCR overview 1

1.1.1.2: Classical activation 2

1.1.1.3: Classical deactivation 3

1.1.2: Rhodopsin signaling 4

1.2: Retinal (re)cycling 6

1.2.1: All-trans retinal recycling 6

1.2.2: Retinal cycle diseases and therapeutics 8

1.2.3: A standing question regarding the retinoid cycle 12

1.3: Rhodopsin structure 12

1.3.1: The retinal binding pocket 13

1.3.2: Constitutive activity 14

1.4: Retinal binding 15

1.4.1: How does retinal enter or exit opsin? 15

1.4.1.1: Ligand channeling through an active-like receptor 16

1.4.1.2: Transient activation model for retinal binding 17

1.5: Dissertation overview 18

Chapter 2: Conformational selection and equilibrium governs the ability of retinals to bind to opsin 38

2.1: Summary 38

2.2: Introduction 39

2.3: Experimental Procedures 44

2.3.1: Buffers 44

2.3.2: Mutant Generation 44

2.3.3: Protein Expression and Purification 45

2.3.4: Absorbance Spectroscopy 45

2.3.5: Fluorescence Spectroscopy 46

2.4: Results 48

2.4.1: Use of Fluorescence to Measure Retinal Uptake 48

2.4.2: The M257Y-CAM$_0$ Opsin Exhibits the Ability to Bind Both Inverse Agonist (11CR) and Agonist (ATR) 50

2.4.3: Shifting the Ops⇌Ops* Equilibrium by a Peptide Mimetic of the G Protein C-Terminus Further Shifts Opsin Affinity From 11CR to ATR 51

2.4.4: G Protein C-terminal Peptide is Sufficient to Stabilize ATR-Bound WT$_0$ Opsin 52

2.4.5: Arrestin "Finger Loop" Peptide also Enhances ATR Binding 53

2.4.6: Conformational Selection of Retinal Isomers by Opsin is Not an Artifact of the Minimal Cysteine Construct 54

2.4.7: Expanding Hole B (TM5/TM6) Does Not Enable ATR Uptake and Actually Slows 11CR Binding 55

2.5: Discussion 56

2.5.1: Conformational Selection of Retinal Isomers by Opsin 56

2.5.2: Palmitoylation of Opsin Does Not Play a Role in Retinal binding to Opsin in Our Detergent System 59

2.5.3: Expanding Hole B (TM5/TM6) Does Not Enable Ops to Bind ATR, but May Play a Role in Stable 11CR Binding 60

2.5.4: Occupancy of the Cytoplasmic Binding Cleft of Opsin by Either G protein C-terminus or Arrestin Finger Loop Peptide Mimics is Sufficient to Enhance ATR Binding..... 61

2.5.5: A Modified Conformational Selection Model for Retinal Binding to Opsin 63

2.5.6: Conclusions..... 65

Chapter 3: Decay of an Active GPCR: Conformational Dynamics Govern Agonist Rebinding and Persistence of an Active, yet Empty Receptor State..... 89

3.1: Summary..... 89

3.2: Introduction..... 90

3.3: Experimental Procedures..... 92

3.3.1: Buffers 92

3.3.2: Mutant generation..... 93

3.3.3: Sample purification and labeling with fluorophore..... 93

3.3.4: Absorbance spectroscopy 94

3.3.5: Bimane emission scans..... 95

3.3.6: Time-resolved steady-state fluorescence spectroscopy..... 95

3.3.7: Hydroxylamine experiments..... 96

3.3.8: Radioactive ligand binding..... 97

3.4: Results..... 98

3.4.1: Stabilization of active-state opsin (Ops*) prevents full retinal release 98

3.4.2: Equilibrium binding, rather than physical trapping, explains the lack of apparent ATR release for Ops* containing samples in the retinal release assays 99

3.4.3: Radioactive ligand binding studies further confirm an ATR binding equilibrium after receptor photoactivation..... 100

3.4.4: Method for simultaneously measuring retinal release and the conversion from active Ops* to inactive Ops receptor conformation 101

3.4.5: ATR dissociation and the conformational change from Ops* to Ops do not always occur simultaneously 102

3.5: Discussion 103

3.5.1: After rhodopsin photoactivation, an equilibrium of ATR release and rebinding is established that depends on the amount of Ops* present 103

3.5.2: Is "retinal release" due to the protein reverting back to an inactive Ops conformation faster than the released ATR can rebind? 106

3.5.3: Opsin can transiently retain an active-like conformation following agonist dissociation 107

3.5.4: Implications for other visual GPCRs 108

3.5.5: Conclusions 109

Chapter 4: Fluorescence sensor for monitoring ligand-induced arrestin and transducin interactions with bovine rhodopsin 122

4.1: Summary 122

4.2: Introduction 123

4.3: Materials and Methods 125

4.3.1: Buffers 125

4.3.2: Mutant Generation 125

4.3.3: Purification, Labeling, and Quality Control 126

4.3.4: Steady-state Fluorescence Spectroscopy 127

4.3.5: Fluorescence Lifetime Spectroscopy 128

4.4: Results 128

4.4.1: Sensor Engineering and Rationale 128

4.4.2: Binding of the fusion construct detected by TrIQ 130

4.4.3: Agonist (ATR) binding can be detected by increased fluorescence quenching in CIM-GtF 131

4.4.4: Non-covalent binding of a G protein antagonist (β-ionone) causes a decrease in fluorescence quenching in the WT-GtF sensor 132
4.4.5: Real-time transfer of ATR from native-source rhodopsin detected by CIM-GtF sensor 133
4.4.6: ArrF sensor increases binding with ATR yet shows little response to β-ionone 135
4.5: Discussion 135
4.5.1: Ligand-binding can be determined by monitoring specific receptor conformations 136
4.5.2: ATR released from photo-activated rhodopsin can transfer to a different opsin 137
4.5.3: Conclusions 138
Chapter 5: Summary and Future Directions 156
5.1: Summary 156
5.1.1: Conformational selection in retinal binding to opsin 156
5.1.2: Equilibrium binding of all-trans retinal 157
5.1.3: Opsin structural states before and after retinal release 158
5.1.4: Fluorescence-based detection of ligand binding to opsin 159
5.2: Future directions 159
5.2.1: How does 11CR bind to opsin? 160
5.2.2: What are the features for the open Ops conformation? 160
5.2.3: Does β-ionone exhibit biased agonism in rhodopsin? 161
5.2.4: Do other ligands exist for rhodopsin? 162
5.3: Concluding remarks 162
References 164
Appendix Chapter 1: Sampling transient molecular states with molecular dynamics simulations 184
A1.1: Simulating tryptophan-induced quenching with lysozyme 185
A1.1.1: Simulation setup 185

A1.1.2: Results 186
A1.2: Simulating inactive opsin in a POPC bilayer 187
A1.2.1: Simulation setup 187
A1.2.2: Results 187
A1.3: Summary 188

Appendix Chapter 2: Kinetic modeling of the transient activation hypothesis confirms its incompatibility with our results in Chapter Two 202
A2.1: Background 202
A2.2: Results 203
A2.3: Summary 204

Appendix Chapter 3: Instrument improvements for improved fluorescent time-course experiments 209

List of Tables

Table 2.1: Complete table of rates of retinal uptake for opsins tested in Chapter 2. 67

Table 3.1: Time to half maximal ATR release and percent remaining complexes prior to HA addition 110

Table 3.2: Retinal release, TM6 movement rates, and activation energies for constructs measuring rates of agonist release and conformational change 111

Table 4.1: Components of fluorescence for CAM, WT, and CIM GtF and ArrF apoproteins 139

List of Figures

Figure 1.1: Basic GPCR architecture 21

Figure 1.2: Simplified liganded GPCR signaling through G protein mediated pathway. 23

Figure 1.3: Rod cell architecture 25

Figure 1.4: Structure of the photoprotein rhodopsin 27

Figure 1.5: Rhodopsin mediated phototransduction 29

Figure 1.6: Recycling of photoisomerized ATR back to 11CR 31

Figure 1.7: Retinal channeling through rhodopsin 34

Figure 1.8: The transient activation model for retinal binding to rhodopsin 36

Figure 2.1: The active rhodopsin structure reveals openings into the retinal binding pocket 73

Figure 2.2: Rates of retinal binding to opsin can be measured by monitoring quenching of the protein intrinsic tryptophan fluorescence. 76

Figure 2.3: A constitutively active mutation (CAM) of opsin, M257Y, binds 11CR slower than WT, yet also gains the ability to bind ATR. 78

Figure 2.4: Shifting the ops→ops* equilibrium by binding of peptide mimetics of the G protein transducin (green, G_t C-term peptide) and arrestin (purple, Arr peptide) enhances the rate of ATR binding, and G_t C-term peptide also slows 11CR binding. 80

Figure 2.5: The presence of palmotylation sites C322 and C323 in WT opsin does not change the effects of shifting the ops→ops* equilibrium using peptide mimetics of the G protein transducin (G_t C-term peptide) and arrestin (Arr peptide) on retinal binding. 83

Figure 2.6: Introducing a permanent enlargement of Hole B (TM5/TM6) is not sufficient to enable ATR binding, and actually slows 11CR binding. 85

Figure 2.7: A conformational selection model for retinal binding to opsin. 87

Figure 3.1: Conformational selection model for retinal binding to opsin (146). 112

Figure 3.2: Evidence that ATR released during decay of photoactivated MII rhodopsin can rebind in an Ops* dependent manner. 114

Figure 3.3: Radioligand binding experiments reveal the ATR produced inside rhodopsin by light bleaching can exchange with an equimolar amount of exogenously added, radioactive (^{3}H-ATR). 116

Figure 3.4: Time-resolved fluorescence assay based on TrIQ for simultaneously monitoring receptor conformational changes and retinal release after rhodopsin photoactivation. 118

Figure 3.5: The time-lag between ATR release and TM6 movement back to the inactive state is increased when retinal release is accelerated. 120

Figure 4.1: Sensor constructs and general ligand-detection scheme 140

Figure 4.2: Demonstration of the GtF and ArrF TrIQ sensor detecting interactions between the opsin and the fusion tail. 142

Figure 4.3: The CIM-GtF sensor reports agonist (ATR) binding in a dose dependent manner. 144

Figure 4.4: Gt antagonist binding detected by increasing sensor fluorescence 146

Figure 4.5: Transfer of ATR from unlabeled rhodopsins to the CIM-GtF sensor. 148

Figure 4.6: Ligand binding detected by arrestin fusion sensors 150

Figure S4.1: Retinal uptake by the different ArrF fusion constructs. 152

Figure S4.2: ATR transfer from photoactivated rhodopsin to Trp-less CIM-GtF construct. 154

Figure A1.1: Experimental data rationalizing the choice of bimane-tryptophan pairs used for the simulations presented here 190

Figure A1.2: Simulation of the probe quencher pairs on T4 lysozyme 192

Figure A1.3: Distance calculations between the Trp and bimane across the three simulations 194

Figure A1.4: Simulation cell of opsin in a POPC bilayer 196

Figure A1.5: TM6 of the simulated opsin remains in the inactive conformation during the experiment 198

Figure A1.6: Comparison of the simulated opsin with Ops and Ops* of the residues flanking Hole A and B 200

Figure A2.1: Transient activation model for retinals binding to opsin 205

Figure A2.2: *In silico* modeling of the transient activation hypothesis confirms that this model cannot reconcile our experimental 11CR binding data 207

Figure A3.1: Setup and testing of the LED augmented fluorometer 210

List of Abbreviations

9CR	9-cis retinal
11CR	11-cis retinal
11CR-ol	11-cis retinol
1D4	monoclonal antibody to rhodopsin
1D4 peptide	peptide recognized by 1D4: TETSQVAPA
A	alanine
α	alpha
A	Arrhenius constant
Å	Angstrom
A2E	N-retinylidene-N-retinyl ethanolamine
ABCA4	ATP-binding cassette transporter
ADRP	Autosomal Dominant Retinitis Pigmentosa
Arr	arrestin
Arr peptide	arrestin peptide: YGQEDIDVMGLSF
ArrF	fusion of Arr peptide to C-terminus of opsin
Asp	aspartate
ATP	adenosine triphosphate
ATR	all-trans retinal
ATR-ol	all-trans retinol
β	beta
B	bimane label
B2AR	β_2 adrenergic receptor
C	cysteine

CAM	constitutively active mutant
CB1	cannabinoid receptor type 1
cGMP	cyclic guanine monophosphate
CIM	constitutively inactive mutant
CNB	Congenital Night Blindness
CRALBP	cellular retinal binding protein
CRBP	cellular retinol binding protein
Cys	cysteine
D	aspartate
DDM	n-dodecyl-β-maltoside
°C	degrees Celsius
DNA	deoxyribonucleic acid
DS	dark-state rhodopsin
ε	extinction coefficient
E (residue)	glutamate
E (protein domain)	extracellular
E_a	energy of activation
EDTA	ethylenediamine-tertraacetic acid
EPR	electron paramagnetic resonance
F	phenylalanine
FRET	fluorescence resonance energy transfer
FTIR	Fourier transform infrared spectroscopy
G	glycine
GDP	guanine diphosphate
Glu	glutamate

GPCR	G protein-coupled receptor
G protein	heterotrimeric guanine nucleotide-binding regulatory protein
Gt	transducin G protein
Gtα	alpha subunit of Gt
G_t C-term Peptide	high-affinity Gt_α C-terminal peptide: VLEDLKSVGLF
GtF	fusion of G_t C-term peptide to C-terminus of opsin
GTP	guanine triphosphate
h	hour
h	Planck's constant
hν	light
HA	hydroxylamine
HEPES	4-(2-hydroxyethyl)-1-piperazineethanesulfonic acid
HPLC	high-pressure liquid chromatography
I (residue)	isoleucine
I (protein domain)	intracellular
IPM	inter-photoreceptor matrix
IRBP	inter-photoreceptor retinol binding protein
k	rate constant
k (residue)	lysine
kcal	kilocalories
L	leucine
λ_{max}	absorbance maximum
LCA	leber congenital amaurosis
LRAT	lecithin retinol acyl transferase

M	molar
M (residue)	methionine
mBBr	monobromobimane
MES	2-(N-morpholino)ethanesulfonic acid
MI	metarhodopsin I photointermediate
MII	metarhodopsin II photointermediate
MIII	metarhodopsin III photointermediate
min	minute
µl	microliter
ml	milliliter
µM	micromolar
mM	millimolar
MW	molecular weight
N	asparagine
NH_2OH	hydroxylamine
nM	nanomolar
NrPE	N-retinulidene- phosphatidylethanolamine
Ops	inactive-state opsin
Ops*	active-state opsin
PBSSC	phosphate-buffered saline
PCR	polymerase chain reaction
PE	phosphatidylethanolamine
PEI	polyethylenimine
pK_a	pH of acid dissociation constant
PMSF	phenylmethanesulfonyl fluoride

PSB	protonated Schiff base
Q	glutamine
θ	rhodopsin background mutant: C140S/C316S/C322S/C323S
R	arginine
RDH	retinol dehydrogenase
Rho	rhodopsin
RK	rhodopsin kinase
RMSD	root mean square deviation
ROS	rod cell outer segment
RP	*retinitis pigmetosa*
RPE	retinal pigment epithelium
s	second
S (residue)	serine
SDFL	site-directed fluorescence labeling
SDSL	site-directed spin labeling
T	threonine
TAH	transient activation hypothesis
tbHA	o-tert-butylhydroxylamine
TCA	trichloroacetic acid
TM	transmembrane
TrIQ	tryptophan-induced quenching
Trp	tryptophan
UV/vis	ultraviolet-visible
V	valine

W	tryptophan
WT	wild-type
Y	tyrosine

Acknowledgements

First and foremost, I would like to thank my graduate mentor, Dr. Dave Farrens. Our spirited debates and scientific discussions have helped shape me to be the scientist I am today.

Additionally, I would like to thank the members of the Farrens lab, Dr. Jon Fay and Dr. Amber Brunette, who have kept the daily grind enjoyable and bearable. I would also thank the former members of the Farrens, Dr. Abhinav Sinha, Dr. Eva Ramon, and Dr. Jay Janz for providing some of the preliminary experiments for this work.

I also would thank my thesis advisory committee, Dr. Michael Chapman, Dr. Ujwal Shinde, Dr. Francis Valiyaveetil, Dr. Matt Whorton, and Dr. Drake Mitchell for their thoughtful comments and guidance.

I would like to thank my family and friends both in Portland and back in Minnesota. You have been a huge source of support and my adventure through graduate school would not have been possible without you all.

Finally, last, but not least, I thank my wonderful partner Ashleigh Murphy, who has suffered through rants, complaints, and endless questions of "is this result interesting enough?" Thank you so much for the support over these years.

Abstract

The dim-light photoreceptor rhodopsin has been a structural model for G protein-coupled receptors (GPCRs) for decades, so much so that the largest class of GPCRs is commonly called “rhodopsin-like.” However, the visual receptor has several unique characteristics that differentiate it from other members of the superfamily. Most notably, rather than interacting through a diffusible ligand, the receptor covalently binds its light-sensitive inverse agonist, 11-cis retinal (11CR), which locks the complex in an “off” state. Activation occurs when the 11CR-rhodopsin complex absorbs light, and isomerizes the ligand into the agonist all-trans retinal (ATR). After activation, the ATR is exchanged for a fresh 11CR in order to reset the protein for further light detection. Therefore, despite the covalent nature of the retinal-rhodopsin interaction, the ligand must be capable of entering and exiting the receptor. So it may come as a surprise that, although rhodopsin was the first solved GPCR crystal structure, how the retinals bind and dissociate from the protein remains unanswered.

This dissertation attempts to address this question. Initially, I tested a standing hypothesis that an active opsin conformation is required for both the 11CR and ATR to transit into or out of the binding pocket. My experiments refuted part of this hypothesis, as I found increasing the relative active population within the opsin sample did not lead to more rapid 11CR binding, but did accelerate the binding of ATR. These results pointed to a conformation selection mechanism governing retinal binding instead of the proposed transient activation model (Chapter 2). Next I expanded on these results and was able to directly observe a conformationally-sensitive binding equilibrium for ATR following

photoactivation and release. Additionally, I observed exchange of the bound ATR for free externally added ATR in solution, even though assays suggested the ATR was covalently bound (Chapter 3). Finally, since these results suggested that rhodopsin can behave like a traditional ligand-binding GPCR, I converted rhodopsin into a fluorescent biosensor to screen for ligands that affect either G protein or arrestin binding (Chapter 4).

In summary, the results presented here have made us reassess how the visual GPCR rhodopsin interacts with its retinal ligands, opening the door for targeting it with therapeutic agents like other, classical GPCRs.

Chapter 1: Introduction

This chapter covers the background and rationale for the pharmacological study of rhodopsin, focusing primarily on the differences between classical "liganded" G protein-coupled receptors (GPCRs) and rhodopsin. The inherent process of retinal cycling within the retina and current hypotheses concerning how retinals bind to rhodopsin are also discussed.

1.1: G protein-coupled receptor signaling

1.1.1: Ligand-binding GPCR signaling

1.1.1.1: GPCR overview

GPCRs represent the largest family of cell surface receptors, constituting over 800 members and ~3% of the human protein-coding genome (1). The receptors respond to a variety of stimuli, including small molecules, peptides, and light. The expansive nature of the protein family has led to extensive efforts for pharmaceutical development, with almost a third of all new drugs on the market targeting a GPCR (2).

Basic GPCR structure involves an extracellular N-terminus followed by seven transmembrane helices (3). These terminate with an amphipathic eighth helix and an intracellular C-terminal tail (Figure 1.1). The receptors can be broken into six distinct classifications. The focus of this dissertation is on the rhodopsin-like subfamily, which contains the namesake rhodopsin and β_2 adrenergic receptor (B2AR), and is the largest of the classes (4).

1.1.1.2: Classical activation

Depicted in Figure 1.2, classic GPCR activation occurs when an agonist ligand binds to the protein and stabilizes an active, G protein-coupling conformation. This change in receptor structure is marked by a translocation of transmembrane helix 6 (TM6) (5-7) and to a lesser extent TM5 (8,9), thus exposing a cleft in the cytoplasmic face that subsequently provides a binding site for the effector G protein (10). The "G protein" is actually a complex of three distinct polypeptides designated α, β, and γ subunits. Coupling involves the Gα subunit's C-terminus binding to the recently exposed cytoplasmic cleft of the GPCR, resulting in a conformational change in the G protein complex that ultimately promotes exchange of GDP for GTP in the Gα protein, thereby activating the G protein (7,10-13).

The G protein then decouples from the receptor, with the Gα dissociating from the Gβ/Gγ subunits, both exposing previously buried surfaces that can interact with various downstream signalers such as adenylate cyclases, phospholipases, and other secondary messenger systems (14-16). In this way, the external stimulus is translated into an internal cellular response. These signals ultimately result in a wide array of effects ranging from neuronal signaling to cellular motility. The beauty of the GPCR system is the ability to massively amplify a signal, since a single ligand can result in many activated G proteins. A rhodopsin molecule, for example, can activate hundreds of G proteins, enabling a single photon to cause a neuron response (discussed below) (17,18).

Binding of the G protein stabilizes a high-affinity agonist binding state of the receptor. This positive cooperatively, where the interaction of one molecule enhances that of another through an allosteric coupling, was first described by Lefkowitz and

colleagues as the ternary complex model (19). This model was later expanded with the discovery of receptor mutations displaying constitutive activity, meaning that they can couple to G proteins and promote guanyl nucleotide exchange in the absence of ligand, to form the extended ternary complex model (20). Rather than describing the receptor population as homogeneous as in the initial ternary complex model, the extension incorporated terms for the receptor's conformation, either active or inactive.

1.1.1.3: Classical deactivation

Termination of signaling is as important as receptor activation. For GPCRs, this deactivation can involve either release of the agonist or initiation of a multistep process initiated by phosphorylation of the C-terminal tail of the active receptor by GPCR kinases (GRKs) (21,22). The addition of these phosphates enhances binding of the ancillary protein arrestin, which physically obstructs the cytoplasmic face of the receptor to prevent further G protein-coupling (23,24). The arrestin protein structure comprises two lobes, aptly named by their proximity to either the N- or C-terminus (25). The primary interacting region of arrestin connects the lobes and is called the "finger loop (26)." Arrestin has been observed to bind in two modes, one interacting with low affinity to the TM7-C-terminal region and another when the finger loop complexes with the cytoplasmic cleft (27-30). A recent crystal structure of a rhodopsin-arrestin fusion protein captures this high affinity state and confirms the finger loop binds into same cytoplasmic cleft as the G protein (28,31).

1.1.2: Rhodopsin signaling

The GPCRs responsible for dim-light vision, rhodopsins, are found in rod-shaped photoreceptor cells in the vertebrate retina (32). These cells are named for their modified and enlarged cilium which gives the outer segment of the cell a rod-like shape, as shown in Figure 1.3. The rod outer segment (ROS) is nearly singular in its purpose of translating the photodetection to cellular signals. The ROS is filled with thousands of stacks of discal organelles that are densely packed with rhodopsin molecules, resulting in a receptor concentration as high 4.6mM (33). This high density of photoactive protein allows for even singular photons that are traversing the rod cell to be captured by a rhodopsin molecule and trigger a signaling cascade (34).

The photoreceptor protein itself is made of two parts, the opsin apoprotein and the light-sensitive chromophore retinal. Before rhodopsin signaling can begin opsin must first take up its inverse agonist 11-*cis* retinal (11CR, retinal structures in Figure 1.4), which binds to the protein through a covalent Schiff base mechanism (35). The small molecule holds the receptor in an inactive "off" state, quenching the very low basal signaling of the opsin (36-38).

Light entering the eye is focused to the retina and causes the isomerization of the bound 11CR to the agonist all-*trans* retinal (ATR) (39). This conversion causes the rhodopsin to cascade through several short-lived photointermediates before settling into the first of three metarhodopsin conformations (40-42). These metarhodopsin states all have a bound ATR agonist, but are separated by different spectral properties. The first of these, metarhodopsin I (MI), absorbs maximally at 480nm, an ~20nm shift from the 500nm for dark-state, 11CR-bound rhodopsin. MI, although bound to the agonist, is a

non-G protein coupling conformation (43,44) and is in equilibrium with the other two metarhodopsins (45), metarhodopsin II (MII) and III (MIII). MIII is also an inactive conformation and has been speculated to represent a storage form of the protein (46). MII exhibits the largest change in spectral properties, with an absorbance shift into the ultraviolet (maximum at 380nm) (Figure 1.4) (35). Additionally, MII is the only form that can activate G proteins, and, as described above, couples with the G protein found only in photoreceptor cells transducin (Gt) to translate the photonic signal to neuronal output (47,48).

A single MII can activate hundreds of transducins, allowing for the massive signal amplification and for effective single photon responses from the cell noted earlier (18). After guanine exchange, the activated Gtα GTP-bound subunit dissociates from the Gtβ/Gtγ subunits, then stimulates activity of cGMP phosphodiesterase (PDE) (49,50), resulting in a decrease in cGMP levels in the ROS. This decrease causes closure of Ca^{2+} channels, stopping the passive transit of the cations into the cell. The resulting hyperpolarization of the rod cell signals through downstream retinal ganglion cells to the brain that a photon has been detected (48,51-53). This phototransduction pathway is depicted in Figure 1.5. Hydrolysis of the bound GTP back to GDP deactivates the Gt allows the rod cell to reset back to dark state conditions (53), and thus be ready for another round of signaling.

Signaling by MII is terminated first by phosphorylation by GRKs and then binding of visual arrestin. Interestingly, recent spectroscopic studies have indicated that all three binding proteins, Gt, GRK, and arrestin, all interact with the same cytoplasmic cleft (see above) (10,21,23,29,30). Final deactivation of the receptor occurs when the

Schiff base is hydrolyzed and ATR is released, then transported to other cells where it is reconverted back to 11CR (discussed below) (54). The loss of the agonist allows the receptor to transition back to the nearly completely inactive opsin state (36,55,56).

1.2: Retinal (re)cycling

With the high-sensitivity of rhodopsin, even small amounts of appropriate wavelength light will result in photoisomerization of the 11CR in some rhodopsins and production of ATR. Therefore, ATR release occurs constantly, and since the enormously high concentration of rhodopsins means a similarly high concentration of ATR, vertebrates have developed a surprisingly elaborate system to deal with the large amount of potentially toxic retinal aldehyde (discussed below).

1.2.1: All-trans retinal recycling

1.2.1.1: ATR transfer from the rod outer segment

After dissociation from the opsin, ATR is recycled back to 11CR through the actions of the so-called retinoid cycle (Figure 1.6). Proper clearance and regulation of the free ATR is essential due to the cytotoxicity of the retinal (a highly reactive aldehyde) especially since relatively high potential concentrations could be achieved if too many of the rhodopsins ejected their agonists all at once (33,57).

Within the membrane, retinal can readily react with phosphatidylethanolamine (PE) to form N-retinylidene-PE (NrPE) (58). Although this reaction is reversible, delayed clearance can react with another ATR creating non-degradable and potentially toxic N-retinylidene-N-retinyl ethanolamine (A2E) (59). Therefore, soon after release, the ATR is

reduced to all-trans retinol (ATR-ol) by retinol dehydrogenase (RDH) 8 and/or 12. Though RDH8 is localized to the outer segment of the rod cells (60) and RDH12 to the inner segment (61,62), mouse models have shown that the dehydrogenase activity is split ~70% RDH8 and ~30% RDH12 (63,64). The activity of these RDHs appears to be isolated to retinal on the cytoplasmic side of the disc—ATR that transitions to the luminal side is not capable of being reduced by the presumably cytoplasmic facing (or within the cytoplasm) RDH8. Therefore, for proper reduction, ATR on the luminal side must be flipped to the cytoplasmic side by ATP-binding cassette transporter 4 (ABCA4) (65). The transition from the discal membrane to the plasma membrane of the outer segment is one of two steps within the retinoid cycle where a chaperoning protein has not been identified, leading to speculation that flexibility within the outer segment allows for the discs to collide with the plasma membrane, thus enabling ATR transfer.

1.2.1.2: ATR-ol is escorted from the rod outer segment to the RPE for storage

From the rod cell plasma membrane, ATR-ol is taken up by inter-photoreceptor retinol binding protein (IRBP) for transport across the inter-photoreceptor matrix (IPM) to the RPE (66,67). IRBP binds both all-*trans* and 11-*cis* isomers and is involved later in the cycle for returning fresh 11CR to the rod cell (68). The retinoid is then passed to the RPE plasma membrane and is picked up by a cellular retinol binding protein (CRBP). The retinoid is then brought to lecithin retinol acyl transferase (LRAT) at the endoplasmic reticulum, anchored by a single membrane-spanning helix (69). LRAT esterifies the ATR-ol to form retinyl-ester, forming the sole substrate for 11-cis retinol

(11CR-ol) production (70-74). Retinyl-esters are used as a storage form of the retinoid, packed in the RPE in retinosomes until needed (75).

1.2.1.3: Conversion back to the 11-cis isomer and return to the rod cell

Deesterification and isomerization of the all-trans retinyl-ester is performed by one enzyme, RPE65. Due to this dual reaction nature, the protein has been referred to as an isomerhydrolase (76-78). It has been argued that the cleavage of the ester from the retinoid provides the necessary source of energy for the isomerization (79). The resulting product of this reaction, 11CR-ol, acts as an inhibitor for RPE65 and slows the production of more 11CR-ol (80,81). Therefore, to accelerate the production of 11-cis isomer, RPE65 complexes with cellular retinal binding protein (CRALBP), which binds to and sequesters the 11CR-ol, preventing inhibition (82,83). 11-cis retinal dehydrogenase (RDH5) is another member of this complex. RDH5 oxidizes 11CR-ol to 11CR reforming the active aldehyde moiety. The binding protein then chaperones new 11CR from the dehydrogenase to the plasma membrane where it is handed off to IRBP once again. IRBP ferries the 11CR back across the IPM to the rod cell where it diffuses across the cytoplasmic space into the discal membrane where it can rebind to an empty opsin molecule and ready the protein for signaling (discussed above).

1.2.2: Retinal cycle diseases and therapeutics

1.2.2.1: Diseases

Due to the large flux of retinoids through the cycle (discussed above), mutations to the enzymes responsible for the process can cause an array of retinal dystrophies and issues. As noted above, after release from rhodopsin, the ATR is first reduced by RDH8

in the rod outer segment. No known disease mutations of RDH8 have yet been identified in humans, despite being the dehydrogenase localized to the outer segment. In contrast, variants have been found for RDH12 (the dehydrogenase found in the rod cell inner segment) in patients with leber congenital amaurosis (LCA) (84,85). However, mice in which RDH8 or RDH12 were knocked out show an accumulation of A2E in the RPE and retinal degeneration under intense illumination (60-62).

Recall that retinals that fail to release to the cytoplasmic side of the disc are unable to be reduced and so must be flipped from the luminal side by the protein ABCA4, to prevent harmful adduct formation. Deficiencies in the flippase result in a form of juvenile macular dystrophy called Stargardt disease, age-related macular degeneration, autosomal recessive cone-rod dystrophy, and autosomal recessive retinitis pigmentosa (86-91). Mouse knockouts of ABCA4 show greater A2E accumulation in the RPE, mild rod degeneration, and delayed dark adaptation of rod cells (92). Neither the RDH nor the ABCA4 knockout mice show the same level of retinal degeneration seen in humans with similar mutations, potentially due to the different requirements of a nocturnal animal (mice) versus a diurnal, cone-dominant species (humans). Interestingly, combining the ABCA4 and RDH8 knockouts greatly exacerbates the retinal dystrophy complete with apoptosis of the photoreceptor cells following bright illumination (93). This can be prevented by pretreating the mice with retinylamine, a retinoid cycle inhibitor (94,95).

Transition from the rod outer segment to the RPE requires IRBP, loss of which is associated with *retinitis pigmentosa* (96) or night blindness. Upon transfer to the RPE, LRAT esterifies the ATR-ol for storage. Mouse knockouts of LRAT have only ATR-ol

present in the eyes without any 11CR formed, illustrating the critical nature of this reaction for proper processing and vision (71,97). Mutations to this enzyme in humans are associated *retinitis pigmentosa* and LCA (98). Likewise, mutations to RPE65, the isomerhydrolase, show similar disease phenotypes in humans (99). Knockouts of the isomerase in mice also show no 11CR production and the formation of extensive retinosomes in the RPE due to accumulation of the retinyl-ester (100). Impairment of the enzyme responsible for final processing to 11CR (RDH5) has been associated with fundus albipunctatus, an abnormality characterized by white dots on the fundus image, night blindness, and cone dystrophy later in life (101,102). Knocking out the 11-cis retinol dehydrogenase in mice resulted in a very benign phenotype with only slight deceleration in dark adaptation (103).

1.2.2.2: Therapeutics

Currently, several therapies to remedy conditions with the visual retinoid cycle fall within two groups, either gene rescue or pharmacological intervention. The first technique, gene therapy, has used adeno-associated virus to replace defective genes. This method has been successful in animals with defective LRAT and RPE65 genes and is undergoing clinical trials for recovering the isomerhydrolase (104-107). By introducing a functioning gene, the disruption of the cycle can be overcome and recycling of the retinal can continue.

Another prominent strategy involves using exogenously added retinoids (108) to either replenish the missing chromophore or slow the process to overcome deficiencies in trafficking. One retinal isomer 9-*cis* retinal (9CR) has very similar properties to 11CR when binding to rhodopsin. Like 11CR, 9CR act as inverse agonists and has a maximal

absorbance that is only slightly blue-shifted from 11CR when bound to opsin (109). However, 9-*cis* retinoids are more stable compared to the 11-cis varieties and therefore be more easily supplemented. Oral supplementation and intraperitoneal injection to RPE65 knockout mice with 9CR has been shown to successfully restore light sensitivity, preserve the retinal morphology, and improve rod cell function up to six months following treatment (110-112). Additionally, retinal activity was recovered in LRAT knockout mice treated orally with 9-*cis* retinoids, preserving pigment at about 50% for 120 days after dosage (107).

However, two concerns arise from simply replacing 11CR with 9CR. First, since a defective RPE is unable to reisomerize the spent ATR, the ligands are only good for a single turnover before they must be replaced. Second, retinals can be converted to retinoic acid within other cell types by RDH1, 2, 3, and 4, a compound that regulates gene expression via RAR and RXR nuclear receptors (113,114).

The final strategy for treating retinoid cycle defects attempts to inhibit the cycle in order to prevent over accumulation of ATR. This method is particularly effective for treating mutations in the "retinal flippase" ABCA4. One example is the commercial acne treatment accutane (isotretinoin or 13-cis retinoic acid), which binds to RDH5 and RPE65, inhibiting 11CR production (115,116). Treatment of albino rats with this compound protected against light-induced retinal damage and treating ABCA4 knockout mice completely blocked new A2E synthesis (117,118). Unfortunately the dosage required for protection in humans would result in adverse side-effects. Another cycle inhibitor is retinylamine, which has also been shown to impair the isomerization reaction

in the RPE (119). This molecule also reduces A2E levels and has the additional benefit of being reversibly N-acylated by LRAT, which prolongs the inhibitory effect (120,121).

1.2.3: A standing question regarding the retinoid cycle

Although, as can be seen above, details about the retinoid cycle are now known, one simple, yet, long-standing question remains—how does the retinal exit and leave the receptor? The lack of understanding of this basic process has likely caused the photoprotein itself to not be the direct subject of therapeutic interventions, aside from replacement of 11CR with 9CR noted above. The focus of this dissertation will be to address how retinal binding occurs and is discussed below.

1.3: Rhodopsin structure

In 2000, rhodopsin became the first GPCR for which a crystal structure was determined (Figure 1.4) (3). For several years after it remained the only family member with atomic level information and thus was used as the template for countless GPCR modeling studies. Since this structure, which represented the 11CR-bound, inactive state, more than twenty different rhodopsin structures have been deposited to the Protein Data Bank (9), including early photointermediates (122,123), active MII with and without Gt C-terminal peptide bound (47), an arrestin-bound fusion structure (31), and the apoprotein opsin, the only empty (non-ligand-bound) GPCR to date (6).

The rhodopsin protein is divided into three general protein domains (Figure 1.5). The first domain is extracellular—technically intradiscal for the photoprotein, however, we have opted to refer to this domain region as extracellular to allow easier comparison

with other GPCRs—and consists of the N-terminus and extracellular loops. These portions of the protein form a tightly packed cap over the retinal binding pocket, protecting the chromophore binding site from discal solvent. On the other side of membrane is the intracellular face of the receptor, which contains the intracellular loops and C-terminus. These provide the scaffolding for interactions with the Gt, GRK, and arrestin signaling proteins. The final domain spans the membrane and contains the transmembrane helices, which include the retinal binding pocket, ionic locks that hold the receptor in the "off" state, and an extensive solvent network that is thought to translate signals from the binding pocket to conformational change on the cytoplasmic face. The features of the retinal binding pocket will be discussed below.

1.3.1: The retinal binding pocket

The binding pocket for the retinal chromophore is buried in the protein near the extracellular side. The pocket contains the lysine residue on TM7 that forms the covalent linkage via a Schiff base between the retinal and the opsin. Other noncovalent interactions between the retinal and opsin are essential for modulating the spectral properties of the photoprotein and maintaining a maximal absorbance at 500nm for the dark-state receptor (44). Key to this task is the protonation of the Schiff base, which is accomplished by a so-called counterion residue at E113 that raises the pK_a of the Schiff base protonation. For example, a constitutively activating mutation, E113Q, drops the pK_a from ~15 to 8 (124-127). Although the covalent bond is not essential for activation by retinoids (128,129), the efficiency of G protein coupling drops dramatically when only noncovalent interactions are included, thus the Schiff base is essential for the high sensitivity of the system (130).

The protonation of the Schiff base can only account for the shift in absorbance of free retinal from 380nm to ~440nm, therefore, other noncovalent interactions must account for the larger specific absorbance maxima seen in some rhodopsin species. Even more importantly, all visual opsins in the vertebrate retina bind the same 11CR chromophore to start their visual cycles, thus, the residues and features of the individual binding pockets must be responsible for the diversity in spectral sensitivity seen for different color-sensing opsins found in cone cells (131). Residues important for the different λ_{max} displayed by the various photoproteins have been identified by site-directed mutagenesis (132-135). These dipolar residues are thought to act electrostatically to influence the absorption states of the chromophore (136).

It has also been observed that the noncovalent interactions within the binding pocket contribute to the long-lived MII state (137). Even though, as stated above, the Schiff base is essential for observing efficient activity (128,130,138), work by Knox and colleagues comparing the ATR dissociation from photoactivated rhodopsin to cone opsin found that although release was much faster from cones, the activation energy for release from both proteins were the same (137). This result indicates that the basic chemistry of the Schiff base is the same in both photoproteins. Therefore, the differences in the rates of ATR dissociation is assumed to be due to the non-covalently associated residues repositioning the retinal so that it reforms the Schiff base as has been previously proposed for 11CR and dark-state rhodopsin (139,140).

1.3.2: Constitutive activity

The mutation E113Q, mentioned above, removes the counterion for the protonated Schiff base. An added effect of this change is the introduction of so-called

"constitutive activity"—an increase in basal G protein signaling of the apoprotein—into the receptor (127). The phenomenon of constitutive activating mutations (CAMs) in opsin is particularly striking due to the low native basal activity, which causes any amount of signal to rise above baseline (36-38). The loss of the counterion is not the only CAM, but rather is a member of well populated list including the loss of the lysine K296, such as in the K296G mutation, indicating that the ionic lock between the two residues is essential for the low basal activity (127). Other CAMs cause congenital stationary night blindness (CSNB) such as G90D, T94I and D, A292E, and A295V, all of which are located near the Schiff base linkage and act to disrupt the E113-K296 interaction (141-147). The resulting rhodopsins inappropriately signal and prevent the rod cell from properly adapting to dark conditions, thereby ruining the high sensitivity and impairing the vision of patients with these variants.

1.4: Retinal binding

1.4.1: How does retinal enter or exit opsin?

As noted above, a long standing question within the rhodopsin community has been how retinal enters and escapes the binding pocket. The original high-resolution crystal structures of the inactive, 11CR-bound receptor further complicated this question, as they showed the binding pocket is entirely occluded from any external space, presenting no obvious openings (148) (Figure 1.7). However, in 2008, the first active-like structure was determined by Ernst and colleagues (6). In addition to the expected translocation of TM6 (5), the structure revealed several surprising features. First, the receptor was in the empty, opsin state, which was unexpected since opsin is well noted to

be almost entirely inactive in physiological conditions (36,55), yet the structure showed an active TM6 position. At first, it was not clear why the structure reflects the non-dominant form of the apoprotein. Subsequent analysis has suggested this active opsin (Ops*) is likely the consequence of the crystallographic conditions, as lower pH (149), unintended presence of a detergent inside the binding pocket (150), or the crystal contacts might cause the protein to adopt the open, active-state.

Additionally, and perhaps more relevant to the question of retinal entry, the active opsin structure also displays an "open" binding pocket, with rotameric changes to several phenylalanine residues. In this active structure, these flanking aromatic residues rotate out into the membranous space, forming two openings, Hole A caused by the rotation of F293 (between TM1 and TM7) and Hole B caused by the rotation of F208 and F273 (between TM5 and TM6) (Figure 1.7) (151,152). These "holes" are present in all subsequent active-state structures (7,47,153,154) and are now thought of as a feature of the active-like conformation. Therefore, the models discussed below were proposed to integrate the active-like opsin structure with how the binding occur.

1.4.1.1: Ligand channeling through an active-like receptor

Even before the active opsins structure, the idea of ligand channeling had been proposed by Hofmann, Palczewski, and colleagues as a means of regulating retinal trafficking and presenting the newly released ATR for reduction by RDH8 (155-157). However these initial reports could not address how the retinal might be traversing the protein, but rather focused on possible secondary retinal binding sites that were proposed to play a role in retinal storage.

The idea of channeling was revisited with the Park et al. structure (6), this time explicitly modeling different retinal conformations inside the binding pocket as though they were transiting through the protein (151,158). The general conclusion from these studies was that the 11CR was likely being taken up for the receptor through Hole A, whereas ATR was released through Hole B. Further modeling experiments using Random Accelerated Molecular Dynamics (RAMD) corroborated that Hole B is the most likely candidate for ATR exit (Figure 1.7) (159). It is important to note that the constriction points between helices in this putative ligand channel are too small to fully accommodate the cross-sectional area of the β-ionone ring of retinal, thus some level of helical flexibility would still be required for retinal to move in and out of these holes.

These modeling studies were followed up with attempts to affect retinal entry and release by mutagenesis throughout the proposed ligand channel (the intraprotein space between Hole A and Hole B, containing the retinal binding pocket) (152). Unexpectedly, the authors observed no obvious pattern among the dozens of mutations tested, and thus the results for many of the mutations could not be rationalized by localized perturbations. Therefore, the authors concluded that the mutations had nonlocalized effects on retinal interactions and were unable to draw direct evidence of the proposed ligand channeling from Hole A to Hole B.

1.4.1.2: Transient activation model for retinal binding

As noted in the previous section, because opsin shows very low levels of activity (basal signaling) in its native state, is has been assumed that the structure of opsin should reflect the 11CR-bound (dark-state) conformation, rather than the active-like opsin seen in the crystal structure (3,7,36). Thus, to account for the lack of obvious entry or exit

avenues in the inactive state, a transient activation model was proposed to explain retinal entry and release (Figure 1.8) (152). A key assumption of this model is that rhodopsin exists essentially as two-states, either closed and inactive or open and active (160). Therefore, in this model, the mostly inactive opsin must transiently adopt an active-like conformation in order to open the binding pocket and allow the retinal bind. Electrophysiology experiments using salamander rod cells partially supported this idea, where transient electrical activity was observed during dark adaptation (161).

Implicit to this model is the proposal that both the inverse agonist 11CR and agonist ATR bind to an active-like conformation of opsin. I directly tested this hypothesis in Chapter Two, the results of which then form the basis for the rest of my dissertation.

1.5: Dissertation overview

The major conclusions of this dissertation are that, contrary to most prior assumptions, the GPCR rhodopsin interacts with its retinal ligands in much the same way as "traditional" ligand-binding receptors. Instead of being a unique or a "black sheep" of the GPCR superfamily, my results show that rhodopsin binds retinals like other GPCRs that bind diffusible ligands. Chapters Two through Four detail my experiments and results leading to the conclusion and applications of opsin being a liganded GPCR.

First, in Chapter Two, I explored the current ideas surrounding how retinal binds to opsin. The current dogma of the transient activation model (described above) posited that an active-state receptor conformation is required for retinals to enter the receptor and form the Schiff base linkage. I tested this idea by probing the rates of retinal binding to opsins of different "activeness." My results indicated that opsin shows classical

conformational selection, where the inverse agonist 11CR binds preferentially to an inactive conformation agonist ATR binds preferentially to an active conformation. This sort of conformational selection is previously unobserved within the visual protein opsin and provides strong evidence for opsin acting as a liganded GPCR.

Chapter Three builds directly on Chapter Two and probes the role of receptor conformation during ATR dissociation after photoisomerization. In line with a conformational selection model for retinal interactions, I found that more stabilized active receptors result in less ATR dissociation. Additionally, this work clearly showed that the ATR in active receptors is in equilibrium and is constantly leaving and rebinding over the course of the experiment. Finally, I simultaneously probed the rates of ATR dissociation and receptor deactivation and found that the protein conformational change from active to inactive was delayed from the agonist release, suggesting that the two events are distinct.

In Chapter Four, I used my observation that retinals bind to opsin as though it were a liganded receptor system to develop a sensor to detect ligand binding. To do this, I combined a selective fluorescence quenching technique with rhodopsin fusion proteins to observe ligand-induced changes in the receptor conformation. These sensors can screen between rhodopsin agonists and antagonists.

Finally, chapter five discusses the overall summary of these studies in the light of opsin as a liganded GPCR and implications to opsin pharmacology, as well as future directions to be undertaken from this work. The appendix to this dissertation details my molecular dynamics modeling efforts to probe events not easily observed experimentally. These include the interactions between a fluorescent probe and tryptophan quencher and

the changes in the inactive opsin structure that might lead to an opening of the binding pocket.

Figure 1.1: Basic GPCR architecture

The classic GPCR structural motif is a seven transmembrane helical fold, with an amphipathic helix eight that lies parallel to the membrane. The N-terminus begins extracellularlly, and with the extracellular loops, forms part of the ligand binding domain, with the transmembrane region forming the rest. The intracellular domain (C-terminus and intracellular loops) form the binding face for G proteins, arrestins, and GPCR kinases (162).

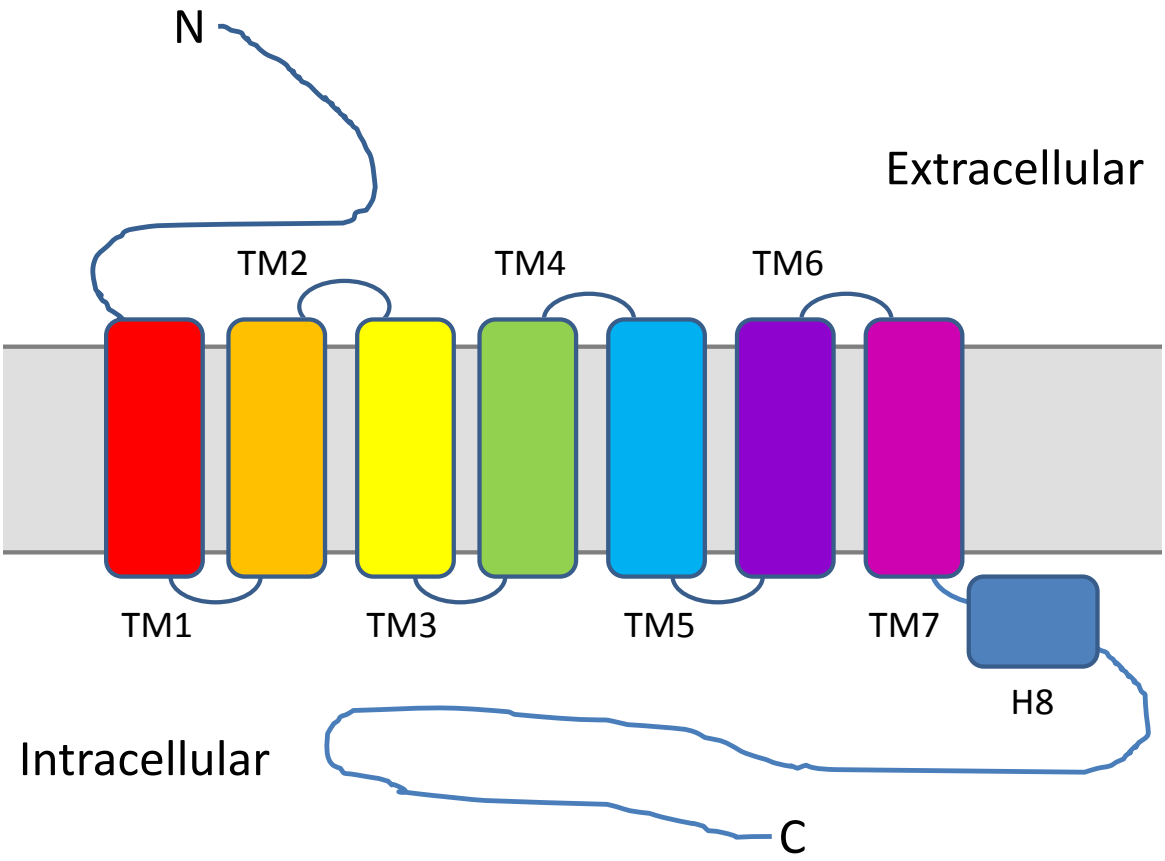
N
Extracellular
TM2
TM4
TM6
TM1
TM3
TM5
TM7
H8
Intracellular
C

Figure 1.2: Simplified liganded GPCR signaling through G protein mediated pathway.

Liganded GPCR signaling is initiated when the apoprotein binds an agonist that stabilizes an active, G protein coupling conformation. Subsequently, the receptor activates the G protein complex by guanine nucleotide exchange of GDP for GTP, which causes the heterotrimeric G protein to split into the Gα and Gβγ subnunits. These subunits then travel into the cell, activating secondary messengers and ultimately eliciting a cellular response from the external stimulus. Alternatively, the empty receptor can bind an antagonist, which stabilizes an inactive conformation that cannot bind G proteins and thus prevents signaling.

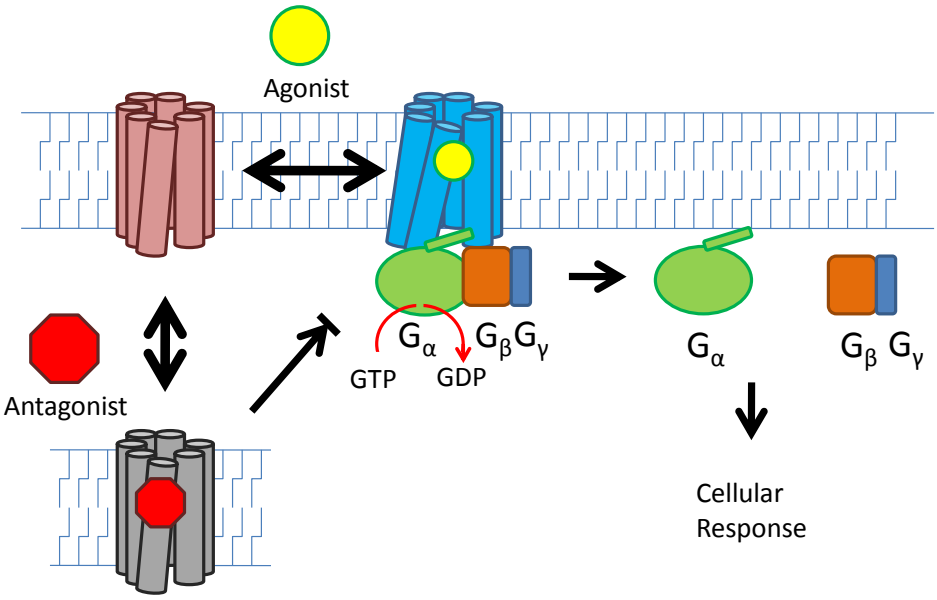
Agonist
Antagonist
GTP
GDP
G_α
$G_\beta G_\gamma$
G_α
G_β G_γ
Cellular
Response

Figure 1.3: Rod cell architecture

The rod cell is specially designed to maximize the ability of rhodopsin molecules to capture photons. The cell itself is composed of an inner segment, containing the cellular machinery such as the nucleus, endoplasmic reticulum, and neuronal signaling apparatus, and the outer segment, containing hundreds of discal organelles, each packed with rhodopsin molecules up to a concentration of about 4.6mM (32,33). The rhodopsins are made up of a transmembrane helical bundle and a bound chromophore which bestows visual spectrum sensitivity onto the photoprotein. Figure taken from (163).

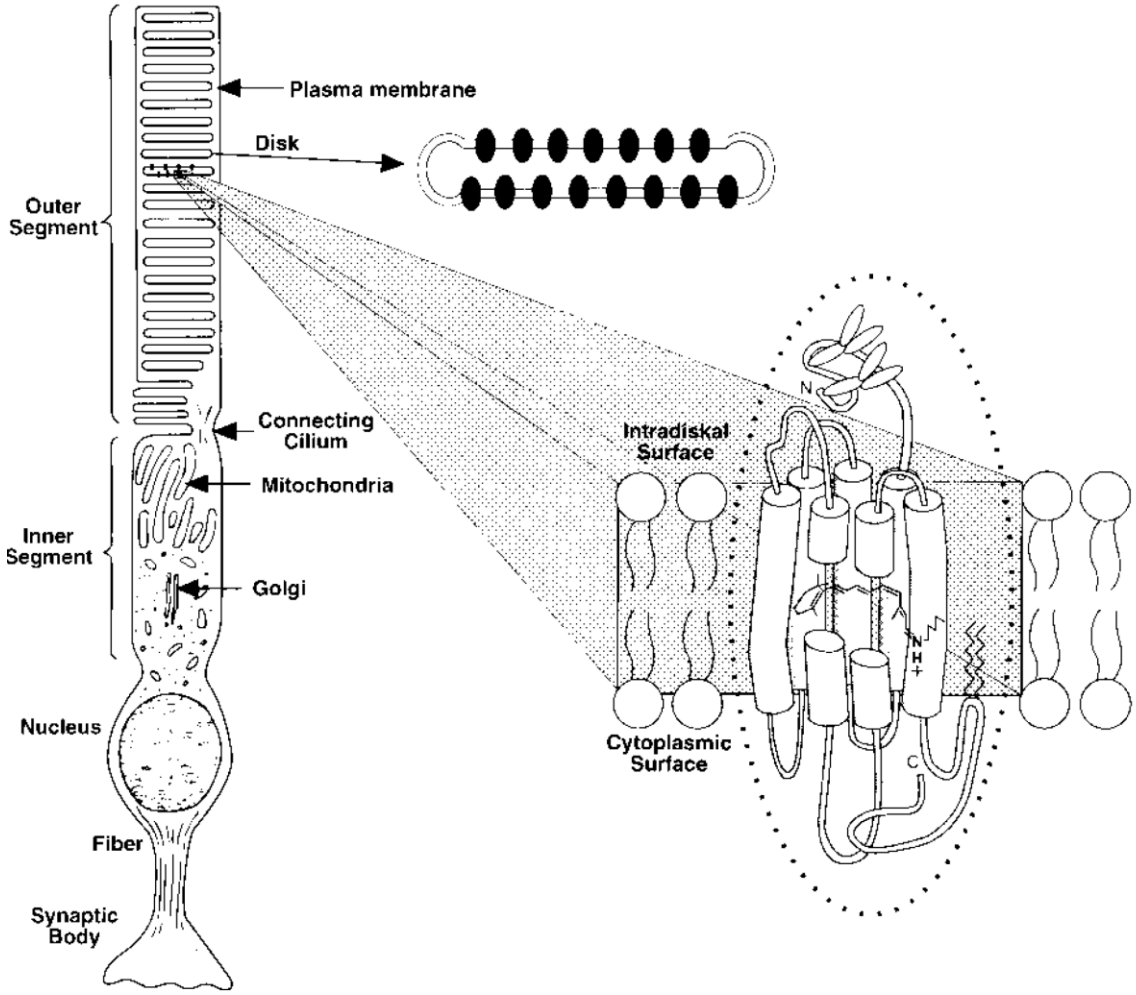
Plasma membrane
Disk
Outer Segment
Connecting Cilium
Mitochondria
Inner Segment
Golgi
Nucleus
Fiber
Synaptic Body
Intradiskal Surface
Cytoplasmic Surface
N
N
H+
C

Figure 1.4: Structure of the photoprotein rhodopsin

The rhodopsin structure is the characteristic class A, or rhodopsin-like, GPCR. A membrane-level view is displayed on the left, which depicts clearly the compact extracellular domain which acts as a closed cap over the retinal (red) in the binding pocket. The three retinal isomers mentioned in this introduction, all-trans, 11-cis, and 9-cis structures are shown above. The seven transmembrane helices are also displayed along with the amphipathic helix 8 leading to the C-terminus on the intracellular side. Depicted on the right are overlay structures of the active (yellow) and inactive (red) conformations as seen from the intracellular face. The largest difference between the structures is the translocation of TM6 away from the helical bundle, exposing a binding cleft for Gt, visual arrestin, and rhodopsin kinase (162). Figure taken from (164).

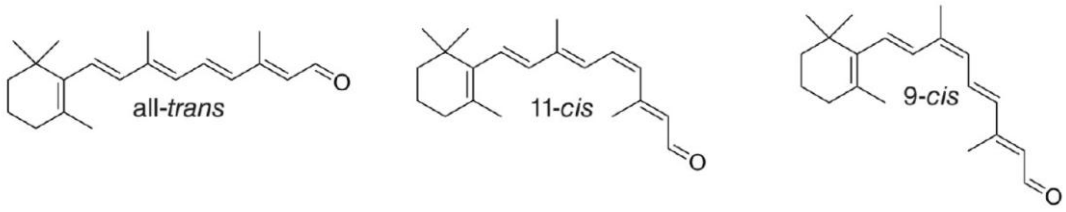
all-trans
11-cis
9-cis
O
O
O

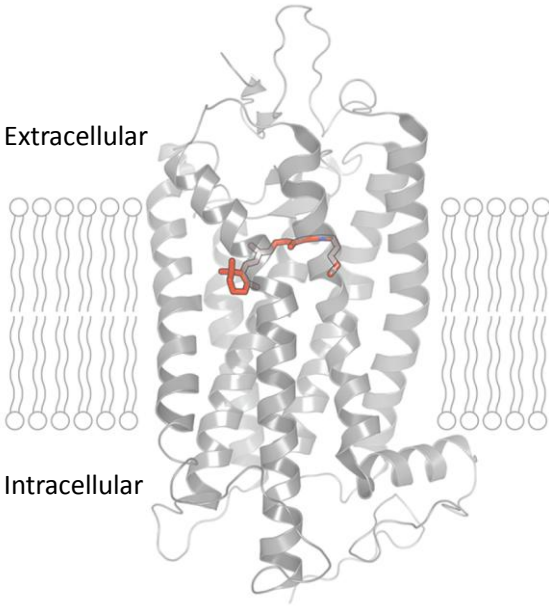
Extracellular
Intracellular

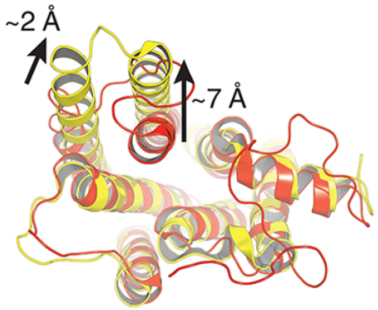
~2 Å
~7 Å

Figure 1.5: Rhodopsin mediated phototransduction

Photoactivation of the 11CR-bound rhodopsin isomerizes the chromophore to the agonist ATR. The conversion event stabilizes the active receptor conformation (MII), which couples to and activates the G protein complex transducin (Gt). The active Gt activates phosodiesterases (PDEs), whose activity reduces the amount of cGMP in the cell. Reduction of the cGMP levels leads to closure of cyclic nucleotide gated cation channels (CNG), blocking the passive diffusion of Ca^{2+} into the cell and hyperpolarizing the rod cell. This hyperpolarization leads to neuronal signaling that indicates to the brain that a photon has been detected. The drop in Ca^{2+} induces a feedback signal through guanylyl cyclase activating proteins (GCAP), which activate guanylate cyclases (GC) and raise cGMP levels to counter signaling. G protein signaling is attenuated at the receptor level first by phosphorylation by rhodopsin kinase and then binding of arrestin to block further Gt interactions. The protein recoverin is a Ca^{2+} mediated inhibitor of GRK activity at high or dark Ca^{2+} levels. Final deactivation occurs when the ATR dissociates from the receptor (not shown). Figure taken from (165) and reviewed in (51-53).

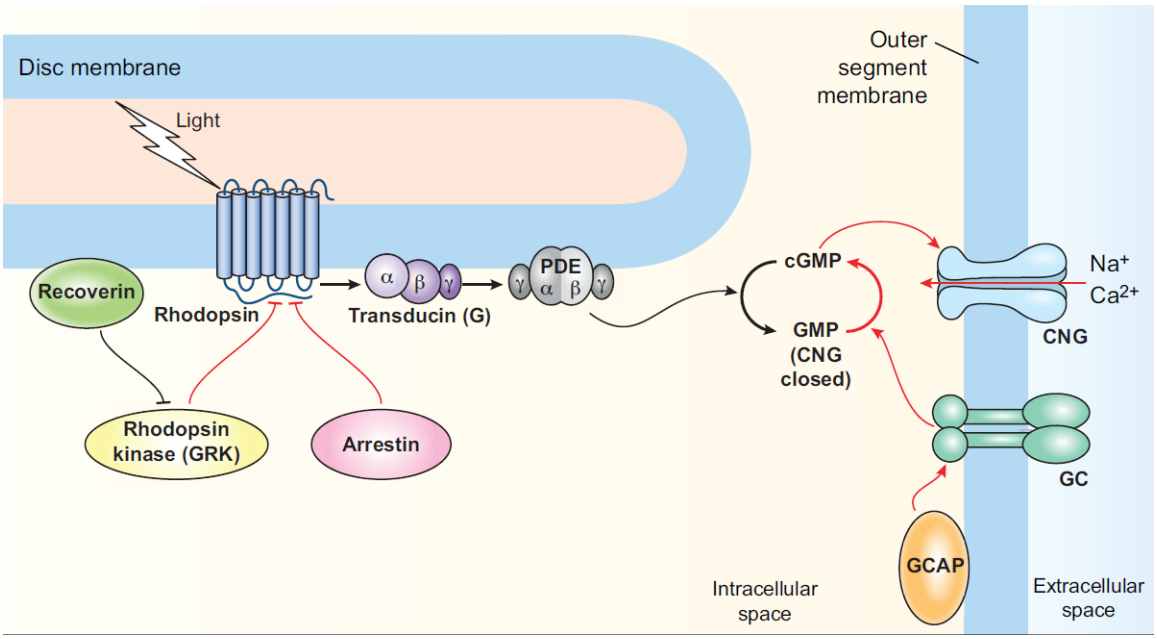
Disc membrane
Light
Outer segment membrane
Recoverin
Rhodopsin
Transducin (G)
PDE
cGMP
GMP (CNG closed)
Na+
Ca2+
CNG
Rhodopsin kinase (GRK)
Arrestin
GC
GCAP
Intracellular space
Extracellular space

Figure 1.6: Recycling of photoisomerized ATR back to 11CR

After ATR release, the spent retinal is recycled back to 11CR through a series of enzymatic steps depicted as cartoons in the top panel. Once free of the protein, ATR is reduced by retinal dehydrogenase (RDH) to form all-trans retinol (ATR-ol), which protects the reactive aldehyde moiety from reacting within the membrane and forming insoluble, phototoxic condensation products. The ATR-ol is then transported across the inter-photoreceptor matrix (IPM) by inter-photoreceptor retinol binding protein (IRBP) to the retinal pigment epithelium (RPE). There the ATR-ol is chaperoned by cellular retinol binding protein (CRBP) to lecithin retinol acyl transferase, which converts the alcohol into a retinyl ester storage form to be converted later. Isomerization and deesterification is a one step process conducted by RPE65 that results in 11CR-ol. 11CR-ol is then oxidized by RDH5 and transported back to the RPE plasma membrane by cellular retinal binding protein (CRALBP), where the molecule is once again ferried across the IPM by IRBP. The fresh 11CR is then released in the rod cell where it can regenerate an opsin.

Retinal cycle diseases (red boxes) and therapeutics (blue boxes) are depicted in the lower panel. This simplified cartoon highlights the sensitivity of the cycle, as deficiencies in individual members lead to larger consequences. For example, *retinitis pigmentosa* (RP), a degradation of the photoreceptor cells resulting in night blindness, is caused by variants in rhodopsin and IRBP, whereas leber congenital amaurosis (LCA), a juvenile form of blindness, is caused by deficient RDH12, LRAT, and RPE65. The disease states are generally speaking the result of an inability to provide new 11CR molecules or, as in ABCA4 mutants for example, accumulation of toxic retinal aldehydes.

The therapeutics shown here (blue boxes) generally target the cycle by replacing 11CR-deficiencies with the more stable 9-cis retinoids or inhibiting the over production of toxic products. For example, retinylamine inhibits RPE65 function, so in cases of accumulation of retinal, particularly ATR, this molecule can slow the cycle. The only nonretinoid displayed here are the primary amines ($R\text{-}NH_2$) which are used to target the released ATR in cases where the clearance is impaired. The $R\text{-}NH_2$ can react with the aldehyde and temporarily protect it from further condensation reactions. Figures taken from and reviewed in (164,166).

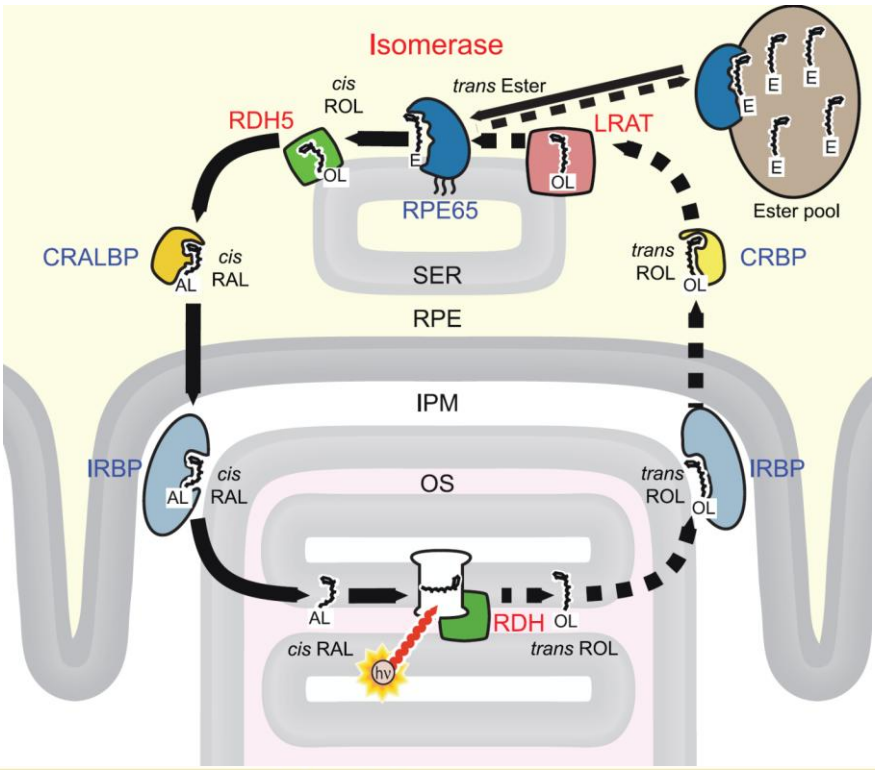
Isomerase
cis ROL
trans Ester
RDH5
LRAT
E
OL
RPE65
Ester pool
CRALBP
cis RAL
AL
SER
trans ROL
CRBP
RPE
IPM
IRBP
OS
RDH
hv

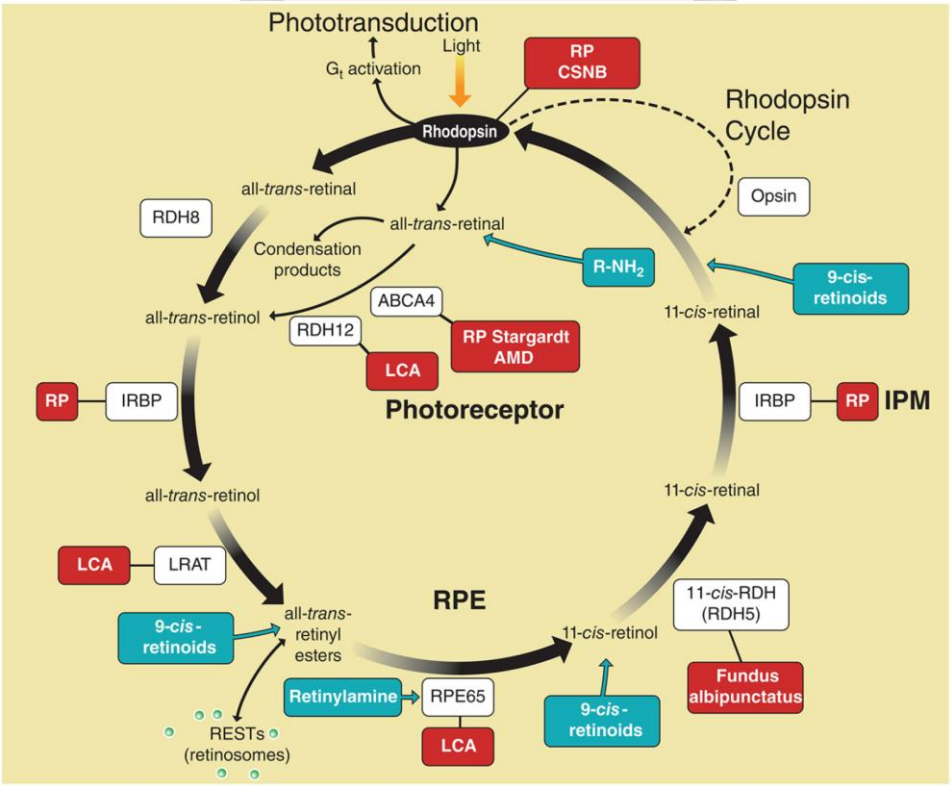
Phototransduction
Light
G_t activation
RP CSNB
Rhodopsin
Rhodopsin Cycle
all-trans-retinal
RDH8
Opsin
Condensation products
R-NH_2
9-cis-retinoids
11-cis-retinal
ABCA4
RDH12
RP Stargardt AMD
LCA
Photoreceptor
RP
IRBP
IPM
all-trans-retinol
LRAT
RPE
all-trans-retinyl esters
11-cis-RDH (RDH5)
Retinylamine
RPE65
Fundus albipunctatus
RESTs (retinosomes)

Figure 1.7: Retinal channeling through rhodopsin

The inactive, 11CR-bound crystal structures of rhodopsin provide no clear avenue for retinal entry or escape (3). Several years later, analysis of a subsequent active-like structure resulted in the proposal that a channel passes through the binding pocket, formed due to rotameric shifts exposing opening between TM1 and TM7 (Hole A) and TM5 and TM6 (Hole B) (6,151). Comparison of the inactive and active binding pockets can be found above. Retinal trafficking (lower) through the protein is illustrated here, where the retinals traverse unidirectionally, entering at Hole A and exiting through Hole B. Figure taken from (148,158).

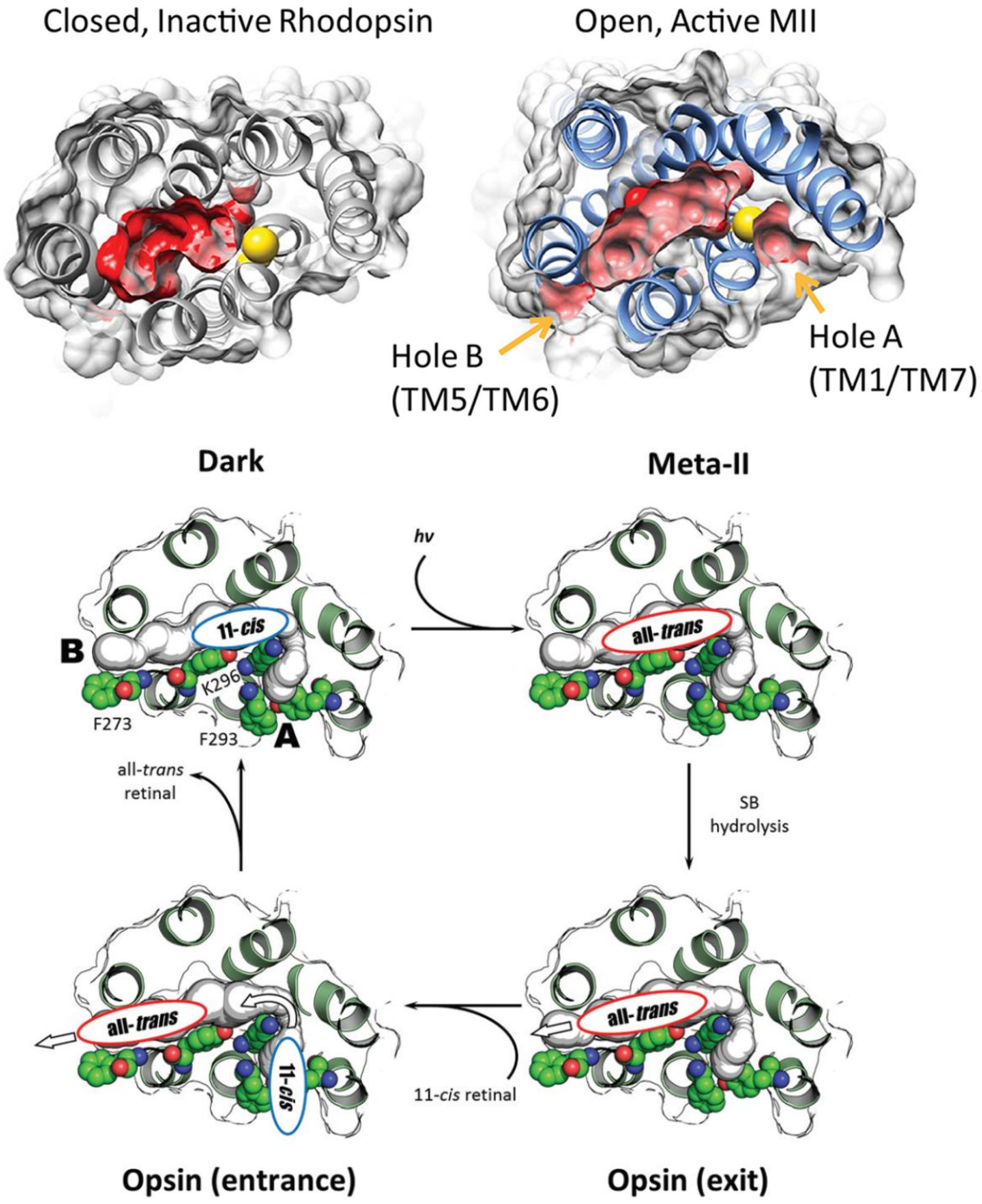
Closed, Inactive Rhodopsin
Open, Active MII
Hole B
(TM5/TM6)
Hole A
(TM1/TM7)
Dark
Meta-II
hv
11-cis
B
K296
F273
F293
A
all-trans
all-trans
retinal
SB
hydrolysis
all-trans
11-cis
11-cis retinal
Opsin (entrance)
Opsin (exit)

Figure 1.8: The transient activation model for retinal binding to rhodopsin

In order to reconcile the structural observations that only the active conformation has the proposed ligand channel and the predominantly inactive apoprotein opsin (36,55), it was proposed by Heck and colleagues that the inactive opsin must transition to an active conformation in order for retinal to enter or exit the protein (152). This binding model, which we have termed the transient activation model, explicitly proposes that the protein must enter an active state for 11CR to bind into the pocket. After this noncovalent binding form is established, the formation of the Schiff base was proposed to trigger lock the protein complex into the inactive conformation. Likewise, after photoactivation, the ATR resulting from isomerization of 11CR exits the protein through the same active conformation. Figure taken from (152).

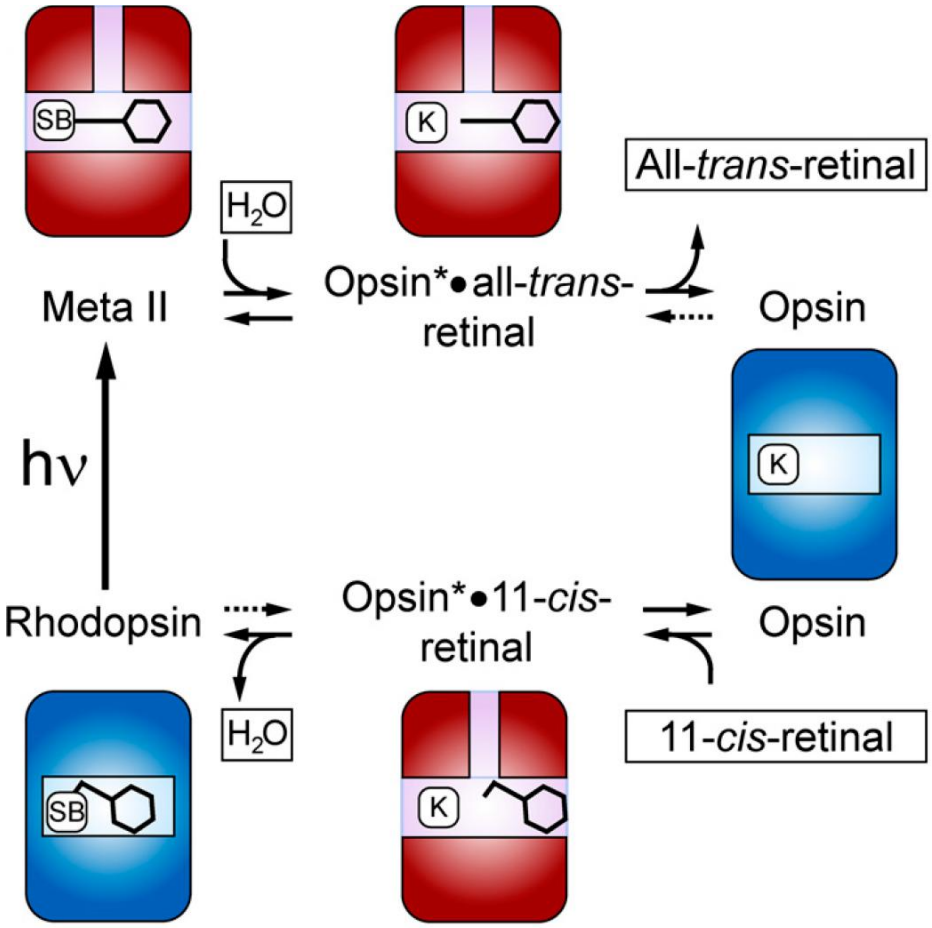
SB
K
All-*trans*-retinal
H_2O
Meta II
Opsin*•all-*trans*-retinal
Opsin
K
hν
Rhodopsin
Opsin*•11-*cis*-retinal
Opsin
SB
H_2O
K
11-*cis*-retinal

Chapter 2: Conformational selection and equilibrium governs the ability of retinals to bind to opsin

Schafer C.T. & Farrens D.L.

2.1: Summary

This chapter addresses the question of how retinal enters and exits the visual G protein-coupled receptor (GPCR) rhodopsin. One clue may lie in two openings between TM1/TM7 and TM5/TM6 in the active receptor structure. Recently, retinal has been proposed to enter the inactive apoprotein (Ops) through these holes when the receptor transiently adopts the active (Ops*) conformation. Here, we directly test this "transient activation" hypothesis (TAH) using a fluorescence-based approach to measure rates of retinal binding to samples containing differing relative fractions of Ops and Ops*. In contrast to what the TAH model would predict, we find binding for the inverse agonist, 11-cis retinal (11CR), slows when the sample contains more Ops* (produced using M257Y, a constitutively activating mutation). Interestingly, the increased presence of Ops* allows for binding of the agonist, all-*trans* retinal (ATR), whereas WT opsin shows none. Shifting the conformational equilibrium towards even more Ops*, using a G protein peptide mimic (either free in solution or fused to the receptor), accelerates the rate of ATR binding and slows 11CR binding. An arrestin peptide mimic shows little effect on 11CR binding, yet stabilizes opsin-ATR complexes. The TM5/TM6 hole is apparently

not involved in this conformational selection. Increasing its size by mutagenesis does not enable ATR binding, but instead, slows 11CR binding, suggesting it may play a role in trapping 11CR. In summary, our results indicate conformational selection dictates stable retinal binding, which we propose involves ATR and 11CR binding to different states, the latter a previously unidentified, open-but-inactive conformation.

All experiments and analysis presented in this chapter was carried out by the author of this dissertation and was published in Schafer, C.T. and Farrens, D.L. (2015) *J. Biol. Chem.* 290(7):4304-4318.

2.2: Introduction

The receptor responsible for dim-light vision, rhodopsin, is unique among G protein-coupled receptors (GPCRs) as its ligand, 11-cis retinal (11CR), is covalently attached to the protein through a Schiff base with the lysine at 296 (35). Protonation of this linkage shifts the absorbance of the ligand from the ultraviolet (380nm) to the visible spectrum (500nm). The 11CR acts as an inverse agonist that quenches basal signaling by trapping the receptor in an inactive conformation. Light absorption causes isomerization of the 11CR to all-*trans* retinal (ATR) (See Fig. 2.1 for ligand structures), which acts as an agonist and induces a series of conformational changes that ultimately push the receptor to the active, G protein-coupling conformation called metarhodopsin II (MII) (5). The MII conformation exposes a cleft on the cytoplasmic face for interactions with ancillary proteins (G protein and arrestins) and is accompanied by deprotonation of the Schiff base and thus a shift in peak retinal absorbance back to 380nm (10,29). Binding of arrestin blocks G protein signaling and subsequent Schiff base hydrolysis results in the

decay of the active species and release of ATR. The now empty receptor, called opsin (ops), has almost no basal G protein coupling ability (36,37,127,167) and appears to have a conformation like that of the inactive 11CR-bound structure (55,168). Rebinding of a fresh 11CR quenches the limited signaling and resets the cycle (169).

Despite rhodopsin being one of the most extensively studied members of the GPCR superfamily, it remains unclear how the very hydrophobic retinal enters or exits the protein. Numerous crystal structures, along with spectroscopic and biochemical data, show rhodopsin exists primarily in two stable conformations, either a closed, inactive conformation (11CR-bound or Ops) or an open, active form (MII or Ops*) (note that other intermediates are transiently formed as the receptor converts between these two states) (3,6,47,55,122,167,168). Although the closed rhodopsin structure shows no means for the retinal to enter or exit the binding pocket, more recent structures of the open, active receptor conformation have identified a possible ligand channel through the protein formed by rotameric shifts of bulky residues between transmembrane helix 1 (TM1) and TM7 (called Hole A) and between TM5 and TM6 (called Hole B) (3,6,7,151,157,159,169,170) (Fig. 2.1A). This structural reorientation exposes the binding pocket to the lipid bilayer and has been speculated to play a role in ligand uptake and/or release (151,152,157,171). The only structure of retinal-free rhodopsin, opsin, currently available most likely does not reflect the "true," inactive opsin state in solution, as it has numerous elements of the open active conformation, including the holes, and a RMSD from MII rhodopsin of only ~0.4Å (6,47,172). Biochemical and spectroscopic studies indicate that opsin, in solution, is more structurally similar to the closed, inactive 11CR-bound rhodopsin (55,167,168).

This conundrum—that 11CR is bound in the binding pocket of the closed, inactive receptor, yet there is no clear way for it to get there—has led to the proposal that the empty state opsin must enter a transient open and active conformation (Ops*) in order for the 11CR to gain access to the binding pocket (152) (Fig. 2.1C). Evidence supporting this "transient activation" hypothesis include whole-cell electrophysiology experiments that show a brief increase in downstream activity during dark adaptation of bleached rod cells (161).

However, direct mutagenesis of the proposed ligand path, shown in Fig. 2.1A, did not yield clear results as to a role for the open-state holes during binding (152). Moreover, in contrast to the hypothesis that 11CR binds the Ops* state, attempts to shift the opsin to more MII-like conformations, either through the lowering the pH or addition of a G protein C-terminal peptide analog (G_t C-term peptide), also failed to accelerate 11CR binding (152,173). Therefore, this "transient activation" model for 11CR binding, although attractive, has remained unsupported by conclusive experimental data.

Here we have directly addressed the question of what governs retinal's ability to bind opsin using a new approach. Traditionally, retinal uptake by rhodopsin has been measured by monitoring formation of the Schiff base between the retinal and the protein after it enters the binding pocket. This is accomplished by measuring the increase in the characteristic absorbance at 500nm. However, this approach requires monitoring the formation of the protonated Schiff base (detection of the 380nm to 500nm shift) and so retinal binding that does not result in a protonated Schiff base goes unnoticed (as both free retinal in detergent and MII absorb maximally near 380nm and thus cannot be easily distinguished by comparing absorbance spectra).

To circumvent this problem, we have established a fluorescent assay to measure the rate of binding of retinal that is independent of protonated Schiff base formation. Essentially, this assay involves running a retinal release assay backwards (54). Our approach tracks the quenching of intrinsic tryptophan fluorescence as the ligand binds in the pocket. A similar general approach has been used in several other works (152,155,156,171,174-176). Here, we established and calibrated our approach to ensure accurate, reproducible measurements so that retinal binding rates, measured by fluorescence, could be directly compared between different conditions. Additionally, we start with naïve opsin in our study, rather than the common approach of using decayed MII formed after photobleaching rhodopsin, as this allows us to measure rates without contamination of other free retinal.

We then used this assay to directly test the transient activation hypothesis for retinal binding. Our strategy was to increase the amount of active Ops* present in a sample, and then use our assay to determine if the rates of retinal binding are faster, as the above hypothesis would predict. Employing the constitutively activating mutation M257Y (M257Y-CAM) (177), we shifted the conformational equilibrium from nearly fully inactive WT opsin to a mixture of inactive (Ops) and active (Ops*) species, and compared the rates of ligand binding between these samples. Unexpectedly, rather than accelerating the rate of 11CR uptake, we found the M257Y-CAM actually slowed 11CR binding, compared to WT opsin. Moreover, stabilizing the Ops* population of M257Y-CAM by conformational trapping with a peptide mimic of G protein C-terminus (G_t C-term peptide) further slowed 11CR binding (178,179). However, we did find partial support for the transient activation hypothesis in experiments using ATR. Although ATR

cannot bind to inactive WT Ops, we find ATR binding is dramatically increased as the Ops* state is stabilized. The novel approach of fusing the G_t C-term peptide to the opsin C-terminus further amplifies these effects.

Together, these observations indicate the transient activation hypothesis must be modified to include a role for conformational selection. In support of this postulate, we demonstrate that stabilizing a minute, fleeting Ops* population present in the WT opsin population with the G_t C-term peptide enables WT opsin to stably bind ATR. Similarly, we found a peptide corresponding to a flexible "finger" loop of arrestin (Arr peptide, residues 67-79) (26) also enhanced ATR binding, yet had little effect on the binding of 11CR. Finally, we tested if Hole B (TM5/TM6), observed in the active Ops* and MII structures (6,47), might play a role in the shift of retinal binding rates. To do this, we expanded the opening with alanine substitutions and measured the effect on 11CR and ATR binding rates. These results showed removing the TM5/TM6 "doors" did not enable ATR uptake, and unexpectedly, slowed 11CR binding.

In summary, we found no evidence to support the hypothesis that transient activation of opsin is required for 11CR binding. In fact, we observed increasing Ops* actually impairs 11CR binding. However, we do find increasing the amount of Ops* enhances ATR binding, providing partial support of the transient activation hypothesis. We also discuss how, together, these data clearly show, in our purified system, classical conformation selection between retinal isomers plays a key role for stable retinal binding, and how this concept can be used to propose a conformational selection based model for retinal binding.

2.3: Experimental Procedures

2.3.1: Buffers

11-cis retinal was generously provided by Dr. R. Crouch (Medical University of South Carolina and the NEI, National Institutes of Health). G_t C-term peptide (VLEDLKSVGLF) (178), Arr peptide (YGQEDIDVMGLSF), and 1D4 peptide (TETSQVAPA) were purchased from GenScript. All other chemicals were purchased from either Sigma Aldrich or Fischer. Buffers used in this report are as follows: PBSSC [137mM NaCl, 2.7mM KCl, 1.5mM KH_2PO_4, 8.0mM Na_2HPO_4, pH 7.2], Buffer B [PBSSC, 1% DDM], Buffer C [PBSSC, 1M NaCl, 2mM $MgCl_2$, 1% DDM], Buffer D [PBSSC, 0.05% DDM], Buffer E [5mM MES, 0.05% DDM, pH 6.0], Elution Buffer [Buffer E, 40mM NaCl].

2.3.2: Mutant Generation

Mutagenesis was performed by overlap extension PCR to generate single site mutants in a synthetic rhodopsin gene (180) and subcloned into a modified version of the original PMT4 expression vector (181). All constructs were confirmed by sequencing. Additionally, each contained the engineered, stabilizing disulfide (N2C, D282C) (182) and minimal reactive cysteines (C140S, C316S, C322S, and C323S) (5,183). This construct, without any additional mutations, has been well characterized and is termed WT_θ throughout this publication (5,181,183). The θ subscript is used to differentiate between the minimal cysteine construct and wild-type (WT) with only the stabilizing disulfide. The minimal cysteine construct was used for direct comparison with previous conformational data determined using site-directed labeling (168). These results were

then confirmed with WT containing all native cysteines. The construct referred to as opsin-G_t C-term peptide fusion had the G_t C-term peptide sequence (described above) fused to the C-terminal tail of the receptor. Four additional glycines were included after the G_t C-term peptide sequence and an additional 1D4 tag for purification finished the sequence. The entire additional sequence is as follows: EEVLEDLKSVGLFGGGGTETSQVAPA. The gene containing this sequence was purchased from GeneScript.

2.3.3: Protein Expression and Purification

Expression and purification of opsin were adapted from previously described methods (168,181). Briefly, COS-1 cells were transiently transfected using PEI and 30μg of DNA per 15cm plate. After 50-65 hours, the plates were washed with 10ml PBSSC and scraped free of the surface. The cells were then pelleted and resuspended in 0.5ml PBSSC/plate with 0.5mM PMSF. Harvested cells were snap frozen in liquid nitrogen and stored at -80°C until use. The thawed cell mass was solubilized in 1% DDM for 1 hour. The solubilized slurry was spun at 100,000xg for 45min. The supernatant from this spin was incubated with 1D4 antibody beads in buffer C for 3 hours. Beads were then transferred to columns with buffer D and washed with at least 100 column volumes in D followed by washing with Buffer E. Elutions were in elution buffer with 200μM 1D4-specific peptide (TETSQVAPA) (168).

2.3.4: Absorbance Spectroscopy

Proper regeneration of the receptors, purity, and rates of Schiff base formation were measured by absorbance spectroscopy using a Shimadzu 1601 spectrophotometer.

Temperature was controlled by a VWR water bath. For experiments well below room temperature, the sample chamber was filled with dry air to prevent condensation on the cuvette viewing window. Testing of newly purified opsin was done with 5x molar excess of 11CR to opsin (2.5μM 11CR added to 0.5μM Opsin—concentration determined by ε_{280}=56500) at 20°C to determine maximal regeneration for the sample by observing increases to the absorbance at 500nm. All samples were capable of greater than 75% regeneration, as indicated by the final absorbance at 500nm. The rate determining experiments using absorbance spectroscopy were conducted using 1μM opsin and 1μM 11CR in 0.1% DM at 10°C. Spectra were measured from 700-350nm in 0.5nm intervals on "fast" setting, giving 35s per spectra. Time between spectra varied between 60 to 300 seconds, depending on the expected length of the experiment. Increase in absorbance at 500nm was fit by a monoexponential rise to maximum using SigmaPlot and the following equation:

$$A(t) = A * (1 - e^{-kt}) + C$$

Acid protonation was achieved by addition of 4μl of 0.4M H_2SO_4 to 77μl of the above binding reactions. Pre and post acid addition spectra were dilution adjusted by matching 280nm absorbance.

2.3.5: Fluorescence Spectroscopy

Protein fluorescence was monitored by steady-state fluorescence using a modified PTI Quantamaster instrument described below. The standard arc lamp excitation source was replaced with a 295nm LED (LLS-295 Ocean Optics). Temperatures were controlled with a VWR water bath and constantly monitored using an Omega Thermister to within 0.5°C of the desired temperature. Retinal binding was observed by quenching of intrinsic

tryptophan fluorescence measured as a decrease in emission at 330nm, essentially the inverse of the retinal release assay (54,152,171,174,175). To minimize rhodopsin bleaching, excitation was tempered by a neutral density (ND 1.7) filter and emission bandwidth was expanded to 20nm. Sample scattering contamination was mitigated using a 310nm long-pass filter before the emission monochromator, and samples were probed for only 1 second every 21 seconds. LED flashing was directed by a 5V TTL pulse from the PTI shutter control.

Unless otherwise stated, all binding studies monitored by fluorescence used the following conditions: 0.5μM opsin, 0.5μM retinal, DDM concentration of 0.1% at a temperature of 10°C. These conditions were found to be optimal for accurate, reproducible binding rate measurements without appreciable nonspecific fluorescence quenching (Fig. 2B). Resulting decay curves described a pseudo-first order binding reaction and were fit by a monoexponential decay using SigmaPlot and the following function:

$$F(t) = A * e^{-kt} + C$$

To enable direct visual comparison of binding rates between conditions, all fluorescence time-courses were normalized by the $(F-F_{final\text{-}11CR})/F_0$, where $F_{final\text{-}11CR}$ was determined from separate 11CR binding measurements. 11CR binds stably under all conditions for these mutants, and thus this normalization approach ensures incomplete ATR binding can be detected, which would be missed if the ATR results were normalized to $F_{final\text{-}ATR}$. Full ATR and 11CR binding produce the same levels of minimal fluorescence (maximum fluorescence quenching) achievable, as indicated by the fact that

the $F_{final\text{-}11CR}$ values match the values obtained for the ATR samples pushed to completion by the addition of G_t C-term peptide fused to the opsin C-terminus.

2.4: Results

2.4.1: Use of Fluorescence to Measure Retinal Uptake

To enable accurate and rapid measurements of rates, and to remove the limitation of requiring protonated Schiff base formation to monitor binding by absorbance spectroscopy, we developed and calibrated a fluorescence assay to measure retinal binding rates to opsin. Essentially, this process entails running a retinal release experiment in reverse (54), where, instead of observing the relief of quenching of intrinsic tryptophan fluorescence by retinal exit, one now monitors the decrease of tryptophan fluorescence emission caused by the tryptophan residues undergoing FRET to the newly bound retinal (152,155,156,171,174-176). In contrast to traditional absorbance-based assays, this approach allows for the detection of any chromophore in the binding pocket and not just those retinals that have formed a protonated Schiff base, thus enabling the study of both 11CR and ATR binding (the latter of which is "spectroscopically silent" in traditional absorbance binding assays). Moreover, the sensitivity of this approach is also at least 10x greater over that of the traditional absorbance assay.

Before embarking on experiments using this assay, we established optimal conditions to enable reproducible binding measurements and removal of non-specific binding signals. We found that bringing the ratio of opsin to ligand to equimolar amounts (1 retinal : 1 opsin) and increasing the detergent concentration to 0.1% (w/v) brought the binding rates into a measurable window that yielded reproducible results, and were at

least an order of magnitude below detergent concentrations that can inhibit 11CR binding (150). These reaction conditions also avoided potential errors due to minor deviations of the specified component concentrations (See Table 2.1 for calibration results). Once we had established these optimal conditions, we began measuring rates of 11CR binding to WT_{θ} opsin (Fig. 2.2B). These initial studies showed that, whereas 11CR rapidly enters the pocket and causes a decrease in the tryptophan fluorescence, incubation with the agonist, ATR, does not elicit any change in the tryptophan emission, indicating no binding of ATR to the WT_{θ} opsin, consistent with previous reports (184). Importantly, we observed a complete lack of nonspecific quenching of the opsin's tryptophan residues for the ATR sample in Fig. 2.2B, indicating the fluorescence drop for 11CR is not simply due to retinal occupying the same detergent micelle and nonspecifically quenching the opsin fluorescence, but rather, reflects actual retinal occupancy of the receptor binding pocket. Therefore, we conclude that the quenching results in the present work accurately monitor retinal binding into the receptor.

We next compared the rates of retinal binding measured by traditional absorbance (Fig. 2.2A) and the new fluorescence approach (Fig. 2.2B) under identical conditions and over a range of temperatures, and carried out Arrhenius analysis to determine the activation energies (E_a) for each method. As shown in Fig. 2.2C, the E_a for binding were the same, within experimental error, for the two assays (12.75±2.1 and 13.0±0.31 kcal/mol for absorbance and fluorescence respectively). This result implies that the two techniques produce essentially equivalent results, and that both report a shared rate limiting step, presumably the rate of Schiff base formation, similar to what is seen for release (54,137).

2.4.2: The M257Y-CAM$_\theta$ Opsin Exhibits the Ability to Bind Both Inverse Agonist (11CR) and Agonist (ATR)

We used the above fluorescence assay to test the hypothesis that an active, Ops* receptor is necessary for 11CR binding. We employed M257Y-CAM$_\theta$ to decrease the conformation transition barrier and convert some of the Ops to Ops*, to determine if the rate of 11CR correspondingly increased as predicted by the transient activation model (152). The M257Y mutation is well documented and has been shown to shift the opsin population's conformational equilibrium from almost completely inactive to one that can more easily transition between the two isomeric states (154,168,177) (Fig. 2.3A). Interestingly, instead of allowing faster binding of 11CR (as the transient activation hypothesis in Fig. 2.1 would predict), we see the rate of 11CR binding to M257Y-CAM$_\theta$ is ~3x slower than it is to the inactive WT$_\theta$ opsin, $k_{WT\theta}$(11CR)=2.55e-3±7.0e-5 s^{-1} vs. $k_{M257Y\text{-}CAM\theta}$(11CR)=1.08e-3±3.7e-5 s^{-1} (Fig. 2.3B&D). See Supplementary Data Table for complete rate results.

An interesting result was observed when we checked the ability of both samples to bind the agonist ATR. WT$_\theta$ showed no ATR binding (Fig. 2.3C). However, M257Y-CAM$_\theta$ showed robust ATR binding (Fig. 2.3E), in corroboration with previous reports (154,177). Using the fluorescence assay, we could directly measure a rate for ATR binding to M257Y-CAM$_\theta$ ($k_{M257Y\text{-}CAM\theta}$(ATR)=1.14e-3±1.6e-5 s^{-1}, Fig. 3E). The rate is approximately equal to that observed for 11CR binding to M257Y-CAM$_\theta$, and likely is a result of significant Ops* presence due to the lower activation energy for transition between the Ops and Ops* conformations (168). Taken together, these results do not support the idea that transient activation of the receptor to Ops* is required for 11CR to

bind, but rather suggest that the inverse agonist prefers ops. However, they do suggest Ops* plays a role in stable ATR binding to the receptor. Together these results suggest that the uptake of retinals by opsin is determined by the conformational state of the protein.

2.4.3: Shifting the Ops ⇌Ops Equilibrium by a Peptide Mimetic of the G Protein C-Terminus Further Shifts Opsin Affinity From 11CR to ATR*

The binding results from the M257Y-CAM$_\theta$ opsin, described above, inspired us to further test the role of conformational selection of the receptor for inverse agonist and agonist. To do this, we next measured the effect of increased Ops* population on retinal binding by including a peptide analog of the C-terminal end of the G protein transducin (G_t C-term peptide) on ATR and 11CR binding (178,179). Binding of this peptide stabilizes the M257Y-CAM$_\theta$ opsin in the active conformation, Ops* (7,154,168,185) (Fig. 2.4A). Indeed, as would be expected if a conformational selection model were correct, adding G_t C-term peptide to the M257Y-CAM$_\theta$ sample resulted in very rapid agonist ATR binding, and even slower binding of 11CR compared to M257Y-CAM$_\theta$ alone ($k_{\text{M257Y-CAM}\theta\text{+Gt C-term peptide}}$(11CR)=0.363e-3±1.7e-5 s^{-1} and $k_{\text{M257Y-CAM}\theta\text{+Gt C-term peptide}}$(ATR)=6.67e-3±4.3e-4 s^{-1}, Fig. 4B&C).

We sought to further increase the amount of Ops* trapped by increasing the apparent concentration of the G_t C-term peptide. This was accomplished by fusing it to the C-terminal tail of the opsin, inspired by a similar approach used by Kobilka and colleagues to study agonist binding to β_2 adrenergic receptor (11). Surprisingly, M257Y-CAM$_\theta$-G_t C-term peptide fusion did not further exacerbate the ligand affinity shift, suggesting that the free peptide was already at saturating conditions. Interestingly, the

amount of binding of ATR to the M257Y-CAM$_\theta$ does not appear to go to 100% completion, but rather, is about 25% less than 11CR to the same protein (Fig 2.4C). This likely reflects a dynamic equilibrium between bound and unbound states resulting from the mixed conformational population.

Stabilizing the Ops* conformation through incubation with G_t C-term peptide, either free in solution or as a fusion, caused the maximal binding of ATR to reach 11CR levels (Fig. 2.4C). These results are reflected in the acid protonation spectra in Fig. 4D. M257Y-CAM$_\theta$ alone does not show complete shift to 440nm with the addition of acid, the characteristic absorbance of a protonated Schiff base. This indicates that free ATR is still present and there is an incomplete occupation of the binding pocket. Free G_t C-term peptide stabilizes the bound complex and the 440nm shift is more complete. G_t C-term peptide incubated with ATR in the absence of opsin shows no absorbance shift with acid (data not shown). Together with the change in rates, these results suggest the conformational state of opsin dictates the affinity for different retinal isomers.

2.4.4: G Protein C-terminal Peptide is Sufficient to Stabilize ATR-Bound WT$_\theta$ Opsin

We also found that the G_t C-term peptide alone enabled WT$_\theta$ opsin to bind ATR (Fig. 2.4F). It has been extensively noted that ATR can interact with opsin inducing guanine nucleotide exchange in G proteins and phosphorylation by rhodopsin kinase (36,129,184,186-190). Only recently has it been shown that interactions with the G protein actually induce proper ATR binding into the binding pocket (176). Here we show that the C-terminus alone is sufficient to form a stable complex with ATR in the retinal binding pocket of WT$_\theta$ opsin, as evidenced by fluorescence data (Fig. 2.4F) and acid

protonation absorbance spectra (Fig. 2.4G). In agreement with previous reports, we found that WT_θ opsin does not show any observable ATR uptake (Fig. 2.4C) (184), and we previously have not seen accumulation of stable interactions of WT_θ opsin with G_t C-term peptide (168). However, combining all three components (opsin, ATR, and G_t C-term peptide) enabled robust ATR binding to inactive WT_θ opsin. Similar to what was observed with the M257Y-CAM_θ alone, the WT_θ opsin+ATR+G_t C-term peptide complex is relatively unstable compared to 11CR, resulting in an incomplete drop in fluorescence (~80% that of 11CR). The free G_t C-term peptide had no effect on the rate of 11CR binding to WT_θ opsin (Fig. 2.4E).

In comparison to M257Y-CAM_θ, which was already saturated by the free peptide, the WT_θ-G_t C-term fusion showed greatly enhanced ATR binding, and the opsin-peptide interaction was strong enough to slow 11CR binding (Fig. 2.4E&F). This construct also completely stabilized the ATR-bound complex, resulting in a fluorescence drop comparable to that induced by 11CR. Acid protonation spectra confirmed Schiff base formation between the ATR and the receptor in the presence of G_t C-term peptide (Fig. 2.4G). Additionally, since WT opsin without G_t C-term peptide shows no presence of a Schiff base upon addition of acid, these data further support our conclusion that the ATR does not form a non-specific Schiff base with a peripheral lysine under our experimental conditions.

2.4.5: Arrestin "Finger Loop" Peptide also Enhances ATR Binding

We also tested if a peptide corresponding to the "finger loop" of bovine arrestin (residues 67-79, Arr Peptide) also affected 11CR or ATR binding to opsin. Similar to the G protein, arrestin has been shown to inhibit ATR release from the photo-activated

receptor (29,191,192). As depicted in Fig. 2.4A, the Arr peptide binds in same cleft in MII as the G_t C-term peptide, shown here as peptide fragments bound in opsin crystal structures (7,27,29,192-194). Interestingly, we found that the Arr peptide increased the rate and amount of ATR binding to M257Y-CAM_θ (Fig. 2.4L) and showed some stabilization of ATR binding to WT_θ (Fig. 2.4I). The presence of a Schiff base with both samples was confirmed by acid protonation spectra (Fig. 2.4J&M). The Arr peptide showed minimal effects on the binding rate of 11CR to either opsin (Fig 2.4H&K), compared to the robust changes observed with G_t C-term peptide, which might be due to the lower affinity and non-optimized state of the Arr peptide (192).

2.4.6: Conformational Selection of Retinal Isomers by Opsin is Not an Artifact of the Minimal Cysteine Construct

To eliminate the possibility that the minimal cysteine background, WT_θ, used for all the experiments in Fig. 4 might be influencing the results, we repeated the experiments with WT opsin containing all native cysteines in addition to the stabilizing disulfide (Fig. 2.5). The WT opsins show identical results across the different conformations (Fig. 2.5A&B). Additionally, we do not observe FRET between WT and ATR, indicating that the native cysteines constituting the palmitoylation sites (C322, C323) do not, at least under our detergent conditions, provide a high-affinity secondary ATR binding site (Fig. 2.5B). The only clear deviation between the minimal cysteine constructs and WT comes from 11CR binding to the M257Y-CAM alone (Fig. 2.5A). With all native cysteines, the rate of 11CR binding is slowed to levels similar to the G_t C-term peptide experiments. This observation might indicate a smaller proportion of ops in the M257Y-CAM sample compared to M257Y-CAM_θ. For all other conditions tested, the

WT variants performed identically to the WT_{θ} and the interpretation of the results from the minimal cysteine construct are valid for the WT protein. See Table 2.1 for complete rate results.

2.4.7: Expanding Hole B (TM5/TM6) Does Not Enable ATR Uptake and Actually Slows 11CR Binding

As discussed in the introduction, crystal structures show that an opening forms Hole B (TM5/TM6) in MII and the active Ops* conformation (Fig. 2.6A) (6,7,47,153,154). This opening has been proposed to form part of a channel for retinal uptake or release (151,157,169). Therefore, we tested if this hole might play a role in the shift in retinal preference that we observed with Ops* stabilization (Fig. 2.4B&C). Hole A was not pursued due to its close proximity to the Schiff base.

To inhibit closure of Hole B, we mutated the flanking phenylalanines to alanines (F208A and F273A) and also constructed a double alanine mutant (F208A-F273A). As shown in Fig. 2.6C, 6E, and 6G, these hole constructs failed to show any detectable ATR binding, despite being predicted to have a more active-like opening to the pocket, suggesting expanding Hole B alone is not sufficient to induce the shift in retinal preference. Moreover, increasing the size of this hole did <u>not</u> increase the rate of 11CR binding (as the transient activation hypothesis would predict), but rather, <u>slowed</u> the rate of binding, with the double mutant being slower than the single sites combined (Fig. 2.6B,D,F).

2.5: Discussion

In this work, we probed the role of structural dynamics in retinal binding to opsin. Our work was initially designed to test a recently proposed "transient activation" hypothesis that postulates retinal binding requires formation of active opsin (Ops*) for the ligand to gain entry into the binding pocket (152). For 11CR, our results are the exact opposite of what this model would predict—as the equilibrium of receptor conformations is shifted from primarily ops (inactive WT opsin) to a mixture of Ops and Ops* (M257Y-CAM), 11CR binding is increasingly slower. However, we also obtained results for ATR that are consisted with the transient activation model—the more we increase the Ops* pool, the faster ATR binds.

As a result of these findings, we propose a new model for retinal binding to naïve opsin with 11CR and ATR binding to different conformations of opsin, consistent with our conformational selection data (Fig. 2.7). Below, we discuss the potential implications of the results of our experiments and new model.

2.5.1: Conformational Selection of Retinal Isomers by Opsin

Is Ops* formation necessary or required for retinal binding? As shown in Fig. 2.3, 4, and 5, increasing the amount of Ops* impairs 11CR binding, yet enables binding of the agonist ATR. Thus, Ops* is clearly important for ATR binding, as inactive Ops shows no ability to bind ATR. Therefore, we propose that the binding of retinals to opsin is primarily dictated by the conformational state of the receptor. This result is consistent with the conformational selection model discussed below (Fig. 2.7).

Why does ATR ever leave the activated photoreceptor if its affinity is higher for the Ops* state than 11CR? We think the answer is the following. Although the protein conformation of Ops* prefers the ATR agonist to the 11CR inverse agonist, the binding of ATR to Ops* is less stable than 11CR to Ops due to the open nature of the Ops* form. In the Ops* state, the retinal-Schiff base linkage becomes exposed to water, due to conformational changes in the protein that open up a solvent channel leading from the retinal binding pocket to the cytoplasmic face. Waters traversing this channel hydrolyze the retinal-opsin Schiff base linkage, resulting in the release of ATR (195). If the ATR leaves the protein after the cleavage event, and the active protein reverts back to the inactive ops form, the ATR will be unable to re-bind until the opsin flickers back to the Ops* state, which is a very low probability event for WT opsin (55). Thus, the Ops*-ATR form is in constant flux and, in the absence of stabilization by G protein or arrestin, the ligand is in equilibrium between the bound and unbound states (12,176,191). This dynamic nature is clearly displayed in the inability of ATR to completely bind without added stabilization by peptides (Fig. 2.4C,F,I,L & 2.5B,E,H,K).

Another way to think of this is that the Ops* converts back to the ops conformation before the ATR can rebind. Of course the system is much more complicated *in vivo* where other proteins, such as retinal dehydrogenase, are also in play to remove free ATR from the system. In fact, the concentration of ATR is tightly regulated by the rod cell, due to free ATR's cytotoxicity at low concentrations, further limiting the possibility of rebinding *in vivo* (57,60,196,197).

Our proposed conformational selection model for ligand binding is in agreement with other well studied GPCRs, such as the β_2 adrenergic receptor (160,198-200).

Additionally, we recapitulate the extended ternary complex model, originally established to explain ligand binding to CAM β_2 adrenergic receptor, for rhodopsin, greatly implying that the dim-light receptor behaves like a ligand-binding GPCR rather than being a special case (20). Interestingly, activation of rhodopsin has been proposed to be an extreme example of an induced fit mechanism, as the inverse agonist isomerizes to the agonist while inside the binding pocket and appears to actively push the inactive conformation to active MII (201). Taken with the data presented here, it appears rhodopsin compartmentally exhibits both classical models of ligand–receptor interactions. The receptor shows clear conformational selection when binding exogenous ligand, yet induced fit when pre-bound 11CR is isomerized by light.

Can the photoactivation event also be interpreted within the confines of a conformational selection model? For example, one can imagine that, after photoisomerization of the 11CR, the protein is no longer restricted to the inactive conformation and can sample other structural states, including the Ops* conformation. Transition to the active state would be quickly stabilized by the high apparent affinity of the agonist covalently bound in the binding pocket. In this model, rather than an induction of the active state, the agonist selects the active conformation as the rhodopsin explores the conformational landscape. An understanding like this might help explain the molecular mechanism behind agonist-induced activation of other GPCRs, such as the AT_1 angiotensin receptor (202).

An aspect of the detergent system is an increased flexibility of the opsins which allows for more consistent occupation of the two conformational extremes and importantly the open conformation. Previous work has shown that a lipid bilayer system

increases the energy barrier for the transition between Ops and Ops* and an impaired conversion to MII upon photobleaching (168,203). Therefore, the conformational selection observed here might be less dramatic in membranes due to a smaller population of Ops* present at any point in time.

2.5.2: Palmitoylation of Opsin Does Not Play a Role in Retinal binding to Opsin in Our Detergent System

Our studies comparing WT opsin and the minimal cysteine opsin, WT_{θ} (lacking palmitoylation due to the C322S and C323S mutations), allow us to speculate the effect of the presence or absence of palmitoylation on retinal binding. Palmitoylation has been shown to improve opsin stability *in vivo* (204), and be essential for G protein induced ATR binding to WT opsin, perhaps by acting as a secondary binding site for retinals (156,205). Here, we see that conformational selection dictates binding rates regardless of palmitoylation status of the opsins, since we do not see significant differences for retinal binding between opsin with (WT) or without (WT_{θ}) palmitoylation, and no major differences on the abilities of exogenous agents, like the G_t C-term peptide, to induce ATR binding (Fig. 2.4&2.5). However, our experiments were carried out using purified, detergent-solubilized receptor, whereas the above cited work was all done using opsin in native membranes. Thus is possible that, in detergent, the putative secondary binding site(s) disappear, suggesting that, if they are present, they are likely low affinity sites.

2.5.3: Expanding Hole B (TM5/TM6) Does Not Enable Ops to Bind ATR, but May Play a Role in Stable 11CR Binding

To test specific aspects of the active conformation that might result in the shift in ligand affinity, we probed the role of opening of the hole between TM5/TM6 by mutating the phenylalanines at positions 208 and 273 to alanines, thereby forcing a hole to be present, regardless of receptor conformation. Experiments on this perforated opsin clearly showed that the presence of a hole between TM5/TM6 is not sufficient for ATR binding, indicating that ATR likely does not use Hole B for entry, but rather might enter through Hole A. Interestingly, 11CR binding rates were drastically slowed by these mutations (Fig. 2.6). This latter observation might indicate Hole B must be closed to help stabilize or "trap" 11CR in the binding pocket.

Could the slow 11CR binding to the Hole B mutants explain why the Ops* conformation slows inverse agonist binding? We speculate that, in the two-state model for receptor activity, this result might indicate that, during binding of 11CR (either entering through the Hole A or Hole B), Hole B must "snap shut" to trap 11CR in the pocket. Forcing Hole B open (as we did here) would prevent the trap from operating correctly, enabling 11CR to "escape" before the Schiff base can form. Alternatively, a third receptor state could be invoked to explain these results, one which has a closed Hole B, yet an open Hole A. In this model, after entering through Hole A, 11CR may simply exit through the enlarged Hole B (caused by the alanine mutation), before proper binding and Schiff base formation can occur. In either case, the TM5/TM6 Hole B appears to be essential for efficient and rapid stable 11CR binding. This interpretation is in agreement

with the proposal that the TM5/TM6 hole might be the avenue for retinal exit from the receptor following activation (151,159,169).

All of our mutants tested here formed a wild-type like chromophore upon addition of 11CR, as indicated by at 500nm peak (data not shown). Thus, we favor the interpretation that F208 and F273 stabilize the retinal for proper binding and do not perturb protein folding. However, we cannot formally rule out the possibility that the effects we see are in part caused by non-localized effects, as has been previously proposed (152).

Furthermore, although mutations F208A and F273Q and L have been previously shown to be non-disruptive to the spectroscopic properties of WT, the F273A and F208A/F273A mutants might have unexpected consequences (152,206).

2.5.4: Occupancy of the Cytoplasmic Binding Cleft of Opsin by Either G protein C-terminus or Arrestin Finger Loop Peptide Mimics is Sufficient to Enhance ATR Binding

The peptides used in this study, G_t C-term and Arr peptide, both stabilized ATR binding to opsin. These results confirm previous speculations about the role of these protein regions based on studies using full-length G protein and arrestin (30,176). Importantly, our observations indicate the well known phenomenon of MII "trapping" by G protein and arrestin needs to be reevaluated (10,12,178,179,191,194,207). Our results indicate G protein and arrestin "trapping" cannot simply be ascribed to these proteins preventing ATR release from the activated MII receptor. Rather, they suggest that some of the "trapping" is almost certainly due to the fact that these proteins stabilize Ops*, and

thus enable released ATR to rebind, due to an increased affinity of the agonist for the receptor by stabilization of the active form.

Interestingly, the increase of Ops* and affinity for ATR appears to be a common consequence of binding something into the cytoplasmic cleft in opsin, since both the G protein and arrestin peptide fragments display this effect (7,10,12,29,191,194,208). Furthermore, these small fragments of the proteins are sufficient to promote an increased affinity for the agonist, suggesting the whole protein is not necessary for the effect to occur, but may increase the magnitude. Our results also show G_t C-term peptide's slowing effect on 11CR binding is not reciprocated by Arr peptide (Fig. 2.4H&K & 2.5G&J), and therefore might indicate a unique receptor conformation (209) that has a higher affinity for ATR, potentially to keep the agonist bound and to protect the rod cell from free ATR accumulation (57,207), and yet does not impair binding of 11CR. This is consistent with a model of physiological arrestin interaction where the arrestin is released from phosphorylated opsin only when the opsin is regenerated by 11CR (210). Although a tempting hypothesis, these differences might just be the result of the affinity for the Arr peptide used here being orders of magnitude lower than the optimized G_t C-term peptide (178,192).

Moreover, these observations also lead to the question: *in vivo*, what prevents ATR from simply rebinding opsin in the presence of G protein or arrestin, such as in the context of high-light bleaching conditions in the retina (197)? One answer may lie in the reduction of the retinal to retinol by retinol dehydrogenase (RDH), which pulls the ATR out of the binding reaction. Thus, RDH proteins may play a key step in preventing futile cyclic ATR binding, as has been previously proposed (60,64,129,187,211).

2.5.5: A Modified Conformational Selection Model for Retinal Binding to Opsin

Our data clearly show that the conformational state of the receptor plays a critical role in determining the rate of retinal binding. The simplest way to fit these results would be to invoke a classical two-state binding model, in which the inverse agonist, 11CR, binds directly to ops and the agonist, ATR, to the open Ops* (160).

The problem with this assumption is that it describes the process, but does not provide a mechanism for how retinal can access the binding pocket. As discussed earlier (Fig. 2.1A), there is no pathway to the binding site in the inactive rhodopsin structures. In contrast, the active rhodopsin conformation does show an access route to the binding pocket, which motivated the proposal (shown in Fig. 2.1C) that both ATR and 11CR bind to the same active receptor conformation (what we refer to here as the transient activation hypothesis or TAH) (3,6,152).

Our results both support and contradict this idea. We find stabilizing the active Ops* state accelerates agonist binding, in agreement with the TAH model. However, in direct contradiction to the TAH model, our data also show creating more active Ops* slows binding of 11CR, the inverse agonist. The latter result strongly suggests the TAH model cannot fully explain all forms of retinal binding.

Why not simply modify the TAH model to include a conformational selection step after retinal binding? Such a model could explain a slower rate of apparent binding and Schiff-base formation for 11CR, since after 11CR enters into the Ops* pocket, the protein would have to revert back to the Ops conformation in order to form a proper Schiff base, and that could take time. However, such an argument breaks down for the

following simple reason—the TAH model still assumes 11CR and ATR can only enter the Ops* conformation, and thus cannot explain why we see the rate of 11CR binding is inversely related to the amount of Ops*. In other words, it does not make sense that the less Ops* there is, the faster 11CR binds, as that would suggest the fastest rate of 11CR binding would occur when there is no Ops* at all, which becomes a nonsensical extrapolation within the confines of the TAH model due to the Ops* requirement for binding.

However, as noted above, there is also an inherent problem with a classical, simple two-state conformational selection model—it does not explain how 11CR enters opsin. Opsin has usually been assumed to be a closed conformation, based on the fact that opsin is functionally inactive, and all inactive rhodopsin structures show no access pathways into the binding pocket. However, there is no experimental evidence that we are aware of indicating inactive opsin has no access pathways to the binding pocket.

Thus, we propose a relatively simple, but little discussed alternate possibility that would circumvent this problem and explain our results—a model in which inactive opsin contains unidentified opening(s) that enable 11CR entry (these could be the same holes observed in the active opsin structure, but do not have to be). Importantly, this hypothetical conformer would lack the conformational changes in the cytoplasmic face that enable G protein and arrestin binding, rendering it still functionally inactive, and thus distinct from Ops*.

Therefore, our new model for retinal binding (presented in Fig. 2.7) contains this new putative, open opsin conformation (in brackets) placed between the fully active Ops* and fully closed off Ops. As discussed above, we speculate that this new state is an

intermediary between the two previously defined conformations. A similar explanation has been invoked to explain results deviating from the simple two-state model in other GPCRs (212-214). Though our model depicts the retinals binding to only one conformation, our results do not preclude the possibility they can also non-preferentially bind to the other opsin state.

2.5.6: Conclusions

In summary, we find shifting the conformational equilibrium in favor of more active state (Ops*) reduces 11CR binding rates, yet enhances the rate of ATR binding, thus the current transient activation hypothesis for 11CR binding to rhodopsin needs modification (152) to include contribution from conformational selection.

However, a number of questions remain unanswered by our present work. Our binding data only measure stable retinal-opsin interactions. Possible roles for transient shifting of the transmembrane helices, rapid flickering of the residues surrounding the binding pocket, or even formation of a third receptor state, as discussed above and proposed for other GPCRs, (212) cannot yet be ruled out as means for retinal entry.

A mechanistic explanation how the retinal enters and exits the receptor still has not been established and may ultimately require the inactive opsin crystal structure to provide structural context to rule out, or reveal, another possible entry pathways into the protein. Interestingly, our data also suggest that using 11CR to shut off a rhodopsin CAM, proposed as a treatment for some retinal diseases, may prove difficult, since the presence of Ops* lowers 11CR affinity. Allosteric ligands may be a better approach for modulating activity in such mutants. Experiments are underway to further test our model of conformational selection, to elucidate what molecular events govern it, and to better

understand retinal-opsin interactions. These topics have clear implications in drug design and protein engineering both for vision and for GPCRs.

Table 2.1: Complete table of rates of retinal uptake for opsins tested in Chapter 2.

Opsin (ligand)	Condition[a]	N[b]	Rate (s^{-1})	R^2	Average Rate (s^{-1})	Error[c] (rate)	$t_{1/2}$ (min)	Error ($t_{1/2}$)
WT_θ (11CR)	Standard Conditions	3	2.39e-3	0.978	2.55e-3	7.00e-5	4.53	1.25e-1
			2.68e-3	0.959				
			2.59e-3	0.914				
	0.05% DDM	1	2.98e-3	0.982	2.98e-3	4.96e-5	3.88	6.47e-2
	0.2% DDM	1	1.68e-3	0.988	1.68e-3	1.69e-5	6.87	6.91e-2
	0.5µM Ops : 1µM 11CR	1	4.65e-3	0.995	4.65e-3	4.53e-5	2.49	2.42e-2
	0.5µM Ops : 0.25µM 11CR	1	2.87e-3	0.986	2.87e-3	3.98e-5	4.02	5.57e-2
	+100µM G_t C-term Peptide	3	2.87e-3	0.981	2.82e-3	2.43e-4	4.10	3.54e-1
			2.28e-3	0.991				
			3.31e-3	0.934				
	G_t C-term Fusion	3	1.42e-3	0.947	1.53e-3	9.94e-5	7.55	4.90e-1
			1.39e-3	0.940				
			1.77e-3	0.935				
	+100µM Arr Peptide	3	2.61e-3	0.741	3.29e-3	2.94e-4	3.51	3.13e-1
			3.83e-3	0.911				
			3.44e-3	0.969				

	+500μM Arr Peptide	3	3.52e-3 4.88e-3 3.52e-3	0.848 0.900 0.926	3.97e-3	3.70e-4	2.91	2.71e-1
WT_{θ} (ATR)	+100μM G_t C-term Peptide	3	1.44e-3 1.02e-3 9.28e-4	0.930 0.984 0.985	1.13e-3	1.29e-4	10.2	1.17e0
	G_t C-term Fusion	3	1.15e-2 1.22e-2 6.82e-3	0.965 0.914 0.927	1.15e-2	1.58e-3	1.00	1.38e-1
	+100μM Arr Peptide	3	3.31e-4 5.45e-4 5.48e-4	0.661 0.711 0.862	4.75e-4	5.86e-5	24.3	3.01e0
	+500μM Arr Peptide	3	3.92e-4 4.36e-4 5.21e-4	0.945 0.863 0.914	4.50e-4	3.09e-5	25.7	1.77e0
M257Y-CAM_{θ} (11CR)	Standard Conditions	3	1.01e-3 1.05e-3 1.16e-3	0.968 0.957 0.976	1.08e-3	3.65e-5	10.7	3.63e-1
	+100μM G_t C-term Peptide	3	4.04e-4 3.49e-4 3.36e-4	0.979 0.979 0.962	3.63e-4	1.69e-5	31.8	1.48e0
	G_t C-term Fusion	3	7.06e-4 6.63e-4 4.70e-4	0.944 0.946 0.955	6.84e-4	7.23e-5	16.9	1.78e0

	+100μM Arr Peptide	3	9.34e-4 1.40e-3 1.09e-3	0.932 0.851 0.961	1.14e-3	1.12e-4	10.1	9.95e-1
	+500μM Arr Peptide	3	1.22e-3 1.12e-3 1.14e-3	0.926 0.798 0.949	1.16e-3	2.51e-5	9.96	2.16e-1
M257Y-CAM_{θ} (ATR)	Standard Conditions	3	1.18e-3 1.13e-3 1.12e-3	0.923 0.968 0.961	1.14e-3	1.56e-5	10.1	1.38e-1
	+100μM G_t C-term Peptide	3	5.83e-3 7.60e-3 6.28e-3	0.941 0.958 0.950	6.57e-3	4.32e-4	1.76	1.16e-1
	G_t C-term Fusion	3	7.15e-3 6.19e-3 1.01e-2	0.927 0.914 0.816	7.81e-3	9.61e-4	1.48	1.82e-1
	+100μM Arr Peptide	3	5.30e-3 7.45e-3 4.28e-3	0.876 0.926 0.909	5.68e-3	7.64e-4	2.04	2.74e-1
	+500μM Arr Peptide	3	1.23e-2 8.02e-3 9.90e-3	0.872 0.918 0.690	1.01e-2	1.01e-3	1.15	1.15e-1
$F208A_{\theta}$ (11CR)	Standard Conditions	3	6.27e-4 7.31e-4 6.62e-4	0.992 0.994 0.990	6.73e-4	2.48e-5	17.2	6.32e-1
$F273A_{\theta}$	Standard	3	1.28e-3	0.985	1.25e-3	3.65e-5	9.28	2.72e-1

(11CR)	Conditions		1.16e-3	0.967				
			1.30e-3	0.947				
F208A-F273A$_\theta$ (11CR)	Standard Conditions	3	3.29e-4	0.993	3.10e-4	7.83e-6	37.3	9.41e-1
			3.05e-4	0.992				
			2.97e-4	0.991				
WT (11CR)	Standard Conditions	3	3.12e-3	0.965	3.92e-3	3.91e-4	2.94	2.93e-1
			4.78e-3	0.975				
			3.87e-3	0.972				
	+100μM G_t C-term Peptide	3	2.58e-3	0.956	3.05e-3	1.95e-4	3.78	2.41e-1
			3.27e-3	0.958				
			3.31e-3	0.888				
	G_t C-term Fusion	3	1.19e-3	0.925	1.17e-3	6.87e-5	9.91	5.84e-1
			1.01e-3	0.953				
			1.30e-3	0.890				
	+100μM Arr Peptide	3	6.89e-3	0.956	5.15e-3	7.40e-4	2.24	3.23e-1
			4.72e-3	0.946				
			3.83e-3	0.971				
	+500μM Arr Peptide	3	4.35e-3	0.935	3.90e-3	3.43e-4	2.96	2.61e-1
			3.06e-3	0.957				
			4.29e-3	0.974				
WT (ATR)	+100μM G_t C-term Peptide	3	1.42e-3	0.958	1.40e-3	3.36e-5	8.26	1.98e-1
			1.32e-3	0.975				
			1.46e-3	0.958				
	G_t C-term Fusion	3	9.08e-3	0.959	1.31e-2	1.79e-3	0.879	1.20e-1
			1.37e-2	0.974				

			1.66e-2	0.762				
	+100μM Arr Peptide	3	4.44e-4 9.41e-4 9.43e-4	0.869 0.761 0.620	7.76e-4	1.35e-4	14.9	2.60e0
	+500μM Arr Peptide	3	3.85e-4 2.51e-4 5.09e-4	0.905 0.922 0.932	3.81e-4	6.08e-5	30.3	4.83e0
M257Y-CAM (11CR)	Standard Conditions	2	6.17e-4 5.88e-4	0.966 0.978	6.02e-4	1.47e-5	19.2	4.68e-1
	+100μM G_t C-term Peptide	2	4.14e-4 4.25e-4	0.951 0.953	4.19e-4	5.35e-6	27.6	3.52e-1
	G_t C-term Fusion	3	4.40e-4 4.96e-4 5.00e-4	0.952 0.948 0.950	4.79e-4	1.59e-5	24.1	8.01e-1
	+100μM Arr Peptide	2	9.00e-4 9.07e-4	0.965 0.968	9.04e-4	3.13e-6	12.8	4.43e-2
	+500μM Arr Peptide	2	1.12e-3 9.54e-4	0.950 0.924	1.04e-3	8.31e-5	11.1	8.93e-1
M257Y-CAM (ATR)	Standard Conditions	2	1.18e-3 1.22e-3	0.943 0.962	1.20e-3	1.87e-5	9.64	1.50e-1
	+100μM G_t C-term Peptide	2	7.53e-3 827e-3	0.935 0.941	7.90e-3	3.68e-4	1.46	6.81e-2
	G_t C-term	3	1.01e-2	0.957	8.44e-3	6.85e-4	1.37	1.11e-1

Fusion		7.24e-3	0.960				
		8.03e-3	0.962				
+100μM Arr Peptide	2	5.95e-3	0.931	5.69e-3	2.65e-4	2.03	9.46e-2
		5.42e-3	0.936				
+500μM Arr Peptide	2	7.74e-3	0.809	6.41e-3	1.33e-3	1.80	3.73e-1
		5.08e-3	0.800				

[a]All conditions used were 0.5μM Ops, 0.5μM Retinal, 0.1% DDM at 10°C. Conditions listed here are in addition to or in place of these listed here.

[b]N refers to number of individual binding time courses performed.

[c]Errors reported are standard error for N=3, standard deviations for N=2, standard error of the rate parameter was determined using a reduced chi-square using the SigmaPlot fitting software for N=1.

Figure 2.1: The active rhodopsin structure reveals openings into the retinal binding pocket

A) Comparison of access to the retinal binding pocket in the inactive, closed rhodopsin state (gray, left) and active, open MII state (blue, right). To enable visualization of the pocket, the bound retinal in each has been removed, and the remaining internal surface "cast," colored red. The models clearly show two avenues for access present in the active conformation that are absent from the inactive. These have been termed Hole A (between TM1/TM7) and Hole B (between TM5/TM6) (151). The C_α carbon of the Schiff base lysine is shown in gold. B) Structures of the chemically identical, but spatially different retinal ligands; the inverse agonist, 11-cis retinal (11CR), and the agonist, all-*trans* retinal (ATR). Currently, only the structure of active opsin, ops*, is known, and is very similar to MII (6,47). Because inactive opsin is thought to be structurally similar to inactive rhodopsin, and thus would have no access pathway to the binding pocket, a "transient activation," or transient conversion of ops→ops*, has been proposed to enable 11CR entry into the binding pocket (152). C) Cartoon of the "transient activation" model in which the apoprotein exists as either ops or ops*. Transition of the inactive ops to ops* is proposed to enable retinal to enter the binding pocket. This non-covalent intermediate is followed by Schiff base formation (shown here as a red star). According to the transient activation hypothesis, both 11CR and ATR enter the ops* state and form the non-covalent intermediate. The subsequent formation of the Schiff base with 11CR locks the receptor in the inactive conformation, while ATR forms a linkage with the active state. Coordinates from PDBID: 1GZM and 3PXO were used for models (47,170). Casting of the binding pocket was done with a 1.4Å radius probe on

the CastP web server (215). Molecular graphics were created using the UCSF Chimera Package (172).

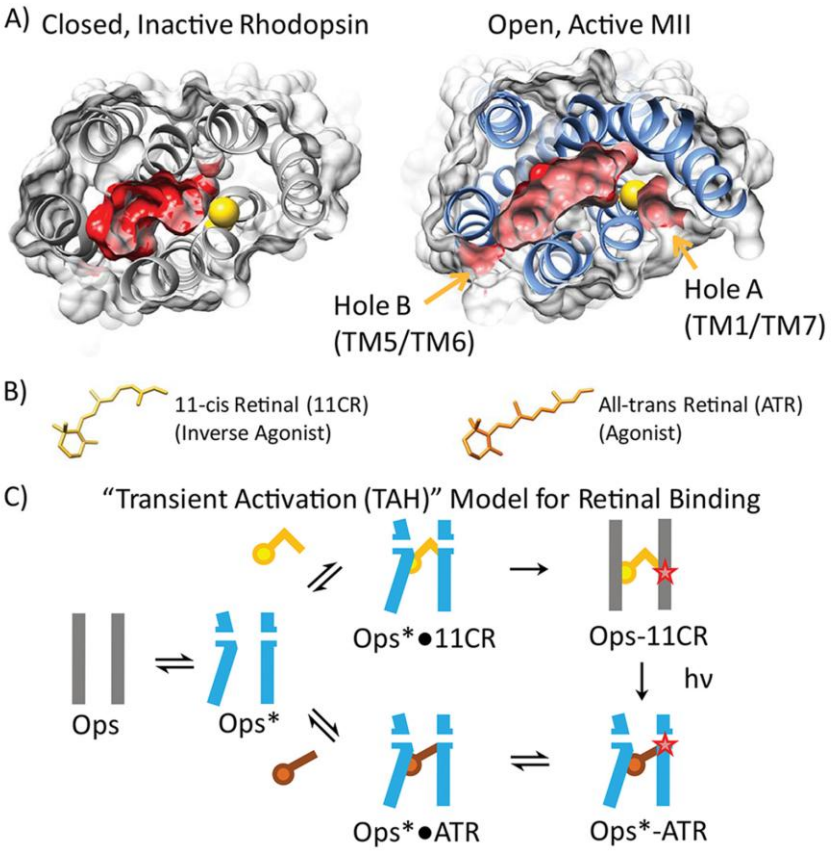
A) Closed, Inactive Rhodopsin
Open, Active MII
Hole B
(TM5/TM6)
Hole A
(TM1/TM7)
B)
11-cis Retinal (11CR)
(Inverse Agonist)
All-trans Retinal (ATR)
(Agonist)
C)
"Transient Activation (TAH)" Model for Retinal Binding
Ops
Ops*
Ops*●11CR
Ops-11CR
hν
Ops*●ATR
Ops*-ATR

Figure 2.2: Rates of retinal binding to opsin can be measured by monitoring quenching of the protein intrinsic tryptophan fluorescence.

A) Example of the traditional approach for monitoring 11CR binding to naïve opsin in which absorbance spectroscopy is used to observe the shift in the maximum absorbance from 380nm to 500nm as 11CR retinal forms a protonated Schiff base linkage with the protein. Inset) The increase of the 500nm absorbance as a function of time can be used to determine the rate of binding. B) Example of 11CR (brown) and ATR (green) retinal binding by monitoring fluorescence of tryptophan residues in WT opsin. The observed decrease indicates 11CR binds to the empty opsin, but ATR does not. Addition of retinal is shown by arrow. C) Arrhenius analysis of the absorbance and fluorescence binding data for 11CR binding to opsin at different temperatures. The plots show that the two methods report essentially the same activation energies, within experimental error (12.75 ± 2.1 and 13.0 ± 0.31 kcal/mole, respectively). Fluorescence binding assays, except where noted, were with 0.5μM opsin and 0.5μM retinal in 5mM MES, 40mM NaCl, 0.1% DDM at pH 6.0 at 10°C. Absorbance assays were conducted with 1μM opsin and 1μM retinal, which was necessary to increase signal over noise. To enable comparison with absorbance data, the Arrhenius analysis of 11CR binding by fluorescence was performed using 1μM opsin and 1μM retinal.

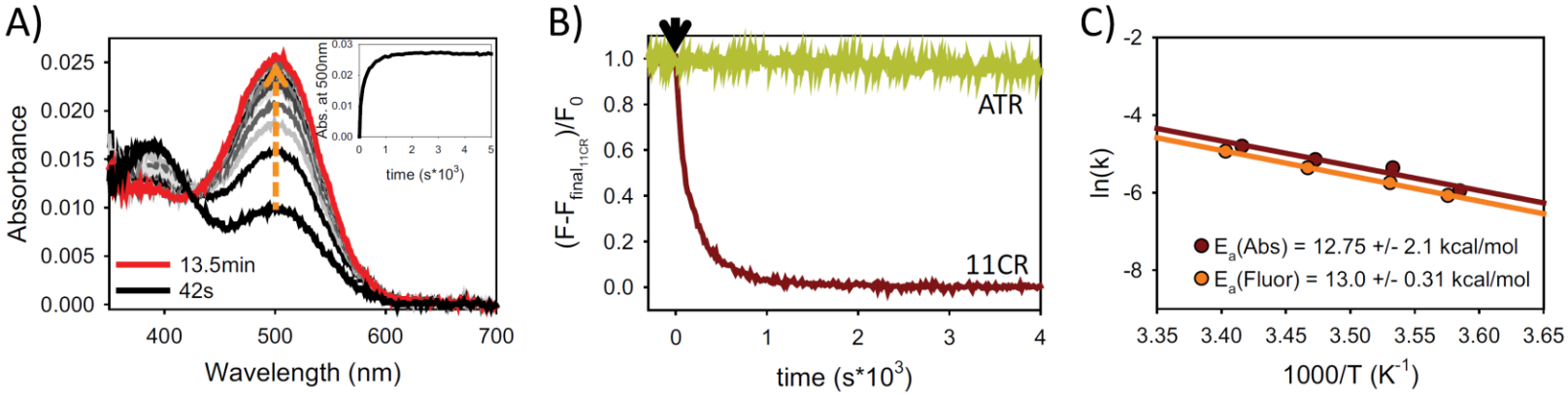
A)
Absorbance
Wavelength (nm)
13.5min
42s
Abs. at 500nm
time (s*10^3)
B)
(F-F final 11CR)/F0
ATR
11CR
time (s*10^3)
C)
ln(k)
Ea(Abs) = 12.75 +/- 2.1 kcal/mol
Ea(Fluor) = 13.0 +/- 0.31 kcal/mol
1000/T (K^-1)

Figure 2.3: A constitutively active mutation (CAM) of opsin, M257Y, binds 11CR slower than WT, yet also gains the ability to bind ATR.

A) Pictorial representation of the effect the M257Y mutation (denoted by the purple star) has on the conformational equilibrium between ops and ops*. The M257Y-CAMθ shifts the equilibrium of the opsin samples from nearly complete inactive (WT) to a mixture of active (Ops*) and inactive (Ops) receptors. B&C) WT_{θ} opsin readily binds 11CR stably, yet is unable to bind ATR. D&E) In contrast, the M257Y-CAM_{θ} can stably bind both 11CR and ATR. Interestingly, 11CR binding is substantially slower for this mutant than it is to the fully inactive WT_{θ}. Experimental conditions were the same as previously described in Fig. 2.2 and Experimental Procedures.

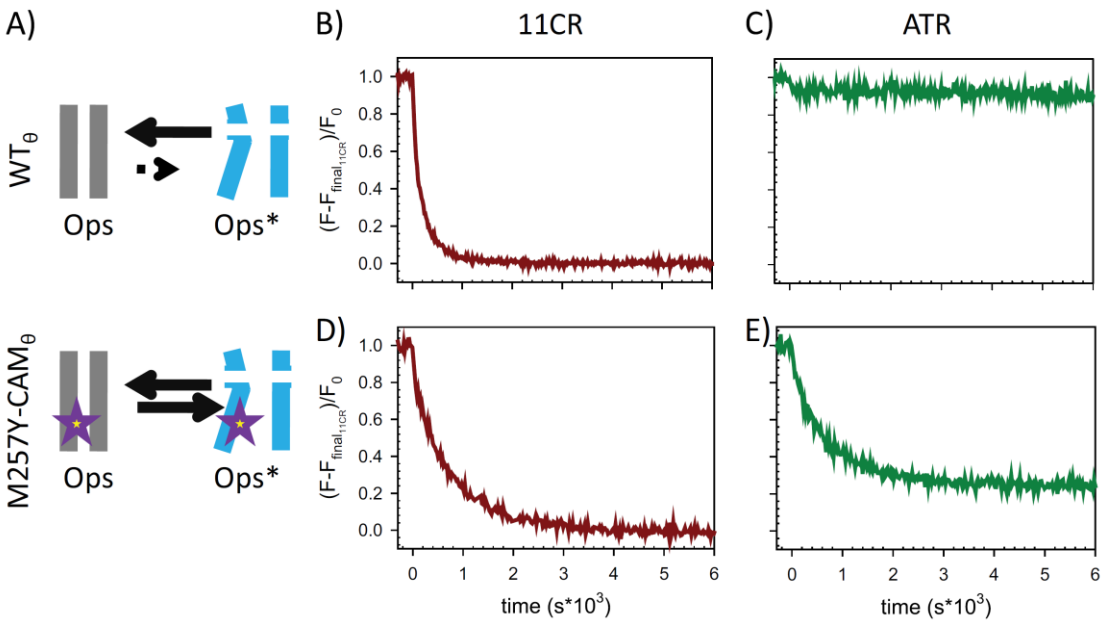
A)
B)
11CR
C)
ATR
WT$_\theta$
Ops
Ops*
M257Y-CAM$_\theta$
Ops
Ops*
D)
E)
(F-F$_{final_{11CR}}$)/F$_0$
1.0
0.8
0.6
0.4
0.2
0.0
0
1
2
3
4
5
6
time (s*10^3)

Figure 2.4: Shifting the ops→ops* equilibrium by binding of peptide mimetics of the G protein transducin (green, G_t C-term peptide) and arrestin (purple, Arr peptide) enhances the rate of ATR binding, and G_t C-term peptide also slows 11CR binding.

A) Cartoons depicting the full length G protein and arrestin and how the G_t C-term and Arr peptide bind in the same cytoplasmic cleft of rhodopsin (10,29). The regions of the full proteins corresponding to the peptides are highlighted in green on the G protein and purple on the arrestin. B&C) Interestingly, while the increased amount of ops* stabilization by the G_t C-term peptide accelerates the rate of ATR, it also significantly slows the rate of 11CR binding. D) Acid protonation spectra show a protonated Schiff base has formed between the opsin and ATR in the M257Y-CAM_θ in the G_t C-term peptide samples by a shift in absorbance to ~440nm. Note the larger shift in the peptide containing sample. E) Addition of free G_t C-term peptide has no effect on the rate of 11CR binding to WT_θ opsin, however, fusing it to the C-terminus of opsin results in impaired 11CR binding. F) Unexpectedly, fusing the G_t C-term peptide to WT_θ opsin induces ATR binding, reaching rates comparable to the peptides effect on M257Y-CAM_θ. G) Acid protonation of ATR bound to WT_θ opsin in the presence of G_t C-term peptide showed Schiff base formation, as indicated by characteristic absorbance shift to ~440nm. In comparison, no shift is detected in the absence of G_t C-term peptide, confirming no stable retinal binding. F) Incubation with Arr "finger loop" peptide mimetic has no effect on the ability of WT opsin's ability to bind either 11CR. G) The Arr peptide stabilizes some ATR binding to WT_θ opsin, but not nearly the amount observed by other conditions. J) Acid protonation spectra also show some Schiff base formation between ATR and WT_θ opsin in the presence of Arr peptide. K) Similarly, Arr

peptide had no effect on 11CR binding to M257Y-CAM_θ. L) The rate of ATR binding to M257Y-CAM_θ was enhanced by incubation with Arr peptide. M) Acid protonation of (L) shows Schiff base formation of ATR with M257Y-CAM_θ in the presence of Arr peptide. 100μM peptide was used for these experiments; all other experimental conditions were as previously specified in Fig. 2.2 and Experimental Procedures. Coordinates from PDBID: 3DQB and 4PXF were used for G_t C-term and Arr peptide-bound to opsin structures respectively (7,194) and 3SN6 and 4J2Q were used for G protein and arrestin models respectively (11,216).

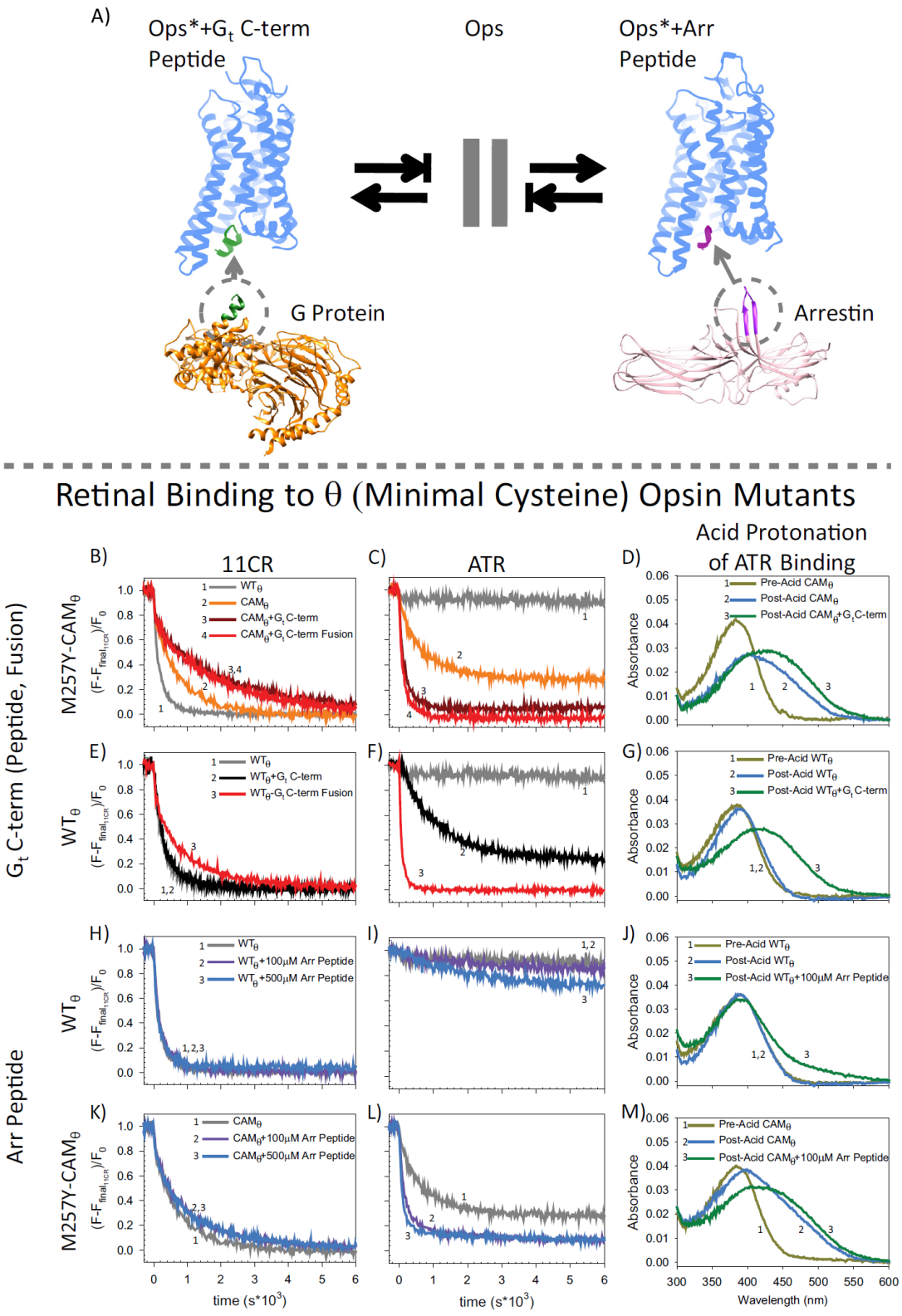
A)
Ops*+Gt C-term Peptide
Ops
Ops*+Arr Peptide
G Protein
Arrestin
Retinal Binding to θ (Minimal Cysteine) Opsin Mutants
Acid Protonation of ATR Binding
11CR
ATR
Gt C-term (Peptide, Fusion)
Arr Peptide
M257Y-CAMθ
WTθ
time (s*10^3)
Wavelength (nm)
Absorbance

Figure 2.5: The presence of palmotylation sites C322 and C323 in WT opsin does not change the effects of shifting the ops→ops* equilibrium using peptide mimetics of the G protein transducin (G_t C-term peptide) and arrestin (Arr peptide) on retinal binding.

A&B) The WT background opsins, with all native cysteines, show the same conformational selection as the WT_θ (Fig. 4B&C). C) Acid protonation confirms that the ATR binding observed in (B) was the results of a stable Schiff base and that G_t C-term peptide increased the total amount linkages. D&E) G_t C-term peptide free in solution assists in the binding of ATR to WT yet has little effect on 11CR binding. When fused to the opsin, the peptide slows 11CR binding and further accelerates formation of stable complexes with ATR. F) Proper binding of ATR induced by G_t C-term peptide is confirmed by acid protonation. G&H) The Arr peptide has little effect on the binding rates of 11CR to WT, it does stabilize some complexes with ATR. I) The ATR+WT+Arr peptide complexes contain a Schiff base, as indicated by 440 nm absorbance produced by acid protonation. J) The Arr peptide has minimal effect on the binding of 11CR to the M257Y-CAM opsin. K) The rate and amount of ATR binding to the M257Y-CAM is enhanced by inclusion of Arr peptide. L) The binding of ATR to the M257Y-CAM by Arr peptide is confirmed by acid protonation. Except where noted, peptide concentration used for these experiments was 100μM. All other experimental conditions were as previously specified in Fig. 2.2, Fig. 2.4, and Experimental Procedures.

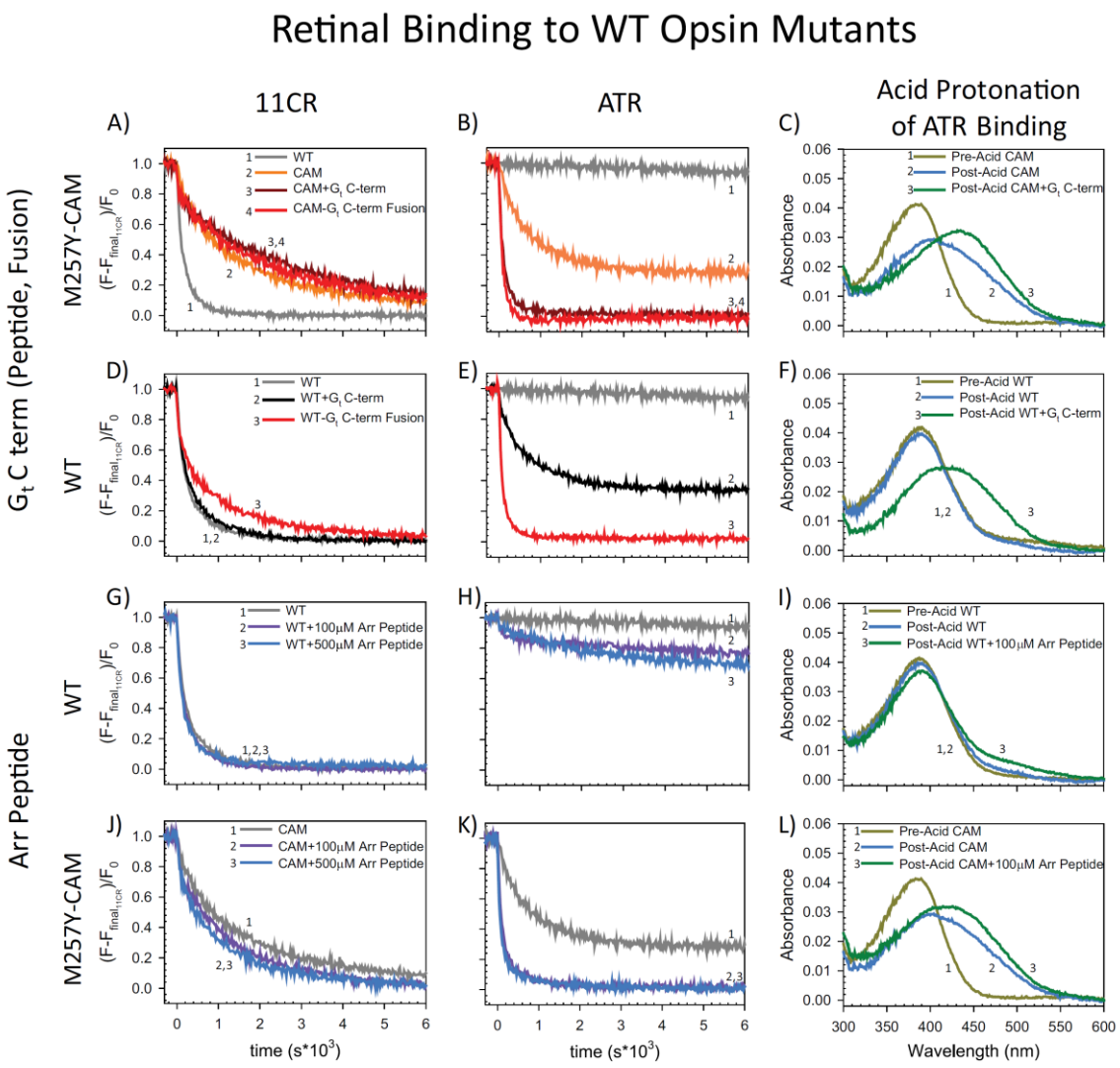
Retinal Binding to WT Opsin Mutants
11CR
ATR
Acid Protonation of ATR Binding
A)
B)
C)
D)
E)
F)
G)
H)
I)
J)
K)
L)
M257Y-CAM
WT
M257Y-CAM
WT
Gt C term (Peptide, Fusion)
Arr Peptide
1 WT
2 CAM
3 CAM+Gt C-term
4 CAM-Gt C-term Fusion
1 WT
2 WT+Gt C-term
3 WT-Gt C-term Fusion
1 WT
2 WT+100μM Arr Peptide
3 WT+500μM Arr Peptide
1 CAM
2 CAM+100μM Arr Peptide
3 CAM+500μM Arr Peptide
1 Pre-Acid CAM
2 Post-Acid CAM
3 Post-Acid CAM+Gt C-term
1 Pre-Acid WT
2 Post-Acid WT
3 Post-Acid WT+Gt C-term
1 Pre-Acid WT
2 Post-Acid WT
3 Post-Acid WT+100μM Arr Peptide
1 Pre-Acid CAM
2 Post-Acid CAM
3 Post-Acid CAM+100μM Arr Peptide
(F-Ffinal11CR)/F0
Absorbance
time (s*10^3)
Wavelength (nm)

Figure 2.6: Introducing a permanent enlargement of Hole B (TM5/TM6) is not sufficient to enable ATR binding, and actually slows 11CR binding.

A) Structural model comparing the position of F208 and F273 at Hole B in the inactive (gray) and active (blue) conformations. The relocation of these residues during formation of the active species results in a hole between TM5 and TM6. To explore the role of the residues constituting this opening, and to see if they play a role in the shifted ligand affinity, each was mutated in turn to an alanine, and the rates of uptake for 11CR and ATR were determined. Interestingly, although the rates of 11CR binding were slower for each of these mutations, F208A (B), F273A (D), or together (F), all were still unable to bind ATR (C,E,G). Taken together, these results suggest that the TM5/TM6 hole is not sufficient to allow ATR binding, yet is essential for rapid 11CR binding, possibly because closing of this hole is necessary to block 11CR escape and enable Schiff base formation. Experimental conditions were the same as previously described in Fig. 2.2 and Experimental Procedures.

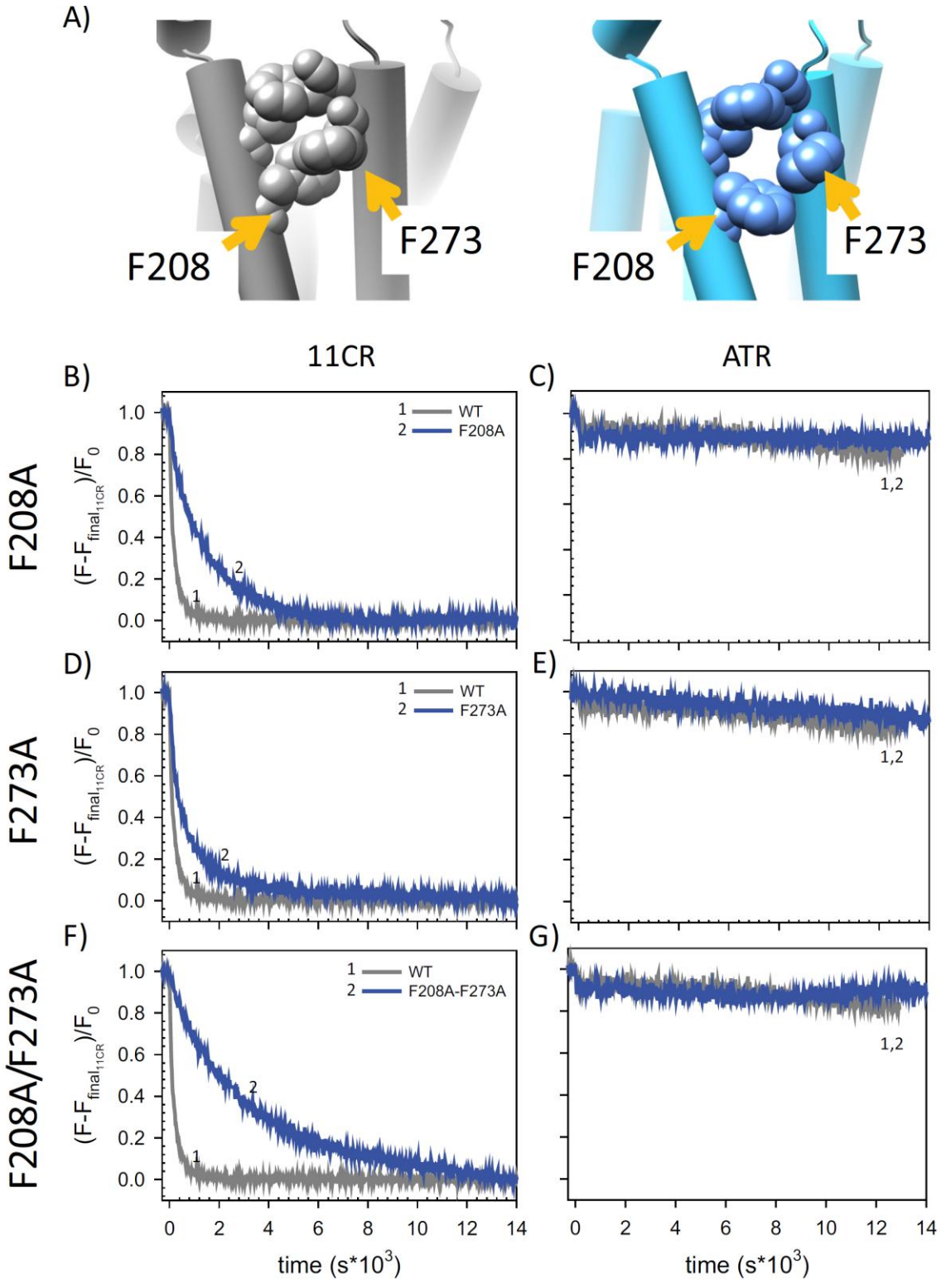
A)
F208
F273
F208
F273
11CR
ATR
B)
C)
F208A
1 WT
2 F208A
1,2
D)
E)
F273A
1 WT
2 F273A
1,2
F)
G)
F208A/F273A
1 WT
2 F208A-F273A
1,2
(F-F final 11CR)/F 0
time (s*10 3)
time (s*10 3)

Figure 2.7: A conformational selection model for retinal binding to opsin.

Our data indicate both ATR and 11CR do not bind to the same active receptor conformation and is consistent with this new model. The model proposes an open, yet inactive opsin form exist that enables 11CR binding (shown in brackets), one that is an intermediary between the closed, inactive and open, active receptor states. In our model, the 11CR molecule enters into this open, inactive conformation (Ops ● 11CR), then the covalent Schiff base is formed (depicted here by a red star). Note that the ATR branch of retinal binding is the same as proposed in the transient activation hypothesis.

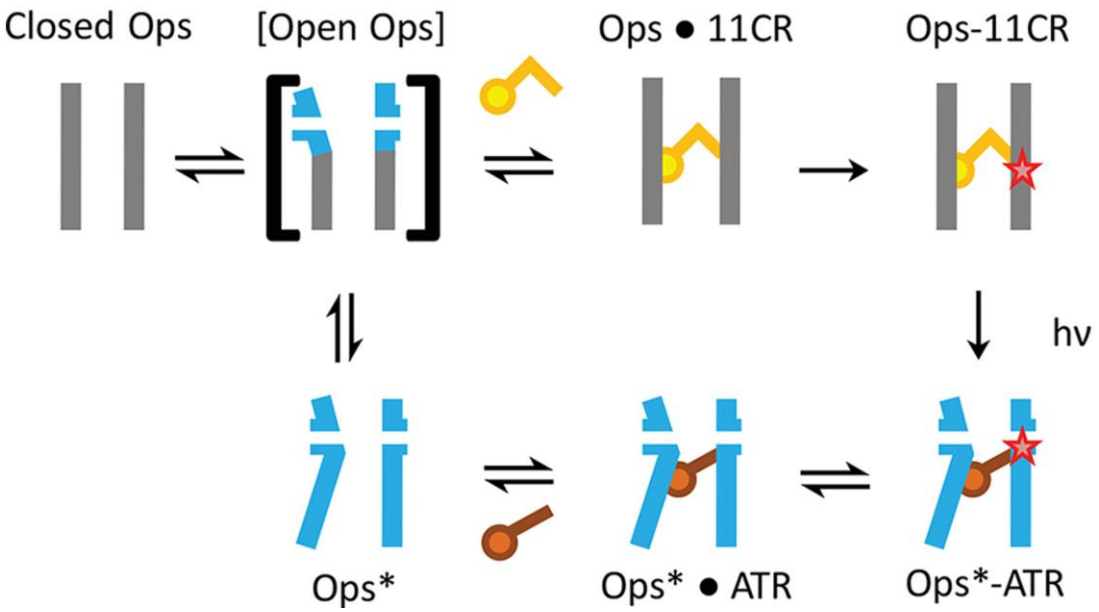
Closed Ops
[Open Ops]
Ops • 11CR
Ops-11CR
hv
Ops*
Ops* • ATR
Ops*-ATR

Chapter 3: Decay of an Active GPCR: Conformational Dynamics Govern Agonist Rebinding and Persistence of an Active, yet Empty Receptor State

Schafer C.T., Fay J.F., Janz J.M., Farrens D.L.

3.1: Summary

In this chapter we describe two new insights into the role of receptor conformational dynamics in the release of agonist (all-trans retinal, ATR) from the visual G protein-coupled receptor (GPCR) rhodopsin. First, we show that after light-activation, ATR continually releases and rebinds to any receptor remaining in an active-like conformation. This equilibrium can be shifted by either promoting the active-like population or increasing the agonist concentration. Second, we find that during decay of the signaling state, an active-like, yet empty receptor conformation transiently persists after retinal release, before the receptor ultimately collapses into an inactive conformation. The latter conclusion is based on our time-resolved, site-directed fluorescence labeling (SDFL) experiments that show a small, but reproducible, lag between the retinal leaving the protein and return of transmembrane helix 6 (TM6) to the inactive conformation, as determined from Tryptophan-induced quenching (TrIQ) studies. Accelerating Schiff base hydrolysis and subsequent ATR dissociation, either by addition of hydroxylamine or introduction of mutations, further increased the time-lag

between ATR release and TM6 movement. These new observations show that rhodopsin can bind its agonist in equilibrium like a traditional GPCR, provides evidence that an active GPCR conformation can persist even after agonist release, and raise the possibility of targeting this key photoreceptor protein by traditional pharmaceutical-based treatments.

The experiments of this chapter were conducted by the author of the dissertation. Dr. Fay provided support and insight into performing the radioactivity experiments and Dr. Janz had performed preliminary experiments when he was a graduate student in the Farrens' lab. This work was submitted in April 2016 to the *Proceedings of the National Academy of Sciences* and is currently under review.

3.2: Introduction

The super-family of G protein-coupled receptors (GPCRs) is one of the largest targets of pharmaceutical drugs in the human genome. Classically, GPCR signaling occurs when a diffusible ligand (such as a drug) binds to the receptor and stabilizes conformations that can couple with and activate intracellular proteins. Our understanding of this process has built on the classical "ternary complex" model of receptor-ligand-G protein interaction (19), a model that, with revisions, has continued to guide our knowledge of how this critical event occurs.

However, this paradigm has faced problems when applied to rhodopsin, the dim-light visual receptor. Rhodopsin does not bind a diffusible ligand, but rather is kept in an "off" state by a covalently-bound inverse agonist, 11-cis retinal (11CR). Light converts the 11CR to an agonist, all-trans retinal (ATR), which enables the receptor to activate its

G protein, transducin (G_t) (19,32,35). The active receptor, metarhodopsin II (MII), continues signaling until the Schiff base linking ATR to the receptor is hydrolyzed, resulting in the release of ATR and the decay of MII into an inactive apoprotein, opsin (Ops) (36,55). Binding of a new 11CR to opsin reforms the dark state (DS), enabling another round of photon detection (169).

Due to this unusual light-activated, covalently-bound ligand, rhodopsin has been considered "different" from the larger superfamily of diffusible ligand-binding GPCRs. However, we recently discovered that rhodopsin behaves more like a traditional ligand-binding GPCR than previously thought (148). Our experiments found that inactive receptor (Ops) preferentially binds inverse agonist (11CR), whereas active-state receptor (Ops*) binds agonist (ATR) (200). To explain these results, we proposed retinal-opsin interactions are governed by the same type of a conformational selection model proposed for other GPCRs (Fig. 3.1).

This new model challenges some long-held assumptions about retinal binding, predicts some unexpected behavior, and contains two new testable hypotheses. First, it predicts that after release, ATR can rebind any receptors remaining in an Ops* conformation. This is in contrast to current assumptions that ATR release is irreversible after Schiff base hydrolysis, and thus can be used to monitor decay of the active MII species (54,152,171). The second new idea builds on the first—if ATR rebinding requires an active-like Ops* conformation, then some active Ops* states may be able to persist after ATR release.

Here we directly tested both hypotheses. First, we measured ATR release for samples containing different amounts of active opsins. The results show the extent of

ATR "release" inversely correlates to the amount of Ops* present—the more Ops*, the less free ATR in solution. Using fluorescence assays and radioligand binding studies, we established the reason this occurs is because during MII decay, ATR release and rebinding are in equilibrium.

Second, we tested if any active Ops* conformers can persist after ATR release by simultaneously measuring ATR in the receptor and the conformational state of the receptor in real-time. Our results show ATR release and the reversion of Ops* to the inactive conformation occur sequentially, but not always simultaneously. The observation that an active-like Ops* state can exist even after agonist release may have wider implications for other GPCRs, and our finding that rhodopsin can bind its agonist ATR in equilibrium opens the possibility of using classical pharmacological methods to both study and ultimately target this key photoreceptor.

3.3: Experimental Procedures

3.3.1: Buffers

11-cis retinal was generously provided by Dr. R. Crouch (Medical University of South Carolina and the NEI, National Institutes of Health). 1D4 peptide (TETSQVAPA) and the $G_{t\alpha}$ fusion gene fragments were purchased from GenScript. ^{3}H-ATR (all-trans retinal [15-3H]) was purchased from American Radiolabeled Chemicals. N-dodecyl-β-D-maltopyranoside (DDM) was purchased from Anatrace. All other chemicals were purchased from either Sigma Aldrich or Fischer. Buffers used were as follows: PBSSC [137mM NaCl, 2.7mM KCl, 1.5mM KH_2PO_4, 8.0mM Na_2HPO_4, pH 7.2], Buffer B [PBSSC, 1% DDM], Buffer C [PBSSC, 1M NaCl, 2mM $MgCl_2$, 1% DDM], Buffer D

[PBSSC, 0.05% DDM], Buffer E [5mM MES, 0.05% DDM, pH 6.0], Buffer Fa [5mM MES, 1mM EDTA, 50mM HEPES, 0.025% DDM, pH 6.8], Buffer Fb [Buffer Fa, 0.2% DDM], Elution Buffer [Buffer E, 40mM NaCl].

3.3.2: Mutant generation

Single site mutations were generated by overlap extension PCR in a synthetic bovine rhodopsin gene and subcloned into the PMT4 expression vector (180,181) Sanger sequencing was used to confirm all constructs. A minimal cysteine construct (C140S, C316S, C322S, C323S) was used as background for all rhodopsins to prevent background fluorescence labeling (5,183). A stabilizing disulfide (N2C/D282C) was introduced in samples testing the ATR equilibrium hypothesis to allow for purification of detergent solubilized apoproteins (182). The $G_{t\alpha}$ C-terminal fusion (GtF) was designed and built as previously described (148).

3.3.3: Sample purification and labeling with fluorophore

Expression and purification of opsin was carried out as previously described (148). Briefly, mutant rhodopsin constructs were expressed in COS-1 cells by transient transfection. 50-65 hours later the cells were washed with PBSSC, scraped free from the plates, and snap frozen in liquid nitrogen and stored at -80°C until use. Cell pellets were thawed and solubilized in 1% DDM for an hour. The slurry was clarified by centrifugation at 100,000xg for 45min, then the supernatant was removed and incubated with 1D4 antibody beads for 3 hours or overnight in Buffer C in a 15ml conical while nutating at 4°C. The rhodopsin-bound beads were transferred to a column and then washed first with Buffer D followed by Buffer E before eluting with elution buffer. Opsin

concentration was determined by absorbance spectroscopy, using an extinction coefficient at 280nm of 56,500$cm^{-1}M^{-1}$. Quality of the samples was evaluated by their ability to bind 11CR (using 5x molar 11CR excess) by monitoring the characteristic absorbance peak at 500nm. All samples thus tested regenerated to at least 75% of the expected absorbance.

Bimane-labeled rhodopsins were prepared using a modification of previous approaches (168,181). Instead of purification as opsin, these constructs were regenerated with 16nmol/plate overnight before solubilization. After the binding of the opsins to the antibody beads and Buffer D wash, the bound proteins were washed with Buffer Fa, then incubated with ~20 molar excess monobromobimane (mBBr) for two hours at 4°C while nutating. Subsequently, the bead pack was washed with Buffer Fa, Fb, Fa, and then finally Buffer E (~30mls each). These washes were done with a 22-gauge needle affixed to the column output, to slow washing rates, thus improving free label removal. After elution, protein quality was determined by the ratio of absorbance between the protein peak at 280nm and the chromophore at 500nm. Concentration of rhodopsin was determined by the absorbance at 500nm using an extinction coefficient of 40,600$cm^{-1}M^{-1}$.

3.3.4: Absorbance spectroscopy

All UV-visual spectra were collected using a Shimadzu UV-1601 at 20°C. Rhodopsin concentration was determined using a molar extinction coefficient of 40,600 at 500nm absorbance. The samples were bleached by 25s of >500nm light from a Techni-Quip Corp T-Q/FOI-1 150W Fiber Optic Illuminator. The bleached spectra were scanned every 5 minutes for 1 hour. Temperature was maintained by an external VWR circulating water bath and confirmed by thermometer before and after each measurement.

3.3.5: Bimane emission scans

Fluorescence spectroscopy was performed using a PTI QuantaMaster steady state fluorescence system with the following modification. The excitation light was produced by an Ocean Optics LLS-405 LED source. Each measurement used 60µl of 0.5µM of rhodopsin sample and temperatures were maintained at 20°C by an external VWR 1160-A water chiller and confirmed by an Omega thermistor probe (44004). The samples were excited with a peak excitation of 405nm and the emission was scanned from 410nm to 600nm. Photobleaching was again carried out with >500nm light for 25s and scans were taken every 5min. The bimane spectra were then normalized to the maximum emission at 460nm. All analysis was performed with SigmaPlot 11.0 (Systat Software, Inc).

3.3.6: Time-resolved steady-state fluorescence spectroscopy

Retinal release and bimane changes with bleaching were observed using a dual-excitation system, as previously described. Briefly, experiments were conducted using a modified PTI QuantaMaster steady state fluorometer in which the excitation source was replaced with Ocean Optics LLS-295 LED and a LLS-405 LED. The light from these sources was attenuated using a neutral density filter (ND1.7) and directed to the sample by way of bifurcated fiber optic cable. Temperature was maintained at 20°C (unless otherwise noted) by an external VWR 1160-a water bath and constantly monitor with an Omega Thermistor probe (44004). ATR equilibrium experiments used 77µl of 0.75µM opsin was incubated with 0.5µM 11CR overnight before each experiment. Rhodopsin experiments used 0.25µM rhodopsin in 65µl.. Emission was simultaneously monitored through two separate monochromators, one set at 460nm and the other at 330nm for

detecting bimane and intrinsic tryptophan fluorescence respectively, with emission slits set at 20nm bandpass. Emission to the 330nm monochromator was additionally attenuated by a 310nm long pass filter to limit scattered light from the LLS-295 LED. For retinal release measurements, fluorescence from the samples was monitored using a cycle of 2 seconds of excitement followed by 28 seconds of rest. After ~5 minutes to ensure stable baseline has been achieved, samples were photobleached in the cuvette by 25s of >500nm light from a Techni-Quip Corp T-Q/FOI-1 150W Fiber Optic Illuminator, this cyclic excitation was repeated until the samples no longer showed a change in fluorescence. The resulting changes to fluorescence were fit to Equation 1 and the time to half max ($t_{1/2}$) for the samples was determined, as previously described (54).

$$F(t) = A(1 - e^{-bt}) + C \text{ Eq(1)}$$

For Arrhenius analysis, a series of retinal release and bimane change experiments were conducted at 10, 15, 20, 25, and 30°C and the rates from these tests were applied to the Arrhenius equation (Equation 2) to determine the activation energy (E_a) of each process (54,133,168).

$$k = Ae\text{^}(-E_a/RT) \text{ Eq(2)}$$

3.3.7: Hydroxylamine experiments

The effect of hydroxylamine hydrolysis of the photobleached sample was observed with time-resolved fluorescence spectroscopy (see above). For the retinal release from increasingly active opsins (Fig. 2), each measurement utilized 77µl of

0.5μM rhodopsin to which 4μl hydroxylamine was added from a freshly prepared 100mM buffered hydroxylamine (HA) stock (500mM MES, pH 6.0) to a final concentration of 5mM HA. This was added after the tryptophan fluorescence had initially plateaued following photoactivation to determine the maximum fluorescence by ensuring any retinal-Schiff bases are hydrolyzed. For experiments with o-tert-butyl-HA (tBHA) which cannot access the retinal binding pocket, the compound were prepared as above and included within the 77μl reaction volume at a final concentration of 10mM prior to photoactivation (209). The higher concentration was used to combat the slower reactivity of the alkylated HA. HA experiments using rhodopsin contained HA at 1mM concentration added before photoactivation. A lower concentration was used due to the high susceptibility of the protein to HA effects of protein without the stabilizing N2C/D282C disulfide which is absent from these samples to preserve a more WT-like construct.

3.3.8: Radioactive ligand binding

Tritiated ATR experiments were tested with opsin proteins regenerated with an excess of 11CR overnight (250nM opsin with 300nM 11CR) to guarantee full occupancy of the proteins. Stocks of 20nM regenerated opsin (determined by opsin concentration) and 20nM ^{3}H-ATR were incubated for ~2 hours at room temperature. During this time, half of the mixture was bleached continuously with >500nm light, while the other half was kept in the dark. The extent of ligand binding was assessed by a modification of a protocol to measure cannabinoid ligands binging to purified CB1 (212). In brief, unbound radiolabeled ATR was removed using mini size-exclusion chromatography columns that had been buffer exchanged to Elution buffer. Separation involved applying 65μl of either

the bleached or unbleached samples to the columns, then spinning the sample at 1500xg in an Eppendorf 5417C centrifuge to obtain the protein free from excess retinal. The flowthrough was then counted by liquid Scintillation to determine the amount of ^{3}H-ATR bound by the proteins.

3.4: Results

3.4.1: Stabilization of active-state opsin (Ops) prevents full retinal release*

A conformational selection model (Fig. 3.1) predicts that, after release, ATR will rebind to any receptor remaining in an active (Ops*) conformation. We tested this idea using opsin samples with varying amounts of active Ops*, monitoring the protein fluorescence increase that occurs as retinal dissociates (54).

For light-activated WT rhodopsin (11CR-bound receptor), these assays show ATR release is complete—tryptophan fluorescence increases and ultimately reaches a plateau that does not increase when hydroxylamine (HA) is added to convert ATR to ATR-oxime (which does not rebind opsin), as well as to cleave any remaining retinal-Schiff base attachments (Fig. 3.2B) (29,54,191).

In contrast, rhodopsin samples that contain stabilized Ops* due to a constitutively activating mutation M257Y (CAM) (154,168,177) do not show full ATR release. Instead, ~60% of the CAM appears to have ATR still bound under steady-state conditions (Fig. 3.2C), and thus show a large fluorescence increase upon HA addition.

Even more dramatic results are observed for rhodopsin samples that have a high-affinity analog of the $G_{t\alpha}$ C-terminus fused to their end (GtF) (148), which stabilizes the active Ops* conformation. After light activation, these samples show almost no apparent

ATR release. All rate values and percent ATR retention for Fig. 3.2 are reported in Table 3.1.

3.4.2: Equilibrium binding, rather than physical trapping, explains the lack of apparent ATR release for Ops containing samples in the retinal release assays*

Two possibilities could explain the results above. Either release is blocked in the samples with more Ops*, or the ATR is continually releasing and rebinding in equilibrium to the stabilized active receptors. To determine which is correct, we exploited a key difference between the two scenarios—retinals involved in equilibrium binding would become exposed to bulk solvent, whereas trapped retinals would not.

Thus, we repeated the ATR release assays in the presence o-tert-butyl HA (tbHA). An alkylated derivative of HA, tBHA is too big to enter the receptor binding pocket and therefore can only react with retinals that have dissociated (209). As expected, tbHA did not affect WT rhodopsin (compare Fig. 3.2E and Fig. 3.2B). However, tbHA caused complete ATR release for the CAM sample (Fig. 3.2F), and even induced ATR release from GtF, although at a slower pace, presumably because some ATR rebinds to Ops* faster than it can collide and react with tbHA (Fig. 3.2G).

These results suggest the apparent incomplete release is due to ATR leaving and rebinding the receptor, rather than being "trapped" inside the binding pocket. Consistent with this interpretation, we found the amount of ATR bound to the CAM increased with increasing amounts of exogenous ATR (Fig. 3.2I), as would be expected for equilibrium binding. Intriguingly, at higher ATR concentrations even WT opsin showed increased binding (Fig. 3.2H), suggesting this phenomenon is not exclusive to mutants with

increased Ops* populations. As expected, the ATR release profile for GtF shows no change with extra ATR, since the receptor is already fully bound with ligand (Fig. 3.2J).

3.4.3: Radioactive ligand binding studies further confirm an ATR binding equilibrium after receptor photoactivation

Radioligand binding studies further confirm that ATR equilibrium is occurring, since ATR produced inside the protein by light can exchange with exogenously added ATR (Fig. 3.3A). In these experiments, we added an equimolar amount of ^{3}H-ATR to each sample, and then measured how much of it had bound to the receptors after light activation. As shown in Fig. 3.3B, the amount of receptor-bound ^{3}H-ATR mirrored the amount of active Ops* present in the samples (Fig. 3.3B).

Expanding on this result, we tested how fast the exchange could occur for the GtF rhodopsin sample. On the surface, the GtF rhodopsin samples appear to have a stably bound ATR after light activation—they show no apparent ATR release in the fluorescence retinal release assay (Fig. 3.2D), and they have a stable Schiff base linkage as determined by a standard acid-protonation assay (Fig. 3.3D). However, within minutes after light activation, these samples show full exchange with exogenously added ^{3}H-ATR (Fig. 3.3C). Interestingly, the receptors show complete expected exchange (calculated from maximal binding experiments (data not shown)) and occurs even faster than retinal release from the WT protein ($t_{1/2}$ GtF exchange of ~5min v. $t_{1/2}$ WT ATR release ~13min).

3.4.4: Method for simultaneously measuring retinal release and the conversion from active Ops to inactive Ops receptor conformation*

Along with equilibrium binding, the conformational selection model predicts another unusual possibility—that an active-like Ops* conformation can persist following the release of bound agonist (Fig. 3.1). We tested this hypothesis by modifying the retinal release assay to simultaneously monitor the receptor conformational state and ATR release (described above). The Ops* state was monitored by tracking the large movement of transmembrane helix 6 (TM6) that occurs during receptor activation, using the Trp-induced quenching (TrIQ) technique (5). TrIQ monitors the quenching of the small fluorescent probe bimane, that only occurs when the Trp and probe are in near contact (217).

Specifically, we attached a bimane to a cysteine on the cytoplasmic end of TM6 (V250C) and introduced a Trp across from it on TM3 (V139W). Previous studies of rhodopsin (218) and the β_2AR (198) have shown activation moves this pair into close contact, resulting in a large decrease in fluorescence (see Fig. 3.4A, Ops*). During decay of MII, TM6 moves back to its starting, inactive position, resulting in a fluorescence increase as the bimane quenching is relieved (Fig. 3.4A, Ops).

Importantly, the absorbance spectra are essentially identical for the V139W/V250B and the V250B control sample. Both show complete conversion to active MII rhodopsin (indicated by the shift from 500nm to 380nm absorbance), and no optical artifacts that could affect direct comparison of their fluorescence properties (Fig. 3.4B,C).

However, their fluorescence emission spectra are strikingly different. For the control, V250B, the bimane fluorescence increases immediately after photoactivation to a

maximal value and stays constant (Fig. 3.4D,F). This increase is caused by the 500 to 380nm shift in retinal absorbance, which removes FRET from the bimane to 11CR in DS rhodopsin (219). In contrast, the V139W/V250B fluorescence does not increase immediately after photoactivation. Rather, it slowly grows with a rate closely matching the profile of retinal release (Fig. 3.4E,G), as the probe on TM6 moves close to (and is quenched by) the Trp on TM3 during MII formation (198,218), then over time returns to its initial inactive position, with a concomitant relief of quenching (198,218,219).

3.4.5: ATR dissociation and the conformational change from Ops to Ops do not always occur simultaneously*

Although TM6 movement and ATR release appear to coincide in the WT rhodopsin (Fig. 3.4G), a closer examination reveals a short, but reproducible, delay between the events (Fig. 3.5A). To see if this lag was real, and could be increased, we repeated these experiments under conditions that accelerate ATR dissociation. Two different approaches were used. First, we carried out the experiments in the presence of HA (Fig. 3.5C) to cleave the retinal-Schiff base linkages immediately after photoactivation (54). As expected, HA treatment dramatically increases the rate of ATR release. However, although TM6 movement was also accelerated in the presence of HA (Fig. 3.5C), it was noticeably delayed in comparison to ATR release.

We also tried decoupling ATR release and TM6 movement by introducing a mutation that promotes ATR dissociation. The mutation, A295S, lies immediately next to the Schiff base lysine at position 296 and greatly increases retinal release rates (133). Indeed, TM6 movement for A295S, although also accelerated, substantially lags behind ATR release (Fig. 3.5E). Together, these results support the model in Figure 1 suggesting

retinal release and conversion of Ops* to Ops are sequential, yet distinct events, with an active-like Ops* conformation transiently persisting after retinal release. All of these experiments were repeated at different temperatures, and the nearly identical results from Arrhenius analyses suggest that the underlying mechanism involved is not altered by either the introduced chemical (HA) or mutation (A295S) (Fig. 3.5B,D,F). Table 3.2 reports the retinal release rates and Arrhenius values for these conditions.

3.5: Discussion

We set out to test two novel questions about how retinal interacts with rhodopsin—can ATR released from activated rhodopsin rebind the receptor, and can an empty yet active receptor conformation (Ops*) transiently persist after ATR is released? Our results and their implications are discussed below.

3.5.1: After rhodopsin photoactivation, an equilibrium of ATR release and rebinding is established that depends on the amount of Ops present*

Binding of either transducin or arrestin can cause incomplete ATR release from photoactivated MII rhodopsin (179,191). The presumption has been that this occurs because retinal release is blocked, resulting in the ATR being "trapped" inside the receptor binding pocket (29,191,207). We find this retinal "trapping" phenomenon can be induced by simply fusing part of transducin (the $G_{t\alpha}$ subunit C-terminal tail) onto the C-terminus of rhodopsin. ATR release is completely inhibited in this mutant, GtF, (Fig. 3.2C) and only occurs upon addition of hydroxylamine (HA) to cleave the retinal-Schiff base linkage.

However, our results with M257Y, a CAM (constitutively active mutant), made us rethink what actually causes retinal "trapping." In the M257Y mutant, although no G protein mimetic is present, retinal does not completely release, but instead reaches an initial plateau that persists until HA is added. While trying to understand this result, we wondered—could the phenomenon of retinal "trapping" actually be caused by an equilibrium being established of ATR releasing and then rebinding?

We first tested this idea using the HA derivative tbHA. Like HA, tbHA chemically modifies the aldehyde moiety in ATR, converting it to a retinal-oxime that cannot rebind to the receptor. However, since tbHA is too large to enter the ligand-binding pocket (209), and thus can only modify those ATR that have exited the protein, retinal release would only be affected if release and rebinding is occurring. In agreement with previous observations, tbHA has little effect on the release of ATR from WT rhodopsin (Fig. 3.2E) (209). However, for the CAM, the tbHA completely abolished the incomplete retinal release plateau (Fig. 3.2F), and even greatly increased the rate of ATR release from the GtF sample (Fig. 3.2G).

Clearly, these results suggest retinal "trapping" is actually due to an equilibrium of ATR release and rebinding for both the CAM and the GtF samples. What could cause this equilibrium? The likely explanation is that the ATR is in flux between the different active and inactive opsin populations present in both mutant samples. Thus, in samples where the completely inactive Ops state is favored (WT), ATR appears to fully release (Fig. 3.2B). In contrast, when an active conformation is stabilized, such as the CAM, an intermediate plateau is observed (Fig. 3.2C). For GtF (the sample with the most Ops*)

ATR release appears fully prevented (Fig. 3.2D). The alteration of these release profiles by tbHA further support the equilibrium hypothesis (Fig. 3.2F, 3.2G).

Our radioligand binding experiments further confirm a retinal release-rebinding equilibrium is occurring. The ATR produced inside the receptor (by light activation) clearly exchanges with externally added, radioactively-tagged ^{3}H-ATR (Fig. 3.3), with the amount of exchange correlating with the amount of stabilized Ops* in the samples (Fig. 3.3B).

The most striking example is seen for the GtF sample. ATR appears to be fully "trapped" in GtF by the fluorescence retinal release assay (Fig. 3.2D). Moreover, the bound ATR appears to form a stable Schiff base linkage, as indicate by the shift to a ~440 nm species upon acid protonation (Fig. 3.3D). However, to our initial surprise, the ATR produced in GtF by light activation rapidly exchanges with externally added ^{3}H-ATR with full exchange being reached within minutes (Fig. 3.3C). Thus, ATR only appears to be "fully bound" because under steady-state conditions, most of the ATR is bound to receptors in Ops* conformation—the "stable" Schiff base linkage attaching ATR to GtF is actually rapidly breaking and reforming as the retinal releases and rebinds the receptor (discussed below).

In retrospect, our results are perhaps not so surprising. Although not interpreted in terms of equilibrium binding, several groups have shown a dose response for ATR-induced G protein activation and arrestin binding (30,129). The ability of ATR to bind to active-stabilized opsins has also been shown (148,154,176). Our results with WT protein (Fig. 3.2H) suggest this ability is not unique to mutants with stabilized Ops*, but a property inherent to opsin, dependent only on relative agonist concentration. How other

rhodopsin photoproducts, metarhodopsin I and III might impact this the binding equilibrium is not clear, since our detergent purified system favors MII formation (Fig. 3.3D). However, although this process may be more complicated in native rod cells, the fundamental conclusions should not change.

3.5.2: Is "retinal release" due to the protein reverting back to an inactive Ops conformation faster than the released ATR can rebind?

Our results show that the extent of apparent ATR release depends on the amount of Ops* present. What insights does this give us about the mechanism underlying ATR dissociation? One intriguing possibility is that "release" simply reflects the protein's inability to rebind the ATR agonist—when the Ops* conformation is stabilized, more ATR binding is observed in the fluorescence release assay (54,133,191).

This interpretation also raises the possibility ATR could be in flux from the moment of photoactivation, as suggested by the rapid exchange with exogenously added ^{3}H-ATR seen in GtF (Fig. 3.3C). If ATR can exchange much more frequently than previously thought, then it may be possible to outcompete the rebinding of ATR with drugs designed to either temper the activity of rhodopsin after light exposure, or alternatively, encourage ATR dissociation from hyperactive rhodopsin mutants and thus enable regeneration with 11CR and proper photocycling.

These results also present interesting implications about the instability of the covalent Schiff base linkage. Previously, based on our studies of the *retinitis pigmentosa* mutant D190N, we postulated that the Schiff base connecting the 11CR to the dark state protein may spontaneously hydrolyze but rebind due to the receptor acting as a "kinetic trap", and perturbations of this trap could lead to a decay of the photoreceptor in some

disease mutations (139). Our current results are consistent with this possibility occurring for ATR in the MII state, and with the rapid Schiff base hydrolysis ($t_{1/2}$ of ~1min) known to occur for model retinal-Schiff base compounds in solution (139).

3.5.3: Opsin can transiently retain an active-like conformation following agonist dissociation

Implicit in both the discussion above and the conformational selection model (Fig. 3.1) is the concept that ATR release and the reversion of Ops* to Ops are sequential, but distinct events. Our results simultaneously monitoring the Ops* conformation while monitoring ATR release support this idea, as they show with the decay of Ops* can lag behind agonist dissociation (Fig. 3.5A). Accelerating the release further exaggerates the disparity between the two events (Fig. 3.5C,E). Together, these data indicate an active, yet empty receptor conformation can persist after agonist release.

This time-lag between agonist release and conformational change is intriguing. Retinal-free rhodopsin is extremely inactive, showing essentially no constitutive activity (36), and hence is normally assumed to only exist as an inactive conformation (55). How then is it possible for an empty, active-like receptor conformation to transiently persist following activation? Presumably, retention of this active state reflects some sort of "protein memory," where the photoreceptor stays active in the absence of the agonist.

Such persistence of "protein memory" might also play a role in signal amplification by other GPCRs. Conformational selection-based ligand-binding mechanisms are well documented for other GPCRs including the β_2 adrenergic and CB1 receptor (198-200,220). Hence, the delay in reversion to the inactive receptor

conformation we observe in rhodopsin might play a heretofore unappreciated role in this and other GPCR signaling systems.

3.5.4: Implications for other visual GPCRs

Our results also have interesting implications for the cone opsins, the mammalian visual opsins responsible for color vision. Recently, Knox and colleagues showed that the process of ATR release from cone opsins is faster than rhodopsin, but exhibit the same activation energy (137). They interpreted these results to mean that while both photoreceptors share a similar mechanism of activation for Schiff base hydrolysis, the differences in rates indicate differences in noncovalent interactions between the retinal and the binding pocket. Our data are consistent with this idea.

Moreover, our results might also help explain other differences between rhodopsin and cone opsins. Cone opsins operate in high-light conditions and thus have to rapidly respond to new photons without losing sensitivity. Therefore their faster recovery to the inactive state (179,221,222), due to a rapid collapse to an inactive (Ops) conformation, would discourage ATR rebinding (and thus persistence of signaling), and be essential for maintaining the ability to discriminate differences in light intensity during daylight conditions (179). In comparison, the dim-light photoreceptor, rhodopsin, needs to convert a single photon to a maximal neuronal signal. Thus, opsin lingering in an active conformation after agonist release, and thus possibly activating more G proteins, would not be detrimental.

3.5.5: Conclusions

Our data provides further evidence that rhodopsin behaves like a ligand-binding GPCR. Despite the uniqueness of its covalently-bound ligand, rhodopsin appears to interact with its retinal ligands in a way consistent with a conformational selection model (148), opening the possibility of using pharmacological approaches to modulate the activity of this key photoreceptor. Additionally, our finding that the active receptor conformation can transiently persists even after release of agonist suggests a phenomenon that may also occur for other ligand-binding GPCRs.

Table 3.1: Time to half maximal ATR release and percent remaining complexes prior to HA addition

	+0.0μM ATR[a]		+0.5μM ATR		+2.0μM ATR		+tbHA[b]	
	$t_{1/2}$ (min)	% Bound	$t_{1/2}$ (min)	% Bound	$t_{1/2}$ (min)	% Bound	$t_{1/2}$ (min)	% Bound
WT[c]	12.5± 1.0[d]	4.63± 0.78	10.9± 0.52	12.1± 2.2	7.17± 0.10	30.4±5.8	10.0±2.3	-0.03±2.1
CAM	3.26± 0.37	62.5±3.1	n.d.[e]	85.6±1.4	n.d.	96.0±3.1	11.2±0.5	2.76±1.0
GtF	n.d.	103±4.3	n.d.	104±1.4	n.d.	107±0.38	24.9± 0.97	23.0±4.2

a: Exongenous ATR added before photoactivation

b: 10mM tbHA added before photoactivation

c: All experiments at 20°C, 0.5μM 11CR incubated overnight with 0.75μM opsin

d: Errors reported are standard deviations.

e: Not Determined (n.d.), rates of release from experiments showing too little initial release for a reliable fit are not reported.

Table 3.2: Retinal release, TM6 movement rates, and activation energies for constructs measuring rates of agonist release and conformational change

	Retinal Release		TM6 Movement	
	$t_{1/2}$ (min)[a]	E_A (kcal/mol)[b]	$t_{1/2}$ (min)	E_A (kcal/mol)
V250B	16.6±1.5[c]	n.d.	n.d.	n.d.
WT[d]	18.4±0.2	23.1±1.4	23.2±0.5	21.6±1.1
+HA	7.9±1.0	19.4±1.2	14.4±1.4	19.2±0.6
A295S	5.1±0.3	20.9±0.8	10.4±0.2	21.6±1.0

a: Experiments were conducted at 20°C with 0.25μM rhodopsin.

b: Activation energies were determined by Arrhenius analysis for experiments conducted at 10, 15, 20, 25, and 30°C.

c: Error reported is standard deviations

d: WT here is the V139W/V250B construct and background for the below constructs

Figure 3.1: Conformational selection model for retinal binding to opsin (148).

The focus of the current work is on the process of ATR dissociation from opsin (enclosed in the dashed circle) testing two hypotheses: first, that ATR will bind in equilibrium depending on the conformation of the opsin (i), and second, that the reversion of Ops* to Ops is distinct from the ligands presence, resulting in the possibility of an active Ops* state can transiently persist in the absence of ligand (ii).

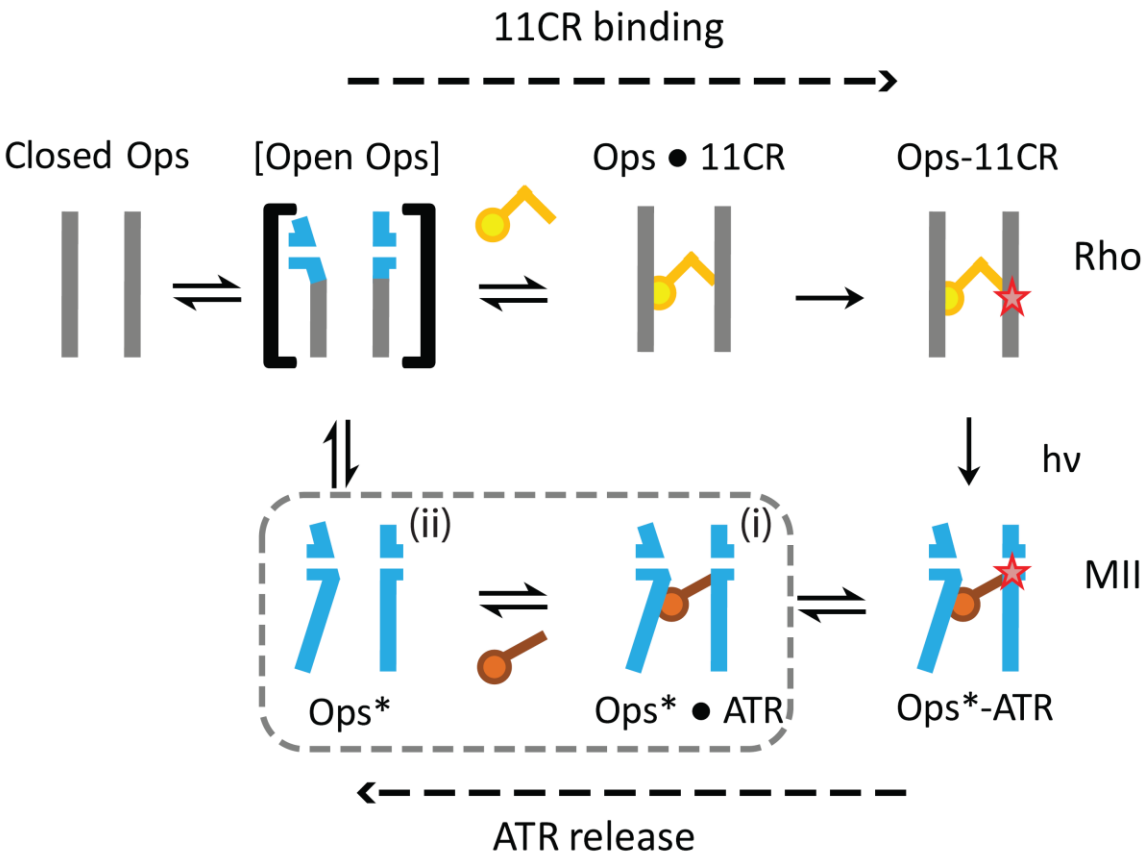
11CR binding
Closed Ops
[Open Ops]
Ops ● 11CR
Ops-11CR
Rho
hv
MII
(ii)
(i)
Ops*
Ops* ● ATR
Ops*-ATR
ATR release

Figure 3.2: Evidence that ATR released during decay of photoactivated MII rhodopsin can rebind in an Ops* dependent manner.

A) Cartoon depiction of how retinal release following light activation can be monitored by an increase in intrinsic protein fluorescence. B) Release trace from WT opsin shows a monoexpontential rise to a plateau. Hydroxylamine (HA) treatment yields no additional release, indicating full ATR dissociation. C) Release from the CAM instead results in some ATR remaining bound to the receptor in an equilibrium that is only relieved when HA is added. D) Photoactivation of GtF, a rhodopsin sample with the $G_{t\alpha}$ C-terminus fused on its end, shows no apparent ATR release until HA is added. E) Addition of tert-butyl-HA (tbHA), a HA derivative that cannot enter the binding pocket (209), had no effect on retinal release for the WT sample (compare with Fig. 2B). F) In contrast, tbHA induces full retinal release from the CAM, resulting in data nearly identical to the WT opsin. G) Similarly, the presence of tbHA induced a (slower) retinal release from GtF. Subsequent assays measured in the presence of increasing amounts of added ATR show a shift in the equilibrium to more bound ATR. H) Results for increasing [ATR] for WT rhodopsin release. I) Extra ATR further shifts the CAM towards the bound state. J) Experiments with GtF and increasing amounts of ATR show no change, as the receptor is already fully bound at the lowest ATR concentration.

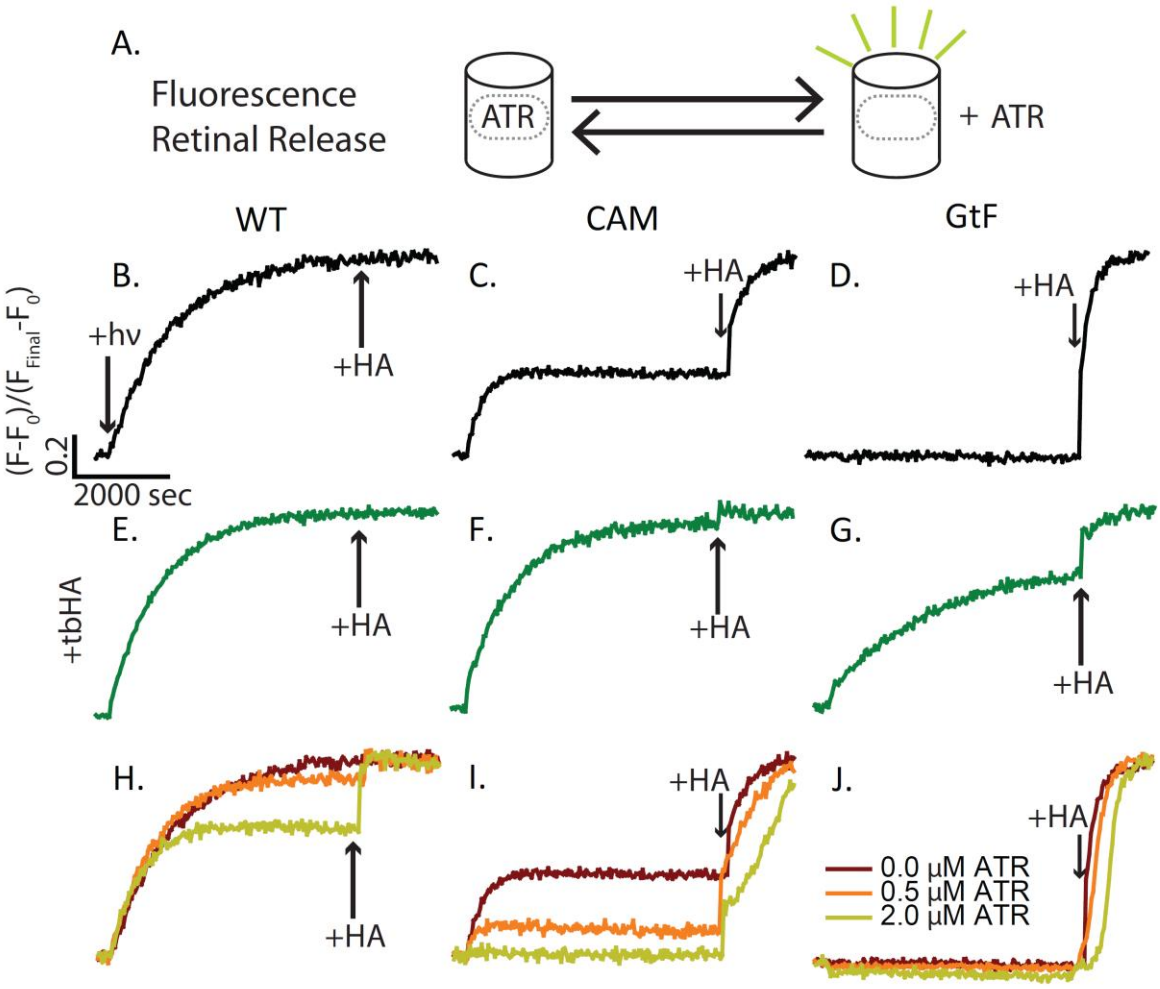
A.
Fluorescence
Retinal Release
ATR
+ ATR
WT
CAM
GtF
B.
C.
D.
+hν
+HA
+HA
+HA
(F-F0)/(FFinal-F0)
0.2
2000 sec
E.
F.
G.
+tbHA
+HA
+HA
+HA
H.
I.
J.
+HA
+HA
+HA
0.0 µM ATR
0.5 µM ATR
2.0 µM ATR

Figure 3.3: Radioligand binding experiments reveal the ATR produced inside rhodopsin by light bleaching can exchange with an equimolar amount of exogenously added, radioactive (^{3}H-ATR).

A) Cartoon depiction of the ATR exchange experiments. B) The amount of radioligand exchange for WT, CAM, and GtF rhodopsins at 2 hours after photoactivation correlates with the amount of active Ops* and retinal "trapping" seen in Figure 2. C) Time course measurement for the GtF construct shows complete and rapid ATR exchange ($t_{1/2}$~4.7min). D) Surprisingly, although GtF clearly shows exchange with exogenous ^{3}H-ATR, acid protonation experiments of the same sample show that after light activation, the ATR-Schiff base linkage in GtF is "stable" during the entire (2 hour) length of the exchange experiment (note the ~440 nm absorbing species indicating a protonated retinal Schiff base (PSB)).

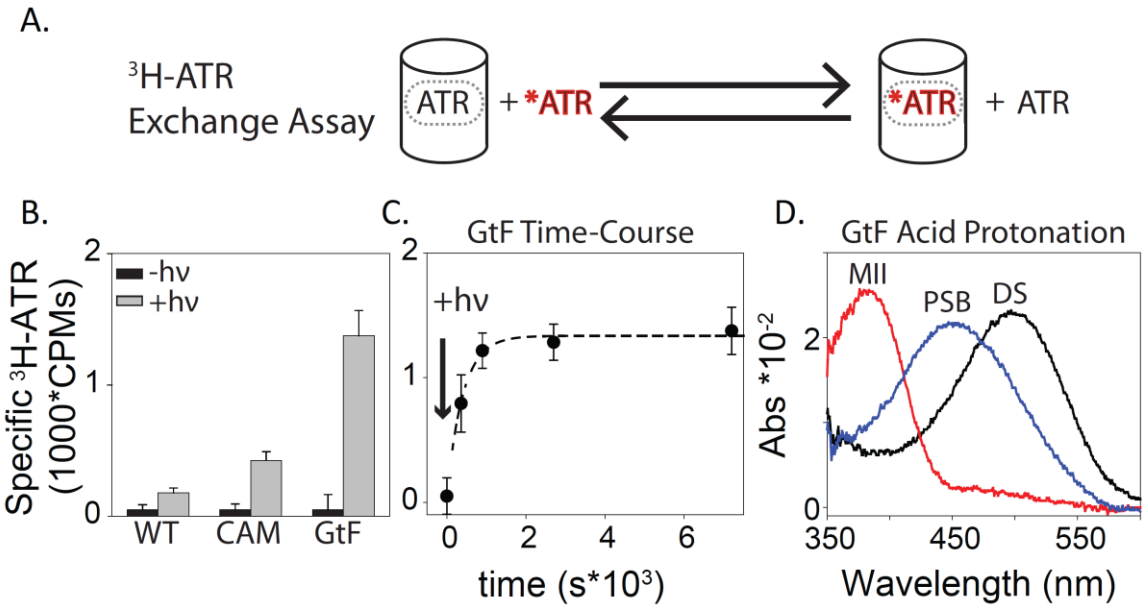
A.
^{3}H-ATR
Exchange Assay
ATR
+ *ATR
*ATR
+ ATR
B.
Specific ^{3}H-ATR
(1000*CPMs)
-hν
+hν
WT
CAM
GtF
C.
GtF Time-Course
+hν
time (s*10^3)
D.
GtF Acid Protonation
MII
PSB
DS
Abs *10^{-2}
Wavelength (nm)

Figure 3.4: Time-resolved fluorescence assay based on TrIQ for simultaneously monitoring receptor conformational changes and retinal release after rhodopsin photoactivation.

A) Model showing activation moves the bimane fluorophore (green) on TM6 into near contact with the quenching Trp (purple) on TM3. Reversion back to the inactive conformation relieves the TrIQ, causing a rise in the bimane emission. B & C) Absorbance spectra indicate both V250B (Trp-less control, (B)) and V139W/V250B (C) are WT-like in their photoactivation properties. Spectra taken before photoactivation and then every five minutes after. D & E) Bimane emission spectra following photoactivation of V250B and V139W/V250B. Spectra were taken first in the dark then every five minutes after bleach. The immediate increase for V250B is due to relief of bimane FRET to the 11CR. Note that for V139W/V250B, the initial increase is absent, rather the emission only slowly increases over time. F & G) Time-course for tryptophan ATR release (Trp fluorescence monitored at 330nm, black trace) with simultaneous measurement of bimane fluorescence (at 460nm, red trace) for V250B and V139W/V250B. A log time scale is used to enable comparison over a wide time range. For V139W/V250B, note the ATR release rate and TM6 movement are very similar, with a very small time lag. Models produced using Chimera and PDB numbers 1GZM and 3PXO (47,170,172).

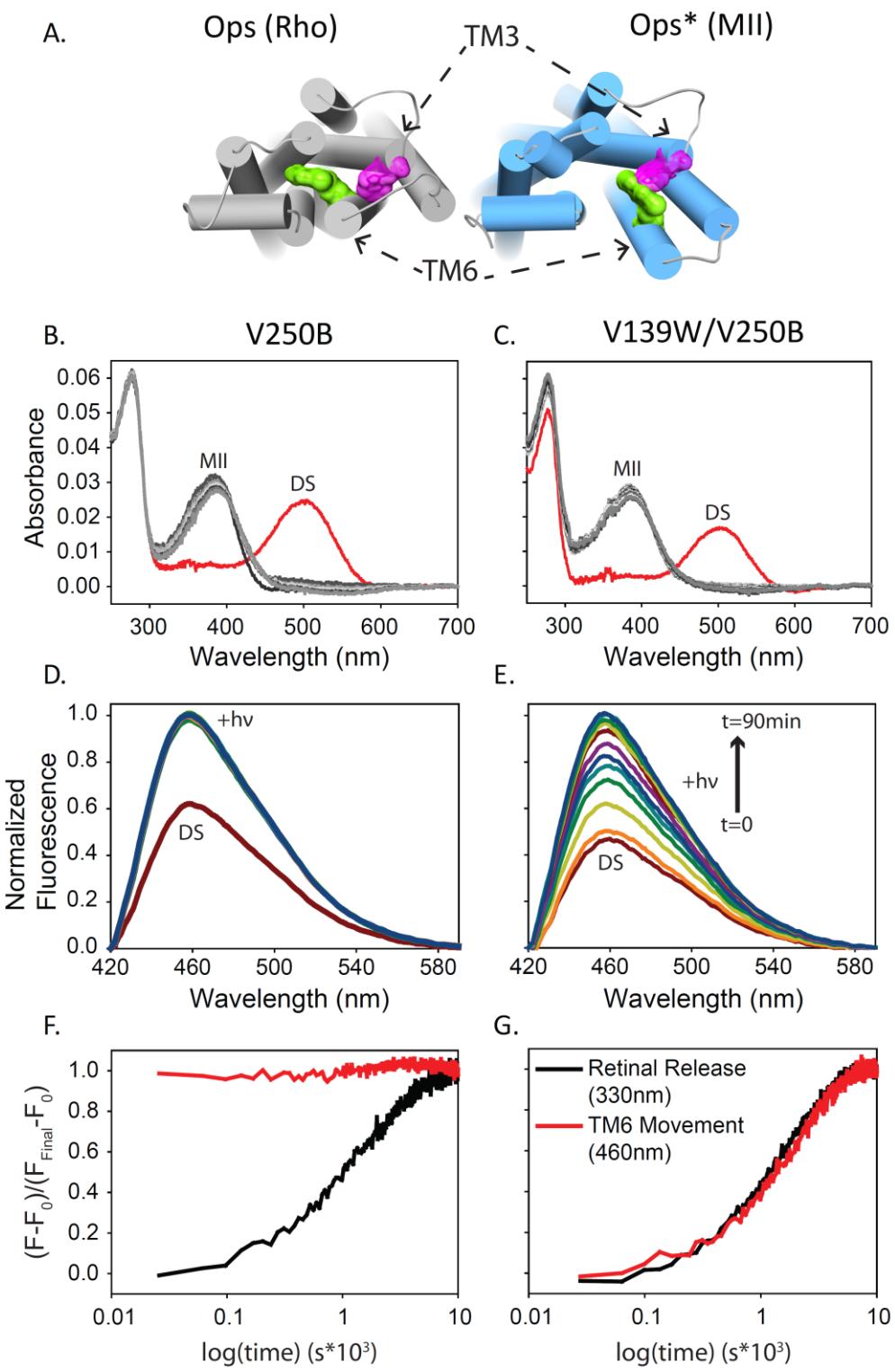
A.
Ops (Rho)
TM3
Ops* (MII)
TM6
B.
V250B
Absorbance
MII
DS
Wavelength (nm)
C.
V139W/V250B
MII
DS
Wavelength (nm)
D.
Normalized Fluorescence
+hν
DS
Wavelength (nm)
E.
t=90min
+hν
t=0
DS
Wavelength (nm)
F.
(F-F0)/(FFinal-F0)
log(time) (s*10³)
G.
Retinal Release (330nm)
TM6 Movement (460nm)
log(time) (s*10³)

Figure 3.5: The time-lag between ATR release and TM6 movement back to the inactive state is increased when retinal release is accelerated.

As with Fig. 4F&G, the plots show simultaneous measurement of tryptophan (black traces) and bimane fluorescence (red traces) as a function of time (note log time scale). A) Data for "WT" (V139W/V250B) receptor. B) Arrhenius analyses show similar activation energies for both events. C) Addition of HA accelerates retinal release faster than the TM6 movement. D) HA does not have a drastic effect on the activation energies of either process. E) Same measurements carried out on rhodopsin mutant, A295S, reveal a similar separation of ATR release and TM6 movement. F) Arrhenius analysis of this construct again shows little change in the activation energy of the two events. Errors reported as standard deviations.

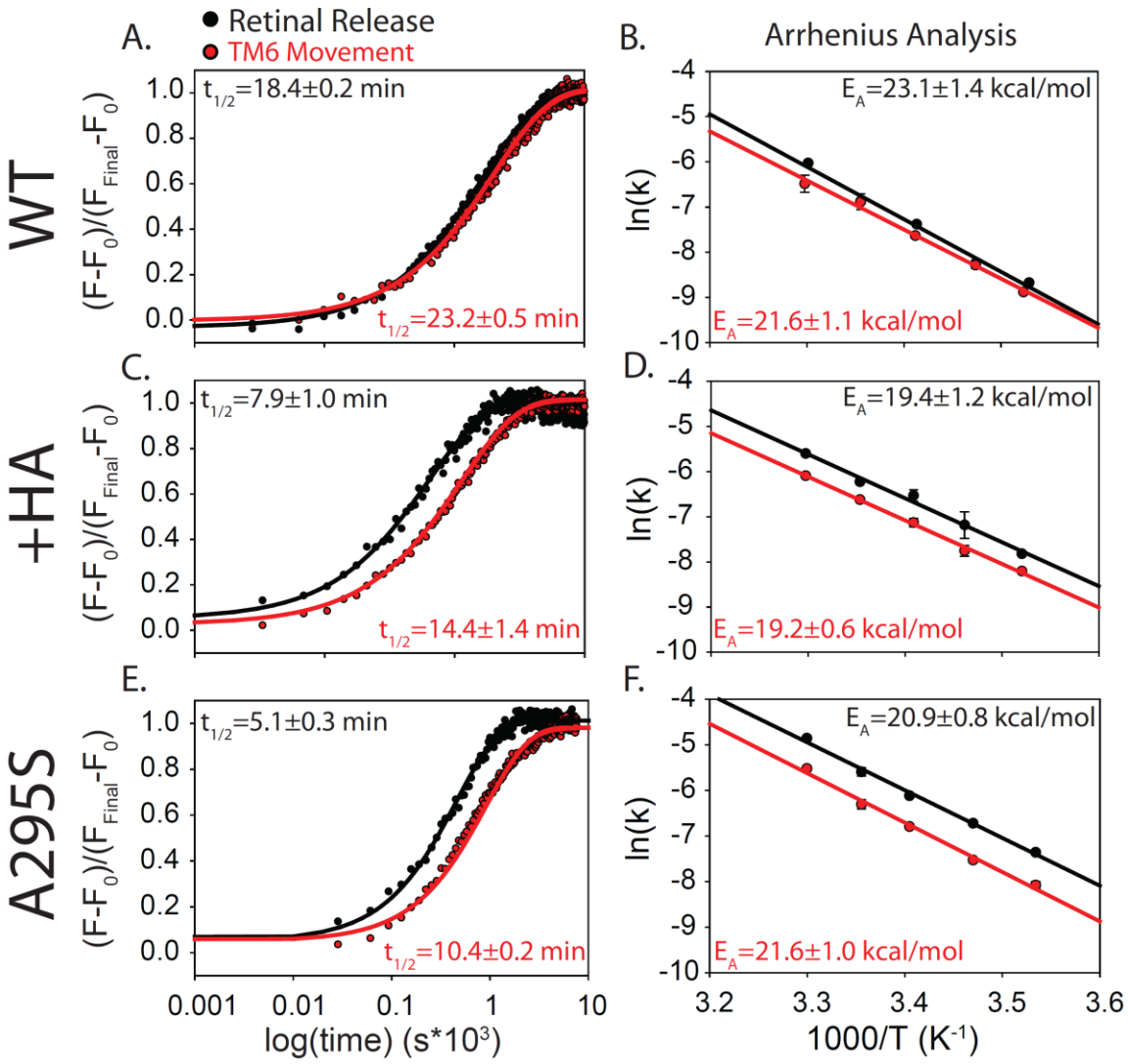
A.
Retinal Release
TM6 Movement
B.
Arrhenius Analysis
WT
+HA
A295S
C.
D.
E.
F.
t1/2=18.4±0.2 min
t1/2=23.2±0.5 min
EA=23.1±1.4 kcal/mol
EA=21.6±1.1 kcal/mol
t1/2=7.9±1.0 min
t1/2=14.4±1.4 min
EA=19.4±1.2 kcal/mol
EA=19.2±0.6 kcal/mol
t1/2=5.1±0.3 min
t1/2=10.4±0.2 min
EA=20.9±0.8 kcal/mol
EA=21.6±1.0 kcal/mol
(F-F0)/(FFinal-F0)
ln(k)
log(time) (s*10³)
1000/T (K⁻¹)

Chapter 4: Fluorescence sensor for monitoring ligand-induced arrestin and transducin interactions with bovine rhodopsin

Schafer C.T., Ramon E., Farrens D.L.

4.1: Summary

In this chapter I describe a new approach for identifying compounds that either induce or inhibit rhodopsin signaling. Our method uses Tryptophan-induced quenching (TrIQ) of fluorescence to directly monitor the binding of fragments of transducin or arrestin fused to the receptor's C-terminus. Using these biosensors, we can detect dose-dependent binding of a known agonist, all-trans retinal (ATR), as well as the non-covalent binding of an antagonist, β-ionone. Finally, we observed that these novel biosensors can monitor, in real time, the release of ATR from unlabeled, photoactivated rhodopsins. Taken together, this approach should prove useful for discovering new ligands for the visual opsin and be applicable for the study of other GPCRs.

Fluorescent sensors and fusion proteins were constructed by the author of this dissertation. All experiments using the fusions and TrIQ-based sensors were also conducted by the author along with all data analysis and interpretation. Dr. Ramon had previously produced the Lineweaver-Burke plot shown in Figure 4.4.

4.2: Introduction

G protein-coupled receptors (GPCRs) are a superfamily of integral membrane proteins that translate external stimuli, such as light and ligands, to a cellular response. Originally, GPCRs signaling was thought to only occur through G proteins, but it is now known these receptors can act through other proteins, such as arrestins (27,223). For these reasons, extensive ligand-discovery efforts continue with the aim of identifying compounds that elicit these different, or biased, effects (224,225).

Rhodopsin, the photosensitive GPCR, has been conspicuously absent from such drug-screening efforts. In part, this has been due to the unique nature of rhodopsin's ligands. Rhodopsin is held in an "off" state by a covalently bound, light-sensitive inverse agonist, called 11-cis retinal (11CR). Light-activation isomerizes the 11CR into an agonist, all-trans retinal (ATR). The combination of these unusual ligands and mode of activation has resulted in limited pharmaceutical studies of this key receptor (32,35).

However, we and others have shown that the interactions of retinals with the rhodopsin apoprotein, opsin, occurs more like classical ligand-binding GPCRs than has previously been realized (30,129,148,176). For instance, we have found that, like other GPCRs, rhodopsin discriminates between inverse agonist and agonist binding by a classic conformational selection mechanism, with the inactive conformation (Ops) preferentially binding 11CR and the active conformation (Ops*) ATR (148). Subsequently, we found that the agonist ATR binds in equilibrium with the active state protein (Chapter Three). As would be expected for a diffusible ligand-binding receptor, this equilibrium can be shifted to more bound ligand by either increasing the proportional active receptor population or simply adding more ATR (148).

With these results in mind, we set out to establish a system that can readily screen for diffusible ligands that bind opsin and alter its ability to interact with the G protein transducin (Gt) and arrestin. This approach builds on our previous discovery that the conformational state of opsin could be modulated by fusing the interacting region of Gt (the last 11 residues) directly after the C-terminal to the receptor sequence, in a construct called GtF (7,10,148,226). Here, we have further expanded this approach to include a new construct, called ArrF, in which the "finger loop" of arrestin (residues 67-79) is fused C-terminally to the receptor. Since this region of arrestin is known to bind in the same cytoplasmic cleft as the Gt C-terminus, we hypothesized it could be similarly used to stabilize the agonist ATR binding receptor conformation (26,29-31,148,227). In order to directly observe the binding of either fusion sequence to opsin, we employed the Tryptophan-induced quenching of fluorescence (TrIQ) technique, which tracks the fluorescence of a small fluorescent probe as it comes into near contact of a genetically encoded quenching Trp (217,228).

These fluorescently-labeled fusion constructs now make it possible to directly identify diffusible ligand binding that specifically impacts Gt or arrestin binding. Furthermore, we show that by introducing constitutively activating or inactivating mutations (CAMs or CIMs, respectively) into these sensors, we can improve or impair the baseline binding of the fusion regions, thus expanding the usable range over which they can detect ligands. Our data clearly show that ATR agonist binding is enhanced for both the GtF and ArrF, consistent with previous reports. Interestingly, we also find that β-ionone, a diffusible, non-covalently binding small molecule, shows antagonistic behavior towards GtF (displacing the Gt fragment from the receptor), yet shows essentially no

effect on the ability of the arrestin-fragment to be displaced from the ArrF protein, suggesting β-ionone may act as a biased ligand. Taken together, our results present a new tool for directly observing ancillary protein interactions caused by different ligands, potentially expanding the repertoire of available agents for the visual protein.

4.3: Materials and Methods

4.3.1: Buffers

11-cis retinal was generously provided by Dr. R Crouch (Medical University of South Carolina and the NEI, National Institutes of Health). 1D4 peptide (TETSQVAPA) and fusion genes were purchased from GenScript. ConA sepharose beads were purchased from GE. All other chemicals were purchased from either Sigma Aldrich or Fisher. Buffers used in this report are as follows: PBSSC [137mM NaCl, 2.7mM KCl, 1.5mM KH_2PO_4, 1mM Na_2HPO_4, pH 7.2], Buffer B [PBSSC, 1% DDM], Buffer C [PBSSC, 1M NaCl, 2mM $MgCl_2$, 1% DDM], Buffer D [PBSSC, 0.05% DDM], Buffer E [5mM MES, 0.05% DDM, pH 6.0], Elution Buffer [Buffer E, 40mM NaCl], Buffer F [5mM MES, 50mM HEPES, 5mM EDTA, 0.025% DDM, pH 6.7], Buffer F_a [5mM MES, 50mM HEPES, 5mM EDTA, 0.2% DDM, pH 6.7].

4.3.2: Mutant generation

Site-directed mutagenesis of a synthetic bovine rhodopsin gene was conducted by overlap extension PCR and subcloned into a modified version of the PMT4 expression vector and confirmed by sequencing (183). Fusion constructs were generated as

previously described (148). The ArrF sequence addition to the opsin is as follows, EEYGQEDIDVMGLSFGGGGTETSQVAPA.

4.3.3: Purification, labeling, and quality control

Proteins were transiently expressed in COS-1 cells and then purified in their apoprotein form as previously described (148,168). Briefly, the cells were scraped free from 15cm plates 50-65 hours post-transfection. After solubilization with Buffer B, the samples were spun at 100,000xg to remove the insoluble particulate. The supernatant from this spin was then incubated with beads coupled to the 1D4 antibody in Buffer C overnight. The beads were transferred to columns and washed with 100 column volumes of Buffer D followed by 100 volumes of Buffer E. Elutions were collected in Elution Buffer with 200μM 1D4-specific peptide.

For labeled samples, after transfer to the columns and washing with Buffer D, the beads were then washed with Buffer F. The columns were then capped and the beads incubated with ~20 molar excess monobromobimane (mBBr) fluorophore in Buffer F for 2 hours while nutating at 4°C. The bead pack was then washed with 50 column volumes of Buffer F, 100 column volumes of Buffer F_a, 50 column volumes Buffer F, and finally 100 column volumes of Buffer E. After labeling, a 22-gauge needle was affixed to the column tip to slow washing and to improve free label removal. Elutions were collected with Elution Buffer containing 200μM 1D4-specific peptide.

Proper folding of the opsins was verified using absorbance spectroscopy by incubating the opsin with 2.5 molar excess of 11CR and measuring the absorbance at 500nm. All samples showed greater than 75% regeneration, indicating an abundance of properly folded and functional opsin molecules. Additionally, all labeled samples were

tested for the presence of free label by TCA precipitation of the protein (229). Less than 10% free bimane was present in all samples.

Purification of native rhodopsin from bovine retinas was carried out as previously described (230). Briefly, the retinas were extensively dounced and the rod outer segment separated by sucrose gradient. The outer segments were then solubilized in DDM before being spun at 100,000xg. The proteins were then bound to ConA sepharose beads, washed, and eluted with 300mM methyl-a-d-mannopyranoside in 20mM HEPES, 140mM NaCl, 2mM $CaCl_2$, 2mM $MgCl_2$, 1mM $MnCl_2$ pH 7.0. Rhodopsin concentration was determined by the absorbance at 500nm and an extinction coefficient of 40,600cm-1M-1.

4.3.4: Steady-state fluorescence spectroscopy

Steady-state fluorescence measurements were conducted using a modified PTI Quantamaster fluorometer in which the standard arc lamp excitation source was replaced with OceanOptic LLS 295 and LLS 405 LEDs. These excitation sources have a spectral peak at 295nm and 405nm, respectively. The LED timing was tied into the shutter control by TTL signaling logic. Sample temperatures were maintained by a VWR water bath and continuously monitored using an Omega thermistor. For fluorescence spectra measured using the 405nm LED and the excitation light was tempered by a 360nm band-pass filter to removed red-edge contamination of the signal from the LED. Emission slits were set at 20nm and the spectra was read from 410-650nm. Total fluorescence for each spectrum was determined by the area under the trace.

Time-resolved fluorescence experiments simultaneously used both the 295nm and 405nm LEDs to excite intrinsic tryptophans and the bimane probes respectively. For

these experiments, the light from these LEDs was attenuated by a neutral density filter (ND 1.7) to minimize bleaching of the rhodospins. Fluorescent emissions were detected by monochrometers set to 330 and 460nm for tryptophan and bimane fluorescence, respectively. Retinal uptake experiments were conducted on the same instrument monitoring only Trp fluorescence as previously described (148).

4.3.5: Fluorescence lifetime spectroscopy

Fluorescence lifetimes of the labeled opsins were measured on a FluoTime 200 TCSPC system (PicoQuant) with a 405nm diode laser. The emission was measured at 490nm using 2.0nm slits and a 470nm long-pass filter. The instrument response function (IRF) was determined using a solution of Ludox, with a FWHM of ~64ps. Decays were analyzed using the PicoQuant FluoFit software by Lorentzian distribution to one or two exponents. The quality of the fit was assessed by a χ^2 of between 0.9 and 1.2. From this analysis the amplitude weighted lifetimes were used to calculate the components of fluorescence as previously detailed (168,217,228).

4.4: Results

4.4.1: Sensor engineering and rationale

This work details a proof-of-principal effort to design a fluorescent sensor for monitoring GPCR conformational states trialed with the visual photoreceptor, rhodopsin. The different mutations and constructs used in this work are detailed in a 2D snake plot in Figure 4.1A. These new sensor proteins build on our recent work fusing a peptide analog of the C-terminus of transducin to the end of opsin sequence (GtF) ((148), Chapter

Three), and also include a construct in which the Gt peptide sequence has been replaced with the sequence of the "finger loop" of bovine visual arrestin (amino acids 67-79) (ArrF) (26,29). Previously, we showed that a peptide corresponding to the finger loop could enhance ATR binding to opsin and here we see this effect is greatly enhanced in the ArrF fusion construct (Figure S4.1) (148). Other features common to all of these constructs include a stabilizing disulfide (N2C/D282C) to allow for detergent purification in the apoprotein form, and replacement of the four most reactive cysteines with serines (C140S/C316S/C322S/C323S) (5,182) to enable introduction of individual cysteines for subsequent specific fluorescent labeling.

The basic idea for using fluorescence to monitor ligand binding to these sensors is shown in Figure 4.1B. In brief, our approach employs a fluorescence technique called tryptophan-induced quenching of fluorescence (TrIQ). TrIQ monitors the loss of emission from a probe affixed to an engineered cysteine, in this case bimane, when a tryptophan comes into near contact (217,228). Here we have attached the bimane probe to the cytoplasmic face of the receptor and introduced a tryptophan residue into the peptide region. Whenever the fusion region (either corresponding to Gt or Arr) binds to the receptor and forms a stable complex, the fluorescence decreases, thereby directly reporting the formation of the binding conformation. Additionally, since the emission of bimane is environmentally sensitive, attaching it to the relatively immobile protein reduces changes to the local probe environment (229), thereby preventing spectral artifacts due to conformational changes that do not reflect direct fragment binding.

4.4.2: Binding of the fusion construct detected by TrIQ

As noted above, the basic strategy is to monitor the loss of bimane fluorescence when binding of the fusion tail moves the encoded Trp into contact with the fluorophore. To generate useful sensors, we thus first had to screen and identify probe-quencher pairs that exhibited substantial fluorescence quenching. Moreover, in order to create sensors that can detect antagonists, we had to introduce a constitutively activating mutation (CAM), M257Y (154,177), to promote binding of the fusion fragments in the receptor apo-state. The results of these experiments showed that approximately 80% quenching for GtF and 50% for ArrF (Figure 4.2A and D). The difference in total quenching is likely due to the different binding modes for the two interacting protein fragments which necessitated different probe-quencher pairs for each.

Reversion of the CAM back to the WT protein lowers the propensity for the opsin to be in the active conformation and weakens the interaction between the fusion sequence and the receptor. Displayed in Figure 4.2B, WT-GtF does not show a decrease in the amount of quenching compared to CAM-GtF, suggesting that the fusion is fully bound in the WT-GtF apoprotein. In contrast, the transition from CAM to WT is sufficient to dislodge the ArrF tail, relieving the quenching (Figure 4.2E). The difference likely is due to the optimized nature of the Gt sequence used for GtF, whereas the native finger loop sequence is used for ArrF.

We also tested the effect of integrating a constitutively inactivating mutation (CIM), Y223A (231,232) into the opsin sequence to reduce the receptor's affinity for the interacting peptide regions. Compared the WT and CAM-GtF discussed above, this CIM-GtF showed little difference in fluorescence between the Trp-containing and Trp-less

sample, indicating that the Gt fragment had not bound to the receptor in the apo state, and thus could be used to detect agonist-like ligands that stabilize Gt binding (Figure 4.2C). In contrast, the fluorescence emission from the CIM-ArrF and Wt-ArrF were very similar (compare Figure 4.2D and Figure 4.2F), suggesting neither sample showed binding of the Arr finger loop fragment in the apo-state. Lifetime and components of fluorescence analysis of the opsin sensors (Table 4.1) showed that the vast majority of the quenching observed was static in nature, confirming stable and direct interaction between the peptide tails and the receptors. We next tested the ability of these sensors to detect binding of a known agonist (ATR) and a small retinoid molecule known to non-covalently bind to opsin, β-ionone.

4.4.3: Agonist (ATR) binding can be detected by increased fluorescence quenching in CIM-GtF

We initially tested if the CIM-GtF could detect binding of the agonist ATR, as indicated by a drop in bimane fluorescence. This construct was chosen as it did not show the high-levels of basal fragment binding seen for both CAM-GtF and WT-GtF (Figure 4.2A and B), and thus should show the largest changes in fluorescence upon agonist binding.

Since the spectral overlap between ATR absorbance and the bimane emission could potentially affect the fluorescence of bimane at high agonist concentrations, we first measured the effect of increasing concentrations of the ATR on the control Trp-less CIM-GtF (Figure 4.3A). Indeed, as anticipated, higher ATR concentrations did cause a marked drop in bimane fluorescence, likely due to FRET from the bimane to the ATR,

attenuation of bimane light excitation due to an inner filter effect, or a combination of both.

However, the effect of ATR on the emission from the Trp-containing CIM-GtF construct was much larger than for the Trp-less control, indicating that increasing concentrations of ATR stabilized the GtF fragment binding (Figure 4.3B). Plotting the ratio of Trp-containing to Trp-less fluorescence as a function of the ATR concentration displays a classic sigmoidal response curve, as would be expected for a receptor binding a ligand in equilibrium (Figure 4.3C). Analysis of these results indicates the CIM-GtF sensor displays micromolar affinity for ATR. Note that the ratio in quenching at the highest tested concentrations matches those of the CAM and WT-GtF, suggesting that the spectral effects of the agonist are not impeding the readout.

4.4.4: Non-covalent binding of a G protein antagonist (β-ionone) causes a decrease in fluorescence quenching in the WT-GtF sensor

We next tested the ability of a putative antagonist for visual rhodopsin, β-ionone, to stabilize the inactive opsin state and dislodge the fusion tails. β-ionone is unusual small retinoid ligand that cannot form a covalent Schiff-base with opsins, and has been reported to have opposing effects on different types of opsins—sometimes acting as an agonist and other times as an antagonist for G protein activation in studies on salamander photoreceptors (233-235). For bovine visual rhodopsin, previous work has shown β-ionone can induce phosphorylation by GRK1 (189) but not Gt activation, thus for our purposes here we are classifying it as a Gt antagonist (236). To our knowledge, the effect of β-ionone on arrestin has not been reported, thus we also tested its effect on our ArrF sensor, discussed below in section 4.4.6. Note that we could not test the most

physiologically relevant inactivating ligand for rhodopsin, 11CR, as its high absorbance and strong spectral overlap with the bimane probe overwhelmed the emission from the sensor.

We first confirmed previous proposals that β-ionone acts as a competitive inhibitor for 11CR binding by carrying Lineweaver-Burke analysis. These data indicate that β-ionone therefore binds in the retinal binding pocket at a single site (Figure 4.4A) (237,238). As β-ionone is an antagonist for Gt, for these experiments we used the WT-GtF sensor to observe the loss of binding through an increase in bimane fluorescence. Compared to ATR, β-ionone has far less spectral overlap with bimane, which enables very high concentrations to be used with little effect on the fluorescent emission as determined by the Trp-less control (Figure 4.4B). In these experiments, the WT-GtF sensor exhibits a dose-dependent increase in the fluorescence of the probe with increasing β-ionone, indicating binding of this compound clearly disrupts the receptor-fragment fusion complex (Figure 4.4C). Plotting the quenching ratio compared to the β-ionone concentration reveals a slow increase in the fluorescence (Figure 4.4D). Unfortunately however, we were unable to achieve saturation conditions before the antagonist precipitated out of our detergent-buffer solution.

4.4.5: Real-time transfer of ATR from native-source rhodopsin detected by CIM-GtF sensor

We next assessed if our sensors could be used to detect increasing concentrations of ATR released from photoactivated rhodopsin in real-time. A schematic representation of this approach is shown in Figure 5.5A. In these experiments, we incubated the CIM-GtF sensor with 4x molar excess of DDM-solubilized rhodopsin from bovine rod outer

segments, and monitored potential ATR transfer by two fluorescence methods. First, we tracked the general ATR occupancy by observing intrinsic protein fluorescence (54) (Chapter Three). When bound to the receptor, ATR quenches Trp fluorescence from the protein and this quenching is relieved (resulting in increasing emission) as the ligand dissociates. The bulk protein fluorescence can be seen in Figure 5.5B as a function of time after photoactivation. Due to the large excess of WT rhodopsins that have low affinity for the ATR after agonist exit, a large increase in fluorescence is observed. Treatment with hydroxylamine (HA) both severs any remaining Schiff bases attaching ATR, and reacts with the ATR to form ATR-oxime, which has much lower affinity for the receptors (54). The further increase in the fluorescence after treatment corresponds to the release of ATR from the CIM-GtF sensors.

Probing the bimane fluorescence allows us to selectively detect any released ATR that has transferred to and bound within the sensor. Following the peak bimane fluorescence emission at 460nm shows direct correlation with quenching of the bimane probe (upon binding of the Gt fragment to the sensor receptor) with the increase in Trp fluorescence as the non-sensor rhodopsins released their ATR, indicating that the ATR is exiting the unlabeled rhodopsins and binding to the sensor (Figure 4.5C). Interestingly, a close examination of this data indicates the loss of bimane fluorescence was slightly delayed from that of the Trp. It is tempting to speculate that this delay reflects a time required for ATR to transition from a rhodopsin in one detergent micelle to a sensor in another. Addition of HA returns the bimane fluorescence to the initial value, confirming that the quenching was due to ATR binding and not some other interaction. Identical experiments with the Trp-less CIM-GtF showed little change in bimane signal for the

duration of the experiment, yet the protein signal matched that of the Trp-containing samples indicating the same transfer event is occurring without the quencher (Figure S4.2).

4.4.6: ArrF sensor increases binding with ATR yet shows little response to β-ionone

The ArrF sensors were also tested for their ability to respond to both ATR and β-ionone. As the interaction of this region of arrestin with receptor is less understood than for the C-terminal tail of Gt, we first screened all three sensors (CAM, WT, and CIM) against a relatively high concentration of either ATR (2μM, Figure 4.6A) or β-ionone (300μM, Figure 4.6B) and noted those sensors that showed the largest changes. Incubation with ATR elicited a response from all of the sensor variants; however the WT-ArrF showed a substantially greater change compared to the apoprotein and thus was chosen for further testing (Figure 4.6C). The response from this sensor is clearly sigmoidal and displays an affinity constant similar to CIM-GtF (~1μM). In contrast, the Gt antagonist β-ionone showed little effect on the binding for any of the ArrF sensors, suggesting that this the ligand does not influence arrestin binding. As no variant showed a change in fluorescence, a dose response for β-ionone binding to ArrF was not conducted.

4.5: Discussion

In the present work we report new tools for GPCR ligand discovery. These sensors are designed to enable direct observation of conformational changes in the receptor that elicit relevant ancillary protein binding. Our method combines the

specificity of the TrIQ technique with fusion constructs encoding only the protein fragments that interact with the cytoplasmic face of the receptor. Of note, we applied this unique method to the visual GPCR opsin, a protein traditionally not considered to exhibit equilibrium ligand binding. However, the results presented here, along with our previous work (148) (Chapter Three), clearly demonstrate rhodopsin can respond to ligands in a way similar to other, classical ligand-binding GPCRs. The implications of our new tool and opsin as a ligand-binding receptor are discussed below.

4.5.1: Ligand-binding can be determined by monitoring specific receptor conformations

GPCRs are known to interact and signal through both G proteins and arrestins. These two signaling methods have been shown to be selectively triggered through ligands eliciting biased agonism. With this in mind, we produced two distinct constructs for observing ligand interactions that result in G protein (GtF) or arrestin (ArrF) binding. The first ligand we tested, ATR, is a well characterized agonist for both G protein and arrestin interactions. As expected, we found that incubation with increasing concentrations of ATR stabilizes the receptor conformations capable of binding the fusion sequences.

The results from β-ionone were far more interesting. Previous reports had shown that β-ionone induces phosphorylation of bovine rhodopsin by GPCR kinase, yet also acts as an antagonist for G protein activation (189,236). Further complicating this observation are conflicting reports that β-ionone shows both G protein agonism and antagonism effects on salamander opsins (233,234). Regardless, to our knowledge the effect of β-ionone on arrestin binding has not been documented. Due to the antagonism β-ionone

displays for bovine opsin Gt activation and the induction of phosphorylation, it is tempting to speculate this small retinoid ligand may exhibit biased agonism properties.

Consistent with the previous results, we observe a stark inhibitory effect of β-ionone on G protein-coupling. Interestingly, we find no effect of β-ionone on the interaction with the fusion tail of ArrF, indicating that the ligand is not acting as an arrestin agonist; however, it also appears to not be acting as an inhibitor, but rather does not break or encourage arrestin finger loop binding. Of course these results do not remove the possibility that biased agonism requires a different region of the arrestin protein to interact with the GPCR, as has been previously speculated by electron microscopy experiments with β_2-adrenergic receptor (27). Additionally, the interface and conformational change for this latter type of arrestin interaction could be completely different from the one occupied by the finger loop, and has been proposed to involve different types of movement in TM7/H8 (220,239).

4.5.2: ATR released from photo-activated rhodopsin can transfer to a different opsin

Another interesting application of our sensor is the real-time observation of increasing ATR concentration following photoactivation of rhodopsins. Although this experiment does not demonstrate the viability of the sensor to report real amounts of ligand *in vivo*, it does clearly demonstrate that released ATR can transfer and bind to any other opsins that are still in an active-like conformation further corroborating our conclusions from Chapter 3. The effect we observe here would be extremely relevant in the context of the outer segment of the rod cell, where the concentration of rhodopsin molecules reach as high as 4.5mM (33). Therefore, activation of a subset of proteins

could result in a chain reaction of ATR dissociating and rebinding, resulting in an overly prolonged photocascade. Previously, we presented data that indicates that one of the mechanisms to prevent this continued signaling is simply the reversion of the active opsin back the native inactive apoprotein (148). However, we subsequently found evidence that even the inactive opsin could bind ATR at sufficiently high concentrations (Chapter Three). Thus relying on the natural collapse of the receptor to an inactive state is a losing strategy. This helps explains the other methods the rod cell has employed to limit ATR concentration, either through rhodopsin storage forms, such as metarhodopsin III (46) or arrestin-binding (30), or rapid chemical modification of ATR to the lower affinity retinol (129).

4.5.3: Conclusions

The present report describes novel reagents for monitoring GPCR interactions with their ligands. We propose these unique fluorescent tools represent a generalizable way to screen for potential drugs that either inhibit or enhance G protein and arrestin interactions. In addition to the potential application to other GPCRs, our results also further demonstrate that rhodopsin can behave like a traditional receptor that binds to diffusible ligands, and thus identification of novel drugs to target this key photoreceptor should be achievable.

Table 4.1: Components of fluorescence for CAM, WT, and CIM GtF and ArrF apoproteins

	γ_0[a]	γ_{DQ}[b]	γ_S[c]
CAM-GtF	0.280±0.006[d]	0.213±0.097	0.507±0.091
WT-GtF	0.232±0.028	0.074±0.119	0.694±0.124
CIM-GtF	0.864±0.086	0.074±0.092	0.062±0.141
CAM-ArrF	0.517±0.045	0.100±0.069	0.383±0.073
WT-ArrF	0.912±0.030	0.030±0.048	0.058±0.060
CIM-ArrF	1.006±0.056	0.007±0.025	-0.013±0.056

[a]: Fractional unquenched fluorescence

[b]: Fractional dynamically quenched fluorescence

[c]: Fractional statically quenching fluorescence

[d]: Errors as standard deviations

Figure 4.1: Sensor constructs and general ligand-detection scheme

General setup for using tryptophan-induced quenching (TrIQ) of the fluorescent probe bimane to detect the binding of a fused peptide corresponding to the C-terminus of transducin (GtF) or the finger loop of arrestin (ArrF). A) 2-dimensional snake plot of the GPCR rhodopsin highlighting the mutations made to the sensor constructs. These constructs contain a stabilizing disulfide (yellow) to allow for detergent-based purification, minimal cysteines (gray), and the locations of the bimane probes on the receptor (magenta) and the quenching tryptophans on the fused peptides (orange). GtF and ArrF are represented in green and purple respectively. Locations of the constitutively activating (M257Y) and inactivating (Y223A) are shown in blue. B) A cartoon of the sensor in action. Simply, a change in receptor conformation is observed by a decrease in fluorescence emission as the quenching tryptophan is brought into contact as the peptide binds.

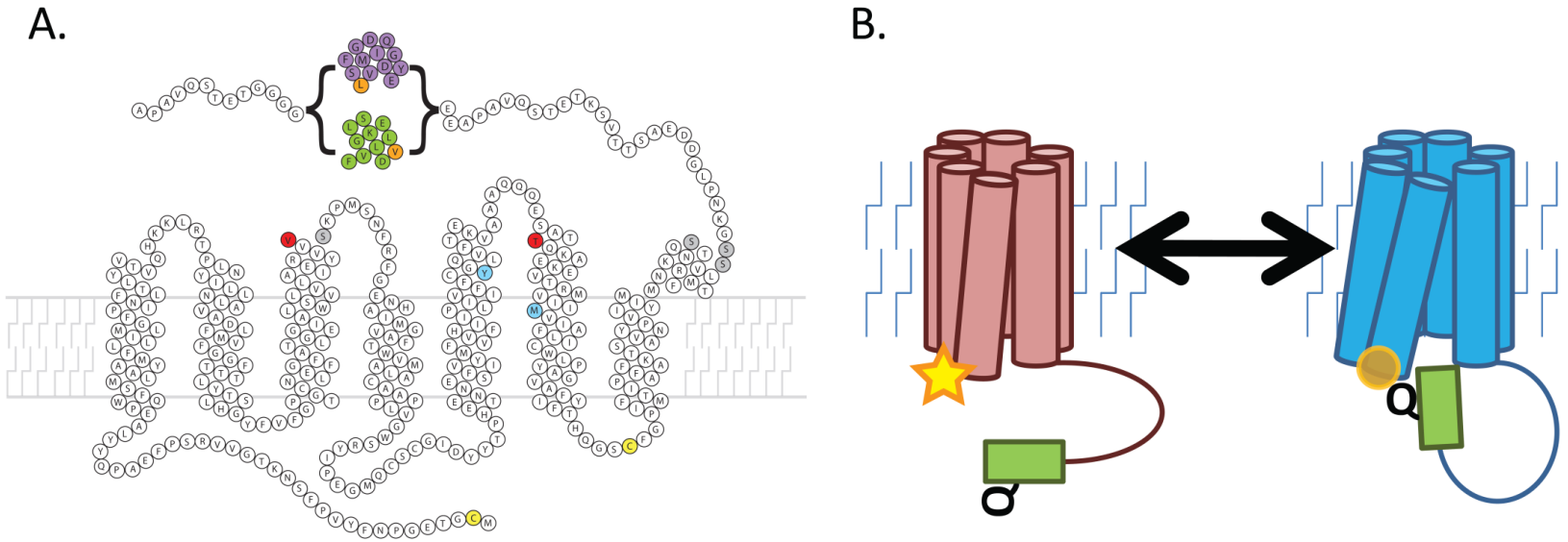
A.
B.
Q
Q

Figure 4.2: Demonstration of the GtF and ArrF TrIQ sensor detecting interactions between the opsin and the fusion tail.

The ability to couple to the fusion region was modulated by introducing constitutively activating and inactivating mutations, CAM and CIM respectively. A) The CAM-GtF sensor presented with (green) and without (brown) the tryptophan in the fusion tail. B) WT-GtF shows a similar level of quenching to the CAM-GtF, indicating that even without the high-affinity mutation, the WT opsin binds to the tail fully. C) Lowering the affinity of the receptor for the tail with a CIM completely reverses the quenching, presenting an apo-sensor with no prebinding. D, E, and F) display TrIQ results for the CAM, WT, and CIM-ArrF respectively. Unlike GtF, only the CAM-ArrF shows prebinding, whereas WT and CIM appear predominantly unbound.

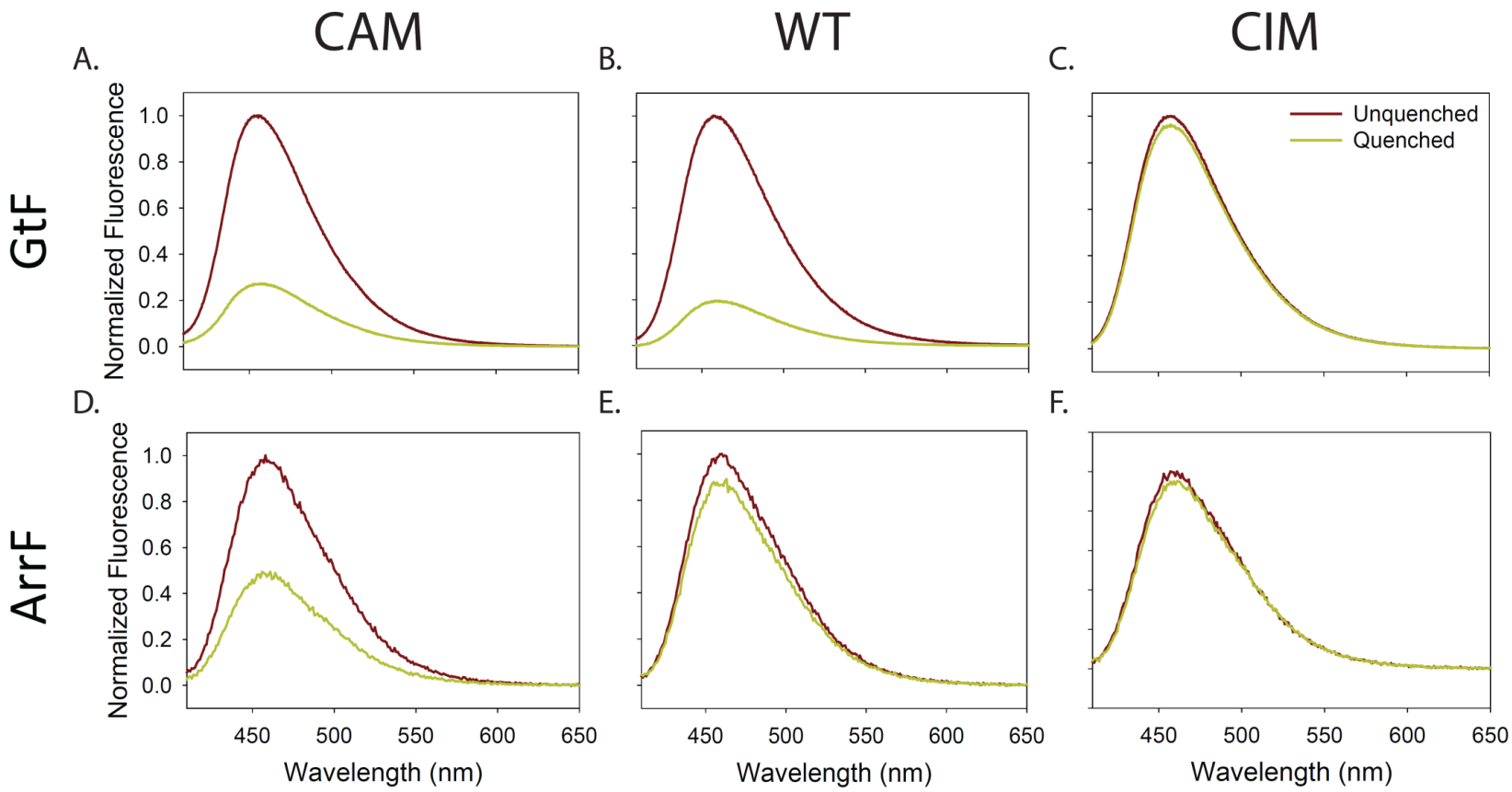
CAM
WT
CIM
A.
B.
C.
D.
E.
F.
GtF
ArrF
Normalized Fluorescence
1.0
0.8
0.6
0.4
0.2
0.0
Unquenched
Quenched
450
500
550
600
650
Wavelength (nm)

Figure 4.3: The CIM-GtF sensor reports agonist (ATR) binding in a dose dependent manner.

A) Addition of ATR has a limited effect on the bimane fluorescence for the sample without the genetically encoded tryptophan resulting from some spectral overlap between the probe and the chromophore. B) Conversely, increased ATR concentration causes a robust quenching of the bimane fluorescence in the Trp-containing sample, indicating that the agonist is stabilizing binding of the fusion tail. C) Comparing the quenching ratio ($F_{Quenched}/F_{Unquenched}$) across the concentrations tested reveals a sigmoidal dose-response curve for ATR stabilized interactions with the fusion.

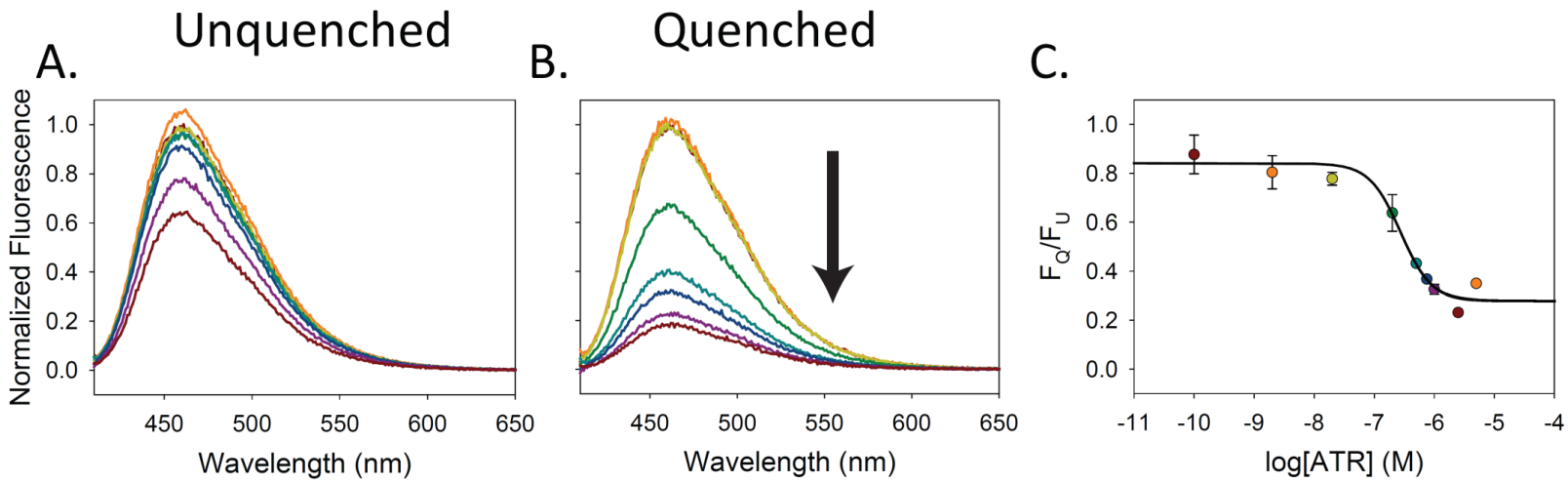
A.
Unquenched
B.
Quenched
C.
Normalized Fluorescence
1.0
0.8
0.6
0.4
0.2
0.0
450
500
550
600
650
Wavelength (nm)
Wavelength (nm)
F_Q/F_U
-11
-10
-9
-8
-7
-6
-5
-4
log[ATR] (M)

Figure 4.4: Gt antagonist binding detected by increasing sensor fluorescence

Non-covalent antagonist (β-ionone) binding to the WT-GtF sensor shows that the increased ligand concentration can dislodge the fusion binding, resulting in an increase in fluorescent emission. A) Lineweaver-Burke competition plot confirming that 11CR and β-ionone compete for the same binding site, in agreement with previous reports (237,238). B) Due to much less spectral overlap between the β-ionone and the probe, much higher concentrations can be used compared to ATR without influencing the emission as shown with the Trp-less control. C) The Trp-containing sample shows a relief of quenching as the concentration of antagonist increases, indicating a stabilization of a non-G protein coupling conformation. D) Dose response curve reflecting the increase in the quenching ratio as the concentration of β-ionone increases. Note that β-ionone began crashing out of our detergent buffer solution at around 1mM.

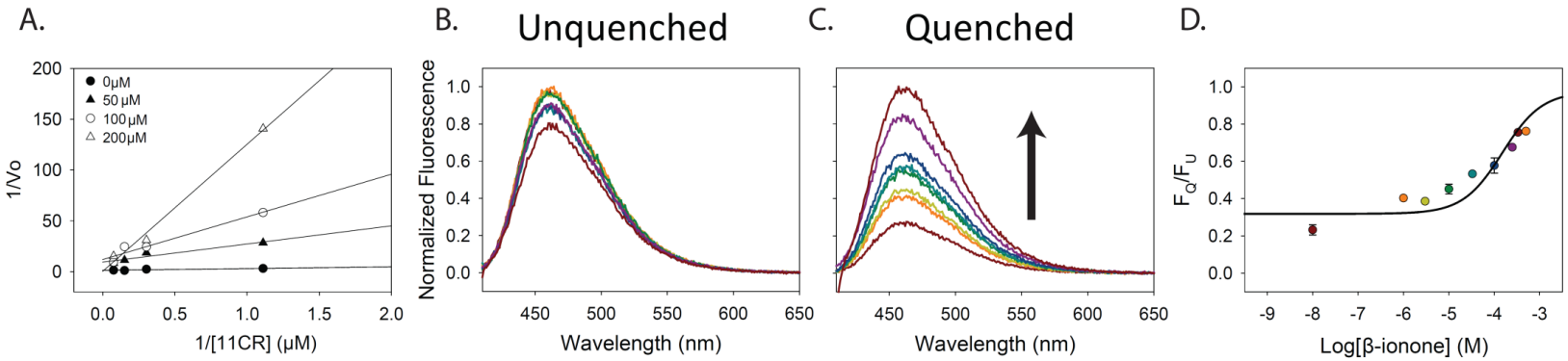
A.
B.
Unquenched
C.
Quenched
D.
1/Vo
0μM
50 μM
100 μM
200μM
1/[11CR] (μM)
Normalized Fluorescence
Wavelength (nm)
Wavelength (nm)
F_Q/F_U
Log[β-ionone] (M)

Figure 4.5: Transfer of ATR from unlabeled rhodopsins to the CIM-GtF sensor.

A) Cartoon of experimental setup, briefly, ATR from photoactivated rhodopsin dissociates from its original receptor resulting in an increase in exogenous ATR concentration. The increased concentration is reflected by a decrease in the bimane signal from the sensor. B) The bimane signal from the sensor construct observed at 460nm shows a steady decrease in fluorescence as the exogenous ATR concentration increases. Addition of hydroxylamine (HA) reverts the bimane fluorescence back to near the original emission. C) Monitoring the intrinsic Trp fluorescence during the course of the experiment reports the release of the ATR from the rhodopsins. HA causes the protein fluorescence to reach a maximum and the change reflects the dissociation of the agonist from the CIM-GtF sensors.

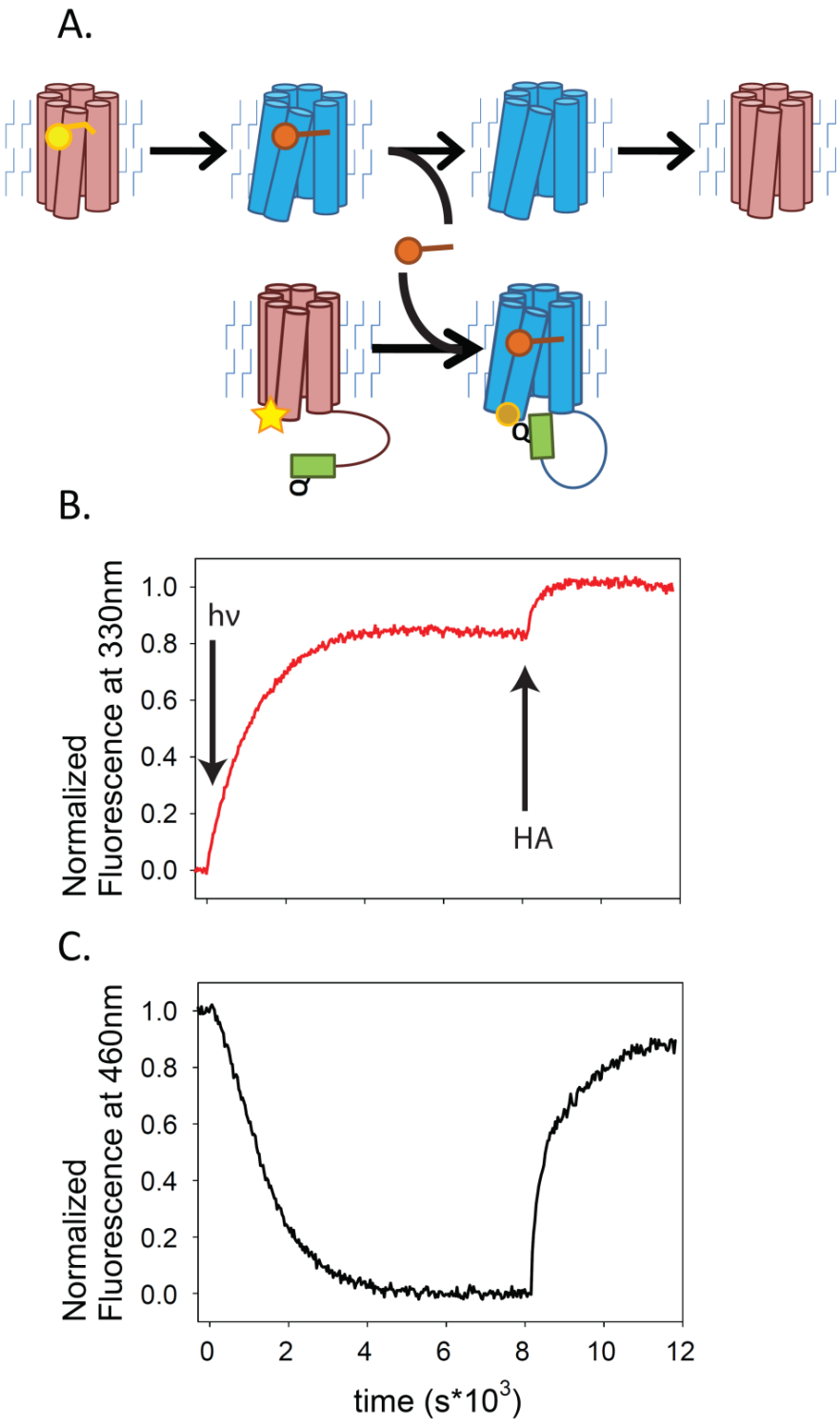
A.
Q
Q
B.
Normalized Fluorescence at 330nm
1.0
0.8
0.6
0.4
0.2
0.0
hν
HA
C.
Normalized Fluorescence at 460nm
1.0
0.8
0.6
0.4
0.2
0.0
0
2
4
6
8
10
12
time (s*10^3)

Figure 4.6: Ligand binding detected by arrestin fusion sensors

ArrF constructs can also detect increasing concentrations of ATR, however, none of the constructs show a β-ionone effect. A) Quenching ratios for CAM, WT, and CIM-ArrF constructs with and without 2μM ATR. B) Quenching ratios with or without 300μM β-ionone demonstrates that none of the constructs (CAM, WT, or CIM) show a change in fluorescence in the presence of the Gt antagonist. C) Since WT-ArrF showed the greatest change in fluorescence (see A.) we challenged the construct with increasing concentrations of ATR to create a dose response.

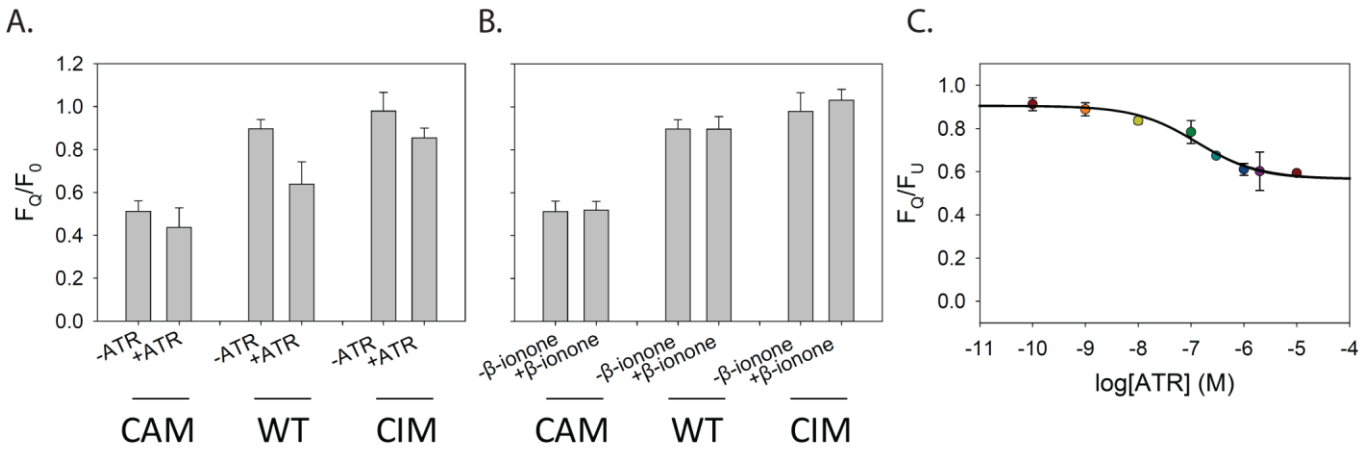
A.
B.
C.
F_Q/F_0
1.2
1.0
0.8
0.6
0.4
0.2
0.0
-ATR
+ATR
-β-ionone
+β-ionone
CAM
WT
CIM
F_Q/F_U
-11
-10
-9
-8
-7
-6
-5
-4
log[ATR] (M)

Figure S4.1: Retinal uptake by the different ArrF fusion constructs.

Uptake of 11CR and ATR by CAM (A.), WT (B.), and CIM (C.) ArrF constructs show that the arrestin fusion increases the rate of ATR binding, yet has no effect on the binding of 11CR. Experiments were conducted as described in Chapter 2 with 1:1 molar ratio of retinal to opsin, 0.1% DDM, at 10°C.

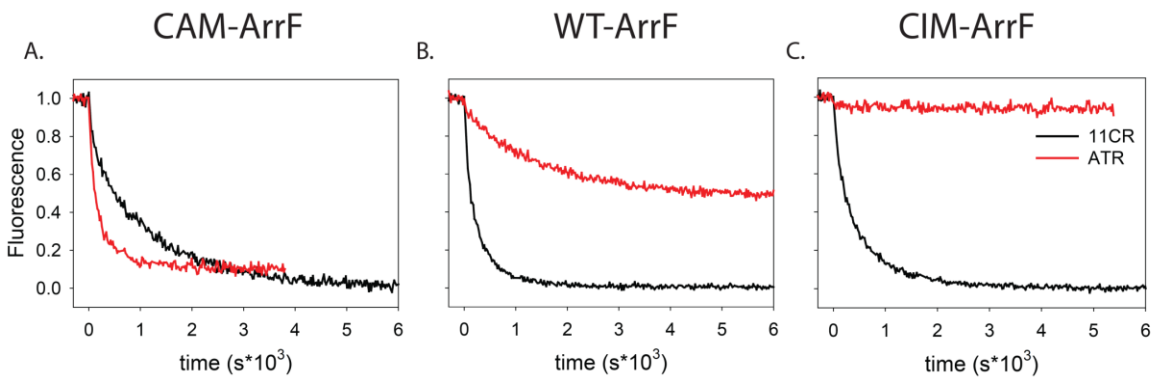
CAM-ArrF
WT-ArrF
CIM-ArrF
A.
B.
C.
Fluorescence
1.0
0.8
0.6
0.4
0.2
0.0
0
1
2
3
4
5
6
time (s*10^3)
11CR
ATR

Figure S4.2: ATR transfer from photoactivated rhodopsin to Trp-less CIM-GtF construct.

A) As no quencher is present in this system, the bimane fluorescent at 460nm doesn't show any substantial changes over the course of the experiment. B) The intrinsic Trp fluorescence reflecting the presence of the ATR in the receptors' binding pockets match the results with the Trp-containing sensor shown in Figure 4.5C.

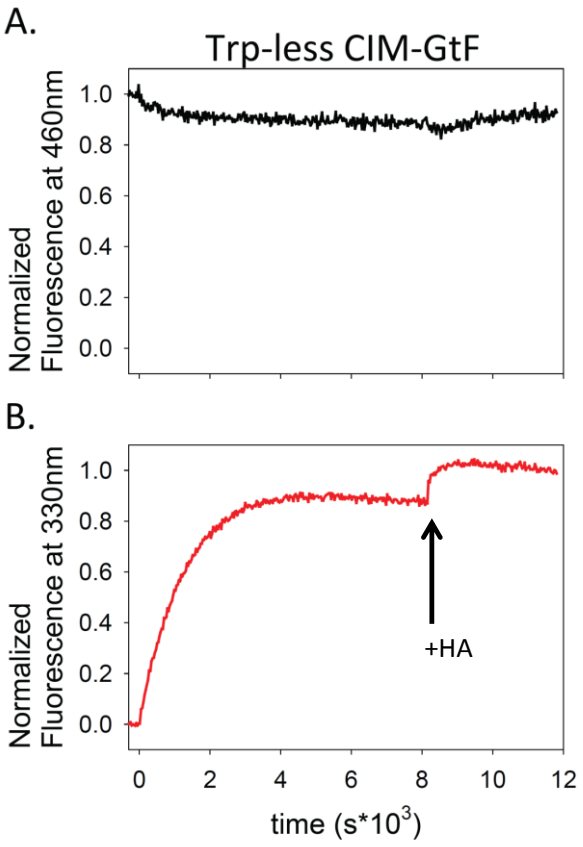
A.
Trp-less CIM-GtF
Normalized Fluorescence at 460nm
1.0
0.8
0.6
0.4
0.2
0.0
B.
Normalized Fluorescence at 330nm
1.0
0.8
0.6
0.4
0.2
0.0
+HA
0
2
4
6
8
10
12
time (s*10^3)

Chapter 5: Summary and Future Directions

5.1: Summary

In this dissertation, I have presented the results from my studies exploring how rhodopsin interacts with its native retinal ligands. The initial work, presented in Chapter 2, focused on testing a prevailing hypothesis that an active-like conformation is necessary for retinals to bind (152). My results showed that, instead of a transient activation, the retinals were discriminated by conformational selection (148). Chapter 3 expanded on our conformational selection model by probing how the conformation of the receptor influences ATR release and rebinding after photoactivation, in addition to evidence that the receptor conformation can persist in an active-like state following agonist release. Finally, in Chapter 4, I used these insights to develop a fluorescence-based ligand-binding sensor to screen for ligands that stabilize either a Gt or arrestin binding conformation.

This chapter will discuss and summarize these findings, along with touching on future questions that remain in the study of how rhodopsin interacts with its ligands.

5.1.1: Conformational selection governs retinal binding to opsin

Our studies into how 11CR enters the rhodopsin retinal binding pocket began with the hypothesis that an active-like state is required to open the protein and allow for retinal entry (152). We tested this idea by measuring binding rates of both 11CR and ATR to opsin samples containing increasing amounts of active-state receptor (148).

Unexpectedly, the results clearly displayed a conformational selection mechanism discriminates between the inverse agonist (11CR) and agonist (ATR). As the transient activation model could not be reconciled with my new experimental data, we proposed a conformational selection model that better describes retinal binding to the receptor, with the inactive Ops binding preferentially binding 11CR and the active Ops* binding ATR. This model was not unique in the world of GPCRs and had been observed for many receptors, first the B2AR and, more recently, for CB1 and the A_{2A} receptor (198-200,220,240). However, application of this model was significant for rhodopsin as it, with other studies, further supports the idea that the visual GPCR can be treated as a ligand-binding receptor (30,129,176,188). Additionally, these results are consistent with the ternary complex model for GPCR, a hallmark of GPCR interactions with agonists (19,20). We show clearly interactions with the G protein transducin kick the receptor into a high-affinity agonist binding conformation, which we have interpreted to be a fully stabilized active opsin.

5.1.2: Equilibrium binding of all-trans retinal

Extrapolating on the implications of this conformational selection model, I explored how receptor conformation also affects ATR release following photoactivation and found that stabilizing the active-like conformation (Ops*) prevented full ATR dissociation. Interestingly, the nearly completely active-state Gt fusion (GtF) displayed no ATR dissociation, in agreement with Ops* having a higher affinity for the agonist than the inactive Ops. Additional experiments revealed that the ATR is not "trapped" in the receptor, as had been previously proposed (191,207), but rather is in flux between release and rebinding, suggesting a binding equilibrium. Subsequent radioligand binding

assays supported this conclusion, as they clearly showed exchange of ATR generated by photoisomerization of 11CR inside the protein with external ATR molecules.

The latter observation has broad implications—it suggests that the Schiff base in rhodopsin, that covalently attaches the retinal to the protein, is transient, similar to what occurs for cone opsins (241-243). Therefore, ligands may possibly be identified that can outcompete the ATR in rhodopsin. So targeting the photoactivated protein is a reasonable pharmacological strategy, particularly to quell inappropriate signaling of constitutively active rhodopsin mutants (147).

5.1.3: Opsin structural states before and after retinal release

Additionally, these results present insights into the inactive Ops structure. Since an active-like conformation is not necessary, and in fact inhibitory, for 11CR binding, there must be an inactive state with an open binding pocket, that is, one that gives access for the retinal to bind. Though this should not be overly surprising, as opsin has been well characterized to be inactive (36,55,168), it does reconcile the biochemical data into a model for opsin regeneration with 11CR. Unfortunately, the only empty crystal structure is of an active Ops*, but based on the combined active and inactive structural data, we propose that the opening of the binding pocket and opening of the cytoplasmic face are separate events (3,5,6), and thus retinal binding can still occur without transient activity.

In addition to the open, inactive conformation, the results in Chapter 3 suggest that an active-like, yet empty opsin structure persists following ATR dissociation. These results imply that the protein can transiently "remember" its conformation, even in absence of agonist, despite the inactive nature of the apo-state (55,168). This protein "memory" might be necessary for signal amplification, by enabling the receptor to linger

in an active state so that the agonist that just dissociated can rebind and continue signal propagation and may be present for other GPCRs.

5.1.4: Fluorescence-based detection of ligand binding to opsin

The results discussed above reinforce the idea that rhodopsin behaves like a traditional, ligand-binding GPCR. However, there are few described ligands for rhodopsin and few that are non-retinoids (129,244). Therefore, we developed a fluorescence-based sensor system to detect critical protein-protein interactions on the cytoplasmic face elicited by different ligands. This system is detailed in Chapter 4. Specifically, the sensors are unimolecular devices that use a fluorescent probe to track the binding of the C-terminus of Gt and the finger loop of arrestin. As expected, both the Gt fusion (GtF) and finger loop fusion (ArrF) sensors show increased interactions with increasing concentrations of the agonist ATR (30,186,188). Interestingly, my tests using the small retinoid β-ionone shows different effects for GtF and ArrF. B-ionone acts as an antagonist for Gt; it does not display an effect for ArrF. With these systems, we are well poised for future opsin ligand-discovery screens, discussed below.

5.2: Future directions

In this section I will detail some future directions and follow up questions for the work presented in this dissertation.

5.2.1: How does 11CR bind to opsin?

The catalyst of this work was the question of how 11CR enters the binding pocket of rhodopsin. Although we found evidence contradicting a current model in the field (the transient activation hypothesis), the conformation selection model we proposed still does not provide a molecular mechanism for 11CR entry. Therefore, the ligand channeling model proposed by Heck, Hofmann and colleagues, remains the prevailing hypothesis (151,155). Recent computational studies further corroborate a unidirectional channeling (158), however, mutagenesis studies failed to provide support or refute this model (152). Our own attempts probing the TM5-TM6 hole by replacing the gating phenylalanines with alanines revealed a role for these residues in maintaining the rapid 11CR uptake displayed by opsin (148). Our data suggests they close to keep 11CR from escaping. Thus, how 11CR enters the protein still remains unknown. Perhaps, in the future, targeted mutagenesis around the TM1-TM7 hole coupled with our calibrated retinal uptake assay might provide insights into what role this opening might play in rhodopsin regeneration.

5.2.2: What are the features for the open Ops conformation?

As mentioned above, we proposed an open inactive opsin conformation for retinal binding in order to reconcile 11CR binding preferentially to the inactive state with crystal structure showing a completely occluded binding pocket (3,148). However, this transient state has not been structurally described and so remains hypothetical, though we propose that this state will meld aspects of the inactive and active conformations, with an inactive cytoplasmic face and an open binding pocket. To get at this idea, I conducted simple molecular dynamics simulations of an inactive apoprotein in a POPC bilayer. The results

of these experiments, detailed in Appendix Chapter 1, revealed that the binding pocket might open, even while the rest of the protein reflects the inactive conformation. These results need to be further investigated by specific spectroscopic techniques, e.g. TrIQ, and structural studies to directly observe the features of this transient state.

5.2.3: Does β-ionone exhibit biased agonism in rhodopsin?

From our work with the fluorescence sensors, it appears that β-ionone has different effects on Gt compared to arrestin. Previously, β-ionone has been shown to act as a Gt antagonist for bovine rhodopsin (236) and can induce phosphorylation of photoreceptor (189), both studies conducted in vitro. This is particularly interesting as phosphorylation is a step in receptor deactivation (53), yet the lack of Gt activity suggests the β-ionone-bound rhodopsin is already inactive. Based on this previous data, it is tempting to speculate that perhaps β-ionone is acting as a biased ligand, where, although it is antagonistic towards Gt signaling, it actually causes signaling through other pathways, such as arrestin (224). Our results in Chapter 4 suggest at minimum a different effect of β-ionone between Gt and arrestin, though it did not appear to elicit an effect on arrestin finger loop binding. However, other interactions between the receptor and arrestin have also been observed and so the sensor might be missing the relevant signaling interactions (27). Therefore, an arrestin signaling assay should be used to expand on these results and to determine if β-ionone does induce arrestin interactions (245). These results would help establish the small molecule as a tool for probing GPCR signaling using rhodopsin as a model system.

5.2.4: Do other ligands exist for rhodopsin?

There is a distinct dearth of ligands targeting the photoreceptor rhodopsin, both those that bind in the retinal binding pocket (orthosteric) or another site (allosteric). This may partially be due to the presumed permanence of the native retinal ligand binding (caused by the Schiff base) discouraging efforts to find such ligands. However, the work presented in this dissertation provides evidence that the native agonist can be displaced by an outside agent. Therefore, targeting the opsin could be a productive avenue for therapeutics treating rhodopsin-related diseases and the sensors presented in Chapter 4 could be used for a high-throughput screen of various compounds for further exploration and potential drug development.

5.3: Concluding remarks

The results presented in this dissertation provide strong evidence for treating the GPCR rhodopsin as a "traditional" liganded GPCR. The opsin protein discriminates between ATR and 11CR by conformational selection, where the agonist binds an active state and the inverse agonist prefers the inactive. Additionally, the interactions between opsin and ATR are more transient and less stable than previously realized, with the agonist existing in a binding equilibrium with active-state receptor, indicating the covalent Schiff base linkage must be breaking and reforming. These results indicate that opsin is pharmacologically targetable, thus, an effort to discover new pharmaceutical agents should be made. As first steps in this process we developed two fluorescence sensors to screen for ligands that influence either Gt or arrestin binding which will be capable of high-throughput screens for new opsin drugs. Although, approximately 30%

of approved pharmaceuticals target GPCRs (2), rhodopsin has not yet been targeted due to the assumed permanency of the Schiff base with the retinal ligand. The work presented in this dissertation conclusively display that the dim-light photoreceptor is targetable and should be the subject of future pharmaceutical development.

References

1. Lagerstrom, M. C., and Schioth, H. B. (2008) Structural diversity of G protein-coupled receptors and significance for drug discovery. *Nature reviews. Drug discovery* **7**, 339-357
2. Brogi, S., Tafi, A., Desaubry, L., and Nebigil, C. G. (2014) Discovery of GPCR ligands for probing signal transduction pathways. *Frontiers in pharmacology* **5**, 255
3. Palczewski, K., Kumasaka, T., Hori, T., Behnke, C. A., Motoshima, H., Fox, B. A., Le Trong, I., Teller, D. C., Okada, T., Stenkamp, R. E., Yamamoto, M., and Miyano, M. (2000) Crystal structure of rhodopsin: A G protein-coupled receptor. *Science* **289**, 739-745
4. Fredriksson, R., Lagerstrom, M. C., Lundin, L. G., and Schioth, H. B. (2003) The G-protein-coupled receptors in the human genome form five main families. Phylogenetic analysis, paralogon groups, and fingerprints. *Molecular pharmacology* **63**, 1256-1272
5. Farrens, D. L., Altenbach, C., Yang, K., Hubbell, W. L., and Khorana, H. G. (1996) Requirement of rigid-body motion of transmembrane helices for light activation of rhodopsin. *Science* **274**, 768-770
6. Park, J. H., Scheerer, P., Hofmann, K. P., Choe, H. W., and Ernst, O. P. (2008) Crystal structure of the ligand-free G-protein-coupled receptor opsin. *Nature* **454**, 183-187
7. Scheerer, P., Park, J. H., Hildebrand, P. W., Kim, Y. J., Krauss, N., Choe, H. W., Hofmann, K. P., and Ernst, O. P. (2008) Crystal structure of opsin in its G-protein-interacting conformation. *Nature* **455**, 497-502
8. Weis, W. I., and Kobilka, B. K. (2008) Structural insights into G-protein-coupled receptor activation. *Current opinion in structural biology* **18**, 734-740
9. Deupi, X. (2014) Relevance of rhodopsin studies for GPCR activation. *Biochimica et biophysica acta* **1837**, 674-682
10. Janz, J. M., and Farrens, D. L. (2004) Rhodopsin activation exposes a key hydrophobic binding site for the transducin alpha-subunit C terminus. *The Journal of biological chemistry* **279**, 29767-29773
11. Rasmussen, S. G., DeVree, B. T., Zou, Y., Kruse, A. C., Chung, K. Y., Kobilka, T. S., Thian, F. S., Chae, P. S., Pardon, E., Calinski, D., Mathiesen, J. M., Shah, S. T., Lyons, J. A., Caffrey, M., Gellman, S. H., Steyaert, J., Skiniotis, G., Weis, W. I., Sunahara, R. K., and Kobilka, B. K. (2011) Crystal structure of the beta2 adrenergic receptor-Gs protein complex. *Nature* **477**, 549-555

12. Dratz, E. A., Furstenau, J. E., Lambert, C. G., Thireault, D. L., Rarick, H., Schepers, T., Pakhlevaniants, S., and Hamm, H. E. (1993) NMR structure of a receptor-bound G-protein peptide. *Nature* **363**, 276-281

13. Bourne, H. R., Sanders, D. A., and McCormick, F. (1991) The GTPase superfamily: conserved structure and molecular mechanism. *Nature* **349**, 117-127

14. Bourne, H. R., Sanders, D. A., and McCormick, F. (1990) The GTPase superfamily: a conserved switch for diverse cell functions. *Nature* **348**, 125-132

15. Hamm, H. E. (1998) The many faces of G protein signaling. *The Journal of biological chemistry* **273**, 669-672

16. Hamm, H. E. (2001) How activated receptors couple to G proteins. *Proceedings of the National Academy of Sciences of the United States of America* **98**, 4819-4821

17. Hecht, S., Shlaer, S., and Pirenne, M. H. (1942) Energy, Quanta, and Vision. *The Journal of general physiology* **25**, 819-840

18. Pugh, E. N., Jr., and Lamb, T. D. (1993) Amplification and kinetics of the activation steps in phototransduction. *Biochimica et biophysica acta* **1141**, 111-149

19. De Lean, A., Stadel, J. M., and Lefkowitz, R. J. (1980) A ternary complex model explains the agonist-specific binding properties of the adenylate cyclase-coupled beta-adrenergic receptor. *The Journal of biological chemistry* **255**, 7108-7117

20. Samama, P., Cotecchia, S., Costa, T., and Lefkowitz, R. J. (1993) A mutation-induced activated state of the beta 2-adrenergic receptor. Extending the ternary complex model. *The Journal of biological chemistry* **268**, 4625-4636

21. Palczewski, K., Buczylko, J., Imami, N. R., McDowell, J. H., and Hargrave, P. A. (1991) Role of the carboxyl-terminal region of arrestin in binding to phosphorylated rhodopsin. *The Journal of biological chemistry* **266**, 15334-15339

22. Palczewski, K., and Benovic, J. L. (1991) G-protein-coupled receptor kinases. *Trends in biochemical sciences* **16**, 387-391

23. Palczewski, K. (1994) Structure and functions of arrestins. *Protein science : a publication of the Protein Society* **3**, 1355-1361

24. Wilden, U., Hall, S. W., and Kuhn, H. (1986) Phosphodiesterase activation by photoexcited rhodopsin is quenched when rhodopsin is phosphorylated and binds the intrinsic 48-kDa protein of rod outer segments. *Proceedings of the National Academy of Sciences of the United States of America* **83**, 1174-1178

25. Granzin, J., Stadler, A., Cousin, A., Schlesinger, R., and Batra-Safferling, R. (2015) Structural evidence for the role of polar core residue Arg175 in arrestin activation. *Scientific reports* **5**, 15808

26. Hanson, S. M., Francis, D. J., Vishnivetskiy, S. A., Kolobova, E. A., Hubbell, W. L., Klug, C. S., and Gurevich, V. V. (2006) Differential interaction of spin-

labeled arrestin with inactive and active phosphorhodopsin. *Proceedings of the National Academy of Sciences of the United States of America* **103**, 4900-4905

27. Shukla, A. K., Westfield, G. H., Xiao, K., Reis, R. I., Huang, L. Y., Tripathi-Shukla, P., Qian, J., Li, S., Blanc, A., Oleskie, A. N., Dosey, A. M., Su, M., Liang, C. R., Gu, L. L., Shan, J. M., Chen, X., Hanna, R., Choi, M., Yao, X. J., Klink, B. U., Kahsai, A. W., Sidhu, S. S., Koide, S., Penczek, P. A., Kossiakoff, A. A., Woods, V. L., Jr., Kobilka, B. K., Skiniotis, G., and Lefkowitz, R. J. (2014) Visualization of arrestin recruitment by a G-protein-coupled receptor. *Nature* **512**, 218-222

28. Pulvermuller, A., Schroder, K., Fischer, T., and Hofmann, K. P. (2000) Interactions of metarhodopsin II. Arrestin peptides compete with arrestin and transducin. *The Journal of biological chemistry* **275**, 37679-37685

29. Sinha, A., Jones Brunette, A. M., Fay, J. F., Schafer, C. T., and Farrens, D. L. (2014) Rhodopsin TM6 can interact with two separate and distinct sites on arrestin: evidence for structural plasticity and multiple docking modes in arrestin-rhodopsin binding. *Biochemistry* **53**, 3294-3307

30. Sommer, M. E., Hofmann, K. P., and Heck, M. (2012) Distinct loops in arrestin differentially regulate ligand binding within the GPCR opsin. *Nature communications* **3**, 995

31. Kang, Y., Zhou, X. E., Gao, X., He, Y., Liu, W., Ishchenko, A., Barty, A., White, T. A., Yefanov, O., Han, G. W., Xu, Q., de Waal, P. W., Ke, J., Tan, M. H., Zhang, C., Moeller, A., West, G. M., Pascal, B. D., Van Eps, N., Caro, L. N., Vishnivetskiy, S. A., Lee, R. J., Suino-Powell, K. M., Gu, X., Pal, K., Ma, J., Zhi, X., Boutet, S., Williams, G. J., Messerschmidt, M., Gati, C., Zatsepin, N. A., Wang, D., James, D., Basu, S., Roy-Chowdhury, S., Conrad, C. E., Coe, J., Liu, H., Lisova, S., Kupitz, C., Grotjohann, I., Fromme, R., Jiang, Y., Tan, M., Yang, H., Li, J., Wang, M., Zheng, Z., Li, D., Howe, N., Zhao, Y., Standfuss, J., Diederichs, K., Dong, Y., Potter, C. S., Carragher, B., Caffrey, M., Jiang, H., Chapman, H. N., Spence, J. C., Fromme, P., Weierstall, U., Ernst, O. P., Katritch, V., Gurevich, V. V., Griffin, P. R., Hubbell, W. L., Stevens, R. C., Cherezov, V., Melcher, K., and Xu, H. E. (2015) Crystal structure of rhodopsin bound to arrestin by femtosecond X-ray laser. *Nature* **523**, 561-567

32. Palczewski, K. (2012) Chemistry and biology of vision. *The Journal of biological chemistry* **287**, 1612-1619

33. Nickell, S., Park, P. S., Baumeister, W., and Palczewski, K. (2007) Three-dimensional architecture of murine rod outer segments determined by cryoelectron tomography. *The Journal of cell biology* **177**, 917-925

34. Baylor, D. A., Lamb, T. D., and Yau, K. W. (1979) Responses of retinal rods to single photons. *The Journal of physiology* **288**, 613-634

35. Wald, G. (1968) The molecular basis of visual excitation. *Nature* **219**, 800-807

36. Surya, A., Foster, K. W., and Knox, B. E. (1995) Transducin activation by the bovine opsin apoprotein. *The Journal of biological chemistry* **270**, 5024-5031

37. Melia, T. J., Jr., Cowan, C. W., Angleson, J. K., and Wensel, T. G. (1997) A comparison of the efficiency of G protein activation by ligand-free and light-activated forms of rhodopsin. *Biophysical journal* **73**, 3182-3191

38. Fan, J., Woodruff, M. L., Cilluffo, M. C., Crouch, R. K., and Fain, G. L. (2005) Opsin activation of transduction in the rods of dark-reared Rpe65 knockout mice. *The Journal of physiology* **568**, 83-95

39. Okada, T., Ernst, O. P., Palczewski, K., and Hofmann, K. P. (2001) Activation of rhodopsin: new insights from structural and biochemical studies. *Trends in biochemical sciences* **26**, 318-324

40. Hubbell, W. L., Altenbach, C., Hubbell, C. M., and Khorana, H. G. (2003) Rhodopsin structure, dynamics, and activation: a perspective from crystallography, site-directed spin labeling, sulfhydryl reactivity, and disulfide cross-linking. *Advances in protein chemistry* **63**, 243-290

41. Ernst, O. P., and Bartl, F. J. (2002) Active states of rhodopsin. *Chembiochem : a European journal of chemical biology* **3**, 968-974

42. Ye, S., Zaitseva, E., Caltabiano, G., Schertler, G. F., Sakmar, T. P., Deupi, X., and Vogel, R. (2010) Tracking G-protein-coupled receptor activation using genetically encoded infrared probes. *Nature* **464**, 1386-1389

43. Ruprecht, J. J., Mielke, T., Vogel, R., Villa, C., and Schertler, G. F. (2004) Electron crystallography reveals the structure of metarhodopsin I. *The EMBO journal* **23**, 3609-3620

44. Wald, G., and Brown, P. K. (1953) The molar extinction of rhodopsin. *The Journal of general physiology* **37**, 189-200

45. Vogel, R., Siebert, F., Zhang, X. Y., Fan, G., and Sheves, M. (2004) Formation of Meta III during the decay of activated rhodopsin proceeds via Meta I and not via Meta II. *Biochemistry* **43**, 9457-9466

46. Heck, M., Schadel, S. A., Maretzki, D., Bartl, F. J., Ritter, E., Palczewski, K., and Hofmann, K. P. (2003) Signaling states of rhodopsin. Formation of the storage form, metarhodopsin III, from active metarhodopsin II. *The Journal of biological chemistry* **278**, 3162-3169

47. Choe, H. W., Kim, Y. J., Park, J. H., Morizumi, T., Pai, E. F., Krauss, N., Hofmann, K. P., Scheerer, P., and Ernst, O. P. (2011) Crystal structure of metarhodopsin II. *Nature* **471**, 651-655

48. Ridge, K. D., Abdulaev, N. G., Sousa, M., and Palczewski, K. (2003) Phototransduction: crystal clear. *Trends in biochemical sciences* **28**, 479-487

49. Beavo, J. A. (1995) Cyclic nucleotide phosphodiesterases: functional implications of multiple isoforms. *Physiological reviews* **75**, 725-748

50. Fain, G. L., Matthews, H. R., Cornwall, M. C., and Koutalos, Y. (2001) Adaptation in vertebrate photoreceptors. *Physiological reviews* **81**, 117-151

51. Ebrey, T., and Koutalos, Y. (2001) Vertebrate photoreceptors. *Progress in retinal and eye research* **20**, 49-94

52. Polans, A., Baehr, W., and Palczewski, K. (1996) Turned on by Ca2+! The physiology and pathology of Ca(2+)-binding proteins in the retina. *Trends in neurosciences* **19**, 547-554

53. Palczewski, K., and Saari, J. C. (1997) Activation and inactivation steps in the visual transduction pathway. *Current opinion in neurobiology* **7**, 500-504

54. Farrens, D. L., and Khorana, H. G. (1995) Structure and function in rhodopsin. Measurement of the rate of metarhodopsin II decay by fluorescence spectroscopy. *The Journal of biological chemistry* **270**, 5073-5076

55. Vogel, R., and Siebert, F. (2001) Conformations of the active and inactive states of opsin. *The Journal of biological chemistry* **276**, 38487-38493

56. Klein-Seetharaman, J., Getmanova, E. V., Loewen, M. C., Reeves, P. J., and Khorana, H. G. (1999) NMR spectroscopy in studies of light-induced structural changes in mammalian rhodopsin: applicability of solution (19)F NMR. *Proceedings of the National Academy of Sciences of the United States of America* **96**, 13744-13749

57. Maeda, A., Maeda, T., Golczak, M., Chou, S., Desai, A., Hoppel, C. L., Matsuyama, S., and Palczewski, K. (2009) Involvement of all-trans-retinal in acute light-induced retinopathy of mice. *The Journal of biological chemistry* **284**, 15173-15183

58. Anderson, R. E., and Maude, M. B. (1970) Phospholipids of bovine outer segments. *Biochemistry* **9**, 3624-3628

59. Ben-Shabat, S., Parish, C. A., Vollmer, H. R., Itagaki, Y., Fishkin, N., Nakanishi, K., and Sparrow, J. R. (2002) Biosynthetic studies of A2E, a major fluorophore of retinal pigment epithelial lipofuscin. *The Journal of biological chemistry* **277**, 7183-7190

60. Maeda, A., Maeda, T., Imanishi, Y., Kuksa, V., Alekseev, A., Bronson, J. D., Zhang, H., Zhu, L., Sun, W., Saperstein, D. A., Rieke, F., Baehr, W., and Palczewski, K. (2005) Role of photoreceptor-specific retinol dehydrogenase in the retinoid cycle in vivo. *The Journal of biological chemistry* **280**, 18822-18832

61. Maeda, A., Maeda, T., Imanishi, Y., Sun, W., Jastrzebska, B., Hatala, D. A., Winkens, H. J., Hofmann, K. P., Janssen, J. J., Baehr, W., Driessen, C. A., and Palczewski, K. (2006) Retinol dehydrogenase (RDH12) protects photoreceptors from light-induced degeneration in mice. *The Journal of biological chemistry* **281**, 37697-37704

62. Kurth, I., Thompson, D. A., Ruther, K., Feathers, K. L., Chrispell, J. D., Schroth, J., McHenry, C. L., Schweizer, M., Skosyrski, S., Gal, A., and Hubner, C. A. (2007) Targeted disruption of the murine retinal dehydrogenase gene Rdh12 does not limit visual cycle function. *Molecular and cellular biology* **27**, 1370-1379

63. Maeda, A., Maeda, T., Sun, W., Zhang, H., Baehr, W., and Palczewski, K. (2007) Redundant and unique roles of retinol dehydrogenases in the mouse retina. *Proceedings of the National Academy of Sciences of the United States of America* **104**, 19565-19570

64. Chen, C., Thompson, D. A., and Koutalos, Y. (2012) Reduction of all-trans-retinal in vertebrate rod photoreceptors requires the combined action of RDH8 and RDH12. *The Journal of biological chemistry* **287**, 24662-24670

65. Quazi, F., Lenevich, S., and Molday, R. S. (2012) ABCA4 is an N-retinylidene-phosphatidylethanolamine and phosphatidylethanolamine importer. *Nature communications* **3**, 925

66. Gonzalez-Fernandez, F. (2002) Evolution of the visual cycle: the role of retinoid-binding proteins. *The Journal of endocrinology* **175**, 75-88

67. Gonzalez-Fernandez, F. (2003) Interphotoreceptor retinoid-binding protein--an old gene for new eyes. *Vision research* **43**, 3021-3036

68. Shaw, N. S., and Noy, N. (2001) Interphotoreceptor retinoid-binding protein contains three retinoid binding sites. *Experimental eye research* **72**, 183-190

69. Moise, A. R., Golczak, M., Imanishi, Y., and Palczewski, K. (2007) Topology and membrane association of lecithin: retinol acyltransferase. *The Journal of biological chemistry* **282**, 2081-2090

70. Trehan, A., Canada, F. J., and Rando, R. R. (1990) Inhibitors of retinyl ester formation also prevent the biosynthesis of 11-cis-retinol. *Biochemistry* **29**, 309-312

71. Batten, M. L., Imanishi, Y., Maeda, T., Tu, D. C., Moise, A. R., Bronson, D., Possin, D., Van Gelder, R. N., Baehr, W., and Palczewski, K. (2004) Lecithin-retinol acyltransferase is essential for accumulation of all-trans-retinyl esters in the eye and in the liver. *The Journal of biological chemistry* **279**, 10422-10432

72. Gollapalli, D. R., Maiti, P., and Rando, R. R. (2003) RPE65 operates in the vertebrate visual cycle by stereospecifically binding all-trans-retinyl esters. *Biochemistry* **42**, 11824-11830

73. Gollapalli, D. R., and Rando, R. R. (2003) All-trans-retinyl esters are the substrates for isomerization in the vertebrate visual cycle. *Biochemistry* **42**, 5809-5818

74. Moiseyev, G., Crouch, R. K., Goletz, P., Oatis, J., Jr., Redmond, T. M., and Ma, J. X. (2003) Retinyl esters are the substrate for isomerohydrolase. *Biochemistry* **42**, 2229-2238

75. Imanishi, Y., Gerke, V., and Palczewski, K. (2004) Retinosomes: new insights into intracellular managing of hydrophobic substances in lipid bodies. *The Journal of cell biology* **166**, 447-453

76. Jin, M., Li, S., Moghrabi, W. N., Sun, H., and Travis, G. H. (2005) Rpe65 is the retinoid isomerase in bovine retinal pigment epithelium. *Cell* **122**, 449-459

77. Moiseyev, G., Chen, Y., Takahashi, Y., Wu, B. X., and Ma, J. X. (2005) RPE65 is the isomerohydrolase in the retinoid visual cycle. *Proceedings of the National Academy of Sciences of the United States of America* **102**, 12413-12418

78. Redmond, T. M., Poliakov, E., Yu, S., Tsai, J. Y., Lu, Z., and Gentleman, S. (2005) Mutation of key residues of RPE65 abolishes its enzymatic role as isomerohydrolase in the visual cycle. *Proceedings of the National Academy of Sciences of the United States of America* **102**, 13658-13663

79. McBee, J. K., Kuksa, V., Alvarez, R., de Lera, A. R., Prezhdo, O., Haeseleer, F., Sokal, I., and Palczewski, K. (2000) Isomerization of all-trans-retinol to cis-retinols in bovine retinal pigment epithelial cells: dependence on the specificity of retinoid-binding proteins. *Biochemistry* **39**, 11370-11380

80. Winston, A., and Rando, R. R. (1998) Regulation of isomerohydrolase activity in the visual cycle. *Biochemistry* **37**, 2044-2050

81. McBee, J. K., Van Hooser, J. P., Jang, G. F., and Palczewski, K. (2001) Isomerization of 11-cis-retinoids to all-trans-retinoids in vitro and in vivo. *The Journal of biological chemistry* **276**, 48483-48493

82. Futterman, S., Saari, J. C., and Blair, S. (1977) Occurrence of a binding protein for 11-cis-retinal in retina. *The Journal of biological chemistry* **252**, 3267-3271

83. Golczak, M., Kiser, P. D., Lodowski, D. T., Maeda, A., and Palczewski, K. (2010) Importance of membrane structural integrity for RPE65 retinoid isomerization activity. *The Journal of biological chemistry* **285**, 9667-9682

84. Perrault, I., Hanein, S., Gerber, S., Barbet, F., Ducroq, D., Dollfus, H., Hamel, C., Dufier, J. L., Munnich, A., Kaplan, J., and Rozet, J. M. (2004) Retinal dehydrogenase 12 (RDH12) mutations in leber congenital amaurosis. *American journal of human genetics* **75**, 639-646

85. Janecke, A. R., Thompson, D. A., Utermann, G., Becker, C., Hubner, C. A., Schmid, E., McHenry, C. L., Nair, A. R., Ruschendorf, F., Heckenlively, J., Wissinger, B., Nurnberg, P., and Gal, A. (2004) Mutations in RDH12 encoding a photoreceptor cell retinol dehydrogenase cause childhood-onset severe retinal dystrophy. *Nature genetics* **36**, 850-854

86. Allikmets, R. (1997) A photoreceptor cell-specific ATP-binding transporter gene (ABCR) is mutated in recessive Stargardt macular dystrophy. *Nature genetics* **17**, 122

87. Allikmets, R., Shroyer, N. F., Singh, N., Seddon, J. M., Lewis, R. A., Bernstein, P. S., Peiffer, A., Zabriskie, N. A., Li, Y., Hutchinson, A., Dean, M., Lupski, J. R., and Leppert, M. (1997) Mutation of the Stargardt disease gene (ABCR) in age-related macular degeneration. *Science* **277**, 1805-1807

88. Fritsche, L. G., Fleckenstein, M., Fiebig, B. S., Schmitz-Valckenberg, S., Bindewald-Wittich, A., Keilhauer, C. N., Renner, A. B., Mackensen, F., Mossner, A., Pauleikhoff, D., Adrion, C., Mansmann, U., Scholl, H. P., Holz, F. G., and Weber, B. H. (2012) A subgroup of age-related macular degeneration is

associated with mono-allelic sequence variants in the ABCA4 gene. *Investigative ophthalmology & visual science* **53**, 2112-2118

89. Maugeri, A., Klevering, B. J., Rohrschneider, K., Blankenagel, A., Brunner, H. G., Deutman, A. F., Hoyng, C. B., and Cremers, F. P. (2000) Mutations in the ABCA4 (ABCR) gene are the major cause of autosomal recessive cone-rod dystrophy. *American journal of human genetics* **67**, 960-966

90. Martinez-Mir, A., Paloma, E., Allikmets, R., Ayuso, C., del Rio, T., Dean, M., Vilageliu, L., Gonzalez-Duarte, R., and Balcells, S. (1998) Retinitis pigmentosa caused by a homozygous mutation in the Stargardt disease gene ABCR. *Nature genetics* **18**, 11-12

91. Rozet, J. M., Gerber, S., Ghazi, I., Perrault, I., Ducroq, D., Souied, E., Cabot, A., Dufier, J. L., Munnich, A., and Kaplan, J. (1999) Mutations of the retinal specific ATP binding transporter gene (ABCR) in a single family segregating both autosomal recessive retinitis pigmentosa RP19 and Stargardt disease: evidence of clinical heterogeneity at this locus. *Journal of medical genetics* **36**, 447-451

92. Wu, L., Nagasaki, T., and Sparrow, J. R. (2010) Photoreceptor cell degeneration in Abcr (-/-) mice. *Advances in experimental medicine and biology* **664**, 533-539

93. Maeda, A., Maeda, T., Golczak, M., and Palczewski, K. (2008) Retinopathy in mice induced by disrupted all-trans-retinal clearance. *The Journal of biological chemistry* **283**, 26684-26693

94. Maeda, A., Golczak, M., Chen, Y., Okano, K., Kohno, H., Shiose, S., Ishikawa, K., Harte, W., Palczewska, G., Maeda, T., and Palczewski, K. (2012) Primary amines protect against retinal degeneration in mouse models of retinopathies. *Nature chemical biology* **8**, 170-178

95. Golczak, M., Maeda, A., Bereta, G., Maeda, T., Kiser, P. D., Hunzelmann, S., von Lintig, J., Blaner, W. S., and Palczewski, K. (2008) Metabolic basis of visual cycle inhibition by retinoid and nonretinoid compounds in the vertebrate retina. *The Journal of biological chemistry* **283**, 9543-9554

96. den Hollander, A. I., McGee, T. L., Ziviello, C., Banfi, S., Dryja, T. P., Gonzalez-Fernandez, F., Ghosh, D., and Berson, E. L. (2009) A homozygous missense mutation in the IRBP gene (RBP3) associated with autosomal recessive retinitis pigmentosa. *Investigative ophthalmology & visual science* **50**, 1864-1872

97. Liu, L., and Gudas, L. J. (2005) Disruption of the lecithin:retinol acyltransferase gene makes mice more susceptible to vitamin A deficiency. *The Journal of biological chemistry* **280**, 40226-40234

98. Thompson, D. A., Li, Y., McHenry, C. L., Carlson, T. J., Ding, X., Sieving, P. A., Apfelstedt-Sylla, E., and Gal, A. (2001) Mutations in the gene encoding lecithin retinol acyltransferase are associated with early-onset severe retinal dystrophy. *Nature genetics* **28**, 123-124

99. Marlhens, F., Bareil, C., Griffoin, J. M., Zrenner, E., Amalric, P., Eliaou, C., Liu, S. Y., Harris, E., Redmond, T. M., Arnaud, B., Claustres, M., and Hamel, C. P.

(1997) Mutations in RPE65 cause Leber's congenital amaurosis. *Nature genetics* **17**, 139-141

100. Znoiko, S. L., Rohrer, B., Lu, K., Lohr, H. R., Crouch, R. K., and Ma, J. X. (2005) Downregulation of cone-specific gene expression and degeneration of cone photoreceptors in the Rpe65-/- mouse at early ages. *Investigative ophthalmology & visual science* **46**, 1473-1479

101. Yamamoto, H., Simon, A., Eriksson, U., Harris, E., Berson, E. L., and Dryja, T. P. (1999) Mutations in the gene encoding 11-cis retinol dehydrogenase cause delayed dark adaptation and fundus albipunctatus. *Nature genetics* **22**, 188-191

102. Nakamura, M., Hotta, Y., Tanikawa, A., Terasaki, H., and Miyake, Y. (2000) A high association with cone dystrophy in Fundus albipunctatus caused by mutations of the RDH5 gene. *Investigative ophthalmology & visual science* **41**, 3925-3932

103. Driessen, C. A., Winkens, H. J., Hoffmann, K., Kuhlmann, L. D., Janssen, B. P., Van Vugt, A. H., Van Hooser, J. P., Wieringa, B. E., Deutman, A. F., Palczewski, K., Ruether, K., and Janssen, J. J. (2000) Disruption of the 11-cis-retinol dehydrogenase gene leads to accumulation of cis-retinols and cis-retinyl esters. *Molecular and cellular biology* **20**, 4275-4287

104. Acland, G. M., Aguirre, G. D., Ray, J., Zhang, Q., Aleman, T. S., Cideciyan, A. V., Pearce-Kelling, S. E., Anand, V., Zeng, Y., Maguire, A. M., Jacobson, S. G., Hauswirth, W. W., and Bennett, J. (2001) Gene therapy restores vision in a canine model of childhood blindness. *Nature genetics* **28**, 92-95

105. Pang, J. J., Chang, B., Kumar, A., Nusinowitz, S., Noorwez, S. M., Li, J., Rani, A., Foster, T. C., Chiodo, V. A., Doyle, T., Li, H., Malhotra, R., Teusner, J. T., McDowell, J. H., Min, S. H., Li, Q., Kaushal, S., and Hauswirth, W. W. (2006) Gene therapy restores vision-dependent behavior as well as retinal structure and function in a mouse model of RPE65 Leber congenital amaurosis. *Molecular therapy : the journal of the American Society of Gene Therapy* **13**, 565-572

106. Hauswirth, W. W. (2005) The consortium project to treat RPE65 deficiency in humans. *Retina* **25**, S60

107. Batten, M. L., Imanishi, Y., Tu, D. C., Doan, T., Zhu, L., Pang, J., Glushakova, L., Moise, A. R., Baehr, W., Van Gelder, R. N., Hauswirth, W. W., Rieke, F., and Palczewski, K. (2005) Pharmacological and rAAV gene therapy rescue of visual functions in a blind mouse model of Leber congenital amaurosis. *PLoS medicine* **2**, e333

108. Travis, G. H., Golczak, M., Moise, A. R., and Palczewski, K. (2007) Diseases caused by defects in the visual cycle: retinoids as potential therapeutic agents. *Annual review of pharmacology and toxicology* **47**, 469-512

109. Hubbard, R., and Wald, G. (1952) Cis-trans isomers of vitamin A and retinene in the rhodopsin system. *The Journal of general physiology* **36**, 269-315

110. Van Hooser, J. P., Aleman, T. S., He, Y. G., Cideciyan, A. V., Kuksa, V., Pittler, S. J., Stone, E. M., Jacobson, S. G., and Palczewski, K. (2000) Rapid restoration

of visual pigment and function with oral retinoid in a mouse model of childhood blindness. *Proceedings of the National Academy of Sciences of the United States of America* **97**, 8623-8628

111. Van Hooser, J. P., Liang, Y., Maeda, T., Kuksa, V., Jang, G. F., He, Y. G., Rieke, F., Fong, H. K., Detwiler, P. B., and Palczewski, K. (2002) Recovery of visual functions in a mouse model of Leber congenital amaurosis. *The Journal of biological chemistry* **277**, 19173-19182

112. Ablonczy, Z., Crouch, R. K., Goletz, P. W., Redmond, T. M., Knapp, D. R., Ma, J. X., and Rohrer, B. (2002) 11-cis-retinal reduces constitutive opsin phosphorylation and improves quantum catch in retinoid-deficient mouse rod photoreceptors. *The Journal of biological chemistry* **277**, 40491-40498

113. Zhao, D., McCaffery, P., Ivins, K. J., Neve, R. L., Hogan, P., Chin, W. W., and Drager, U. C. (1996) Molecular identification of a major retinoic-acid-synthesizing enzyme, a retinaldehyde-specific dehydrogenase. *European journal of biochemistry / FEBS* **240**, 15-22

114. Chambon, P. (1996) A decade of molecular biology of retinoic acid receptors. *FASEB journal : official publication of the Federation of American Societies for Experimental Biology* **10**, 940-954

115. Gamble, M. V., Mata, N. L., Tsin, A. T., Mertz, J. R., and Blaner, W. S. (2000) Substrate specificities and 13-cis-retinoic acid inhibition of human, mouse and bovine cis-retinol dehydrogenases. *Biochimica et biophysica acta* **1476**, 3-8

116. Gollapalli, D. R., and Rando, R. R. (2004) The specific binding of retinoic acid to RPE65 and approaches to the treatment of macular degeneration. *Proceedings of the National Academy of Sciences of the United States of America* **101**, 10030-10035

117. Radu, R. A., Mata, N. L., Nusinowitz, S., Liu, X., Sieving, P. A., and Travis, G. H. (2003) Treatment with isotretinoin inhibits lipofuscin accumulation in a mouse model of recessive Stargardt's macular degeneration. *Proceedings of the National Academy of Sciences of the United States of America* **100**, 4742-4747

118. Radu, R. A., Mata, N. L., Bagla, A., and Travis, G. H. (2004) Light exposure stimulates formation of A2E oxiranes in a mouse model of Stargardt's macular degeneration. *Proceedings of the National Academy of Sciences of the United States of America* **101**, 5928-5933

119. Golczak, M., Kuksa, V., Maeda, T., Moise, A. R., and Palczewski, K. (2005) Positively charged retinoids are potent and selective inhibitors of the trans-cis isomerization in the retinoid (visual) cycle. *Proceedings of the National Academy of Sciences of the United States of America* **102**, 8162-8167

120. Maiti, P., Kong, J., Kim, S. R., Sparrow, J. R., Allikmets, R., and Rando, R. R. (2006) Small molecule RPE65 antagonists limit the visual cycle and prevent lipofuscin formation. *Biochemistry* **45**, 852-860

121. Golczak, M., Imanishi, Y., Kuksa, V., Maeda, T., Kubota, R., and Palczewski, K. (2005) Lecithin:retinol acyltransferase is responsible for amidation of

retinylamine, a potent inhibitor of the retinoid cycle. *The Journal of biological chemistry* **280**, 42263-42273

122. Salom, D., Lodowski, D. T., Stenkamp, R. E., Le Trong, I., Golczak, M., Jastrzebska, B., Harris, T., Ballesteros, J. A., and Palczewski, K. (2006) Crystal structure of a photoactivated deprotonated intermediate of rhodopsin. *Proceedings of the National Academy of Sciences of the United States of America* **103**, 16123-16128

123. Nakamichi, H., and Okada, T. (2006) Crystallographic analysis of primary visual photochemistry. *Angewandte Chemie* **45**, 4270-4273

124. Sakmar, T. P., Franke, R. R., and Khorana, H. G. (1989) Glutamic acid-113 serves as the retinylidene Schiff base counterion in bovine rhodopsin. *Proceedings of the National Academy of Sciences of the United States of America* **86**, 8309-8313

125. Zhukovsky, E. A., and Oprian, D. D. (1989) Effect of carboxylic acid side chains on the absorption maximum of visual pigments. *Science* **246**, 928-930

126. Nathans, J. (1990) Determinants of visual pigment absorbance: identification of the retinylidene Schiff's base counterion in bovine rhodopsin. *Biochemistry* **29**, 9746-9752

127. Cohen, G. B., Oprian, D. D., and Robinson, P. R. (1992) Mechanism of activation and inactivation of opsin: role of Glu113 and Lys296. *Biochemistry* **31**, 12592-12601

128. Zhukovsky, E. A., Robinson, P. R., and Oprian, D. D. (1991) Transducin activation by rhodopsin without a covalent bond to the 11-cis-retinal chromophore. *Science* **251**, 558-560

129. Kono, M., Goletz, P. W., and Crouch, R. K. (2008) 11-cis- and all-trans-retinols can activate rod opsin: rational design of the visual cycle. *Biochemistry* **47**, 7567-7571

130. Matsuyama, T., Yamashita, T., Imai, H., and Shichida, Y. (2010) Covalent bond between ligand and receptor required for efficient activation in rhodopsin. *The Journal of biological chemistry* **285**, 8114-8121

131. Imamoto, Y., and Shichida, Y. (2014) Cone visual pigments. *Biochimica et biophysica acta* **1837**, 664-673

132. Lin, S. W., and Sakmar, T. P. (1999) Colour tuning mechanisms of visual pigments. *Novartis Foundation symposium* **224**, 124-135; discussion 135-141, 181-190

133. Janz, J. M., and Farrens, D. L. (2001) Engineering a functional blue-wavelength-shifted rhodopsin mutant. *Biochemistry* **40**, 7219-7227

134. Lin, S. W., Kochendoerfer, G. G., Carroll, K. S., Wang, D., Mathies, R. A., and Sakmar, T. P. (1998) Mechanisms of spectral tuning in blue cone visual pigments. Visible and raman spectroscopy of blue-shifted rhodopsin mutants. *The Journal of biological chemistry* **273**, 24583-24591

135. Sekharan, S., Mooney, V. L., Rivalta, I., Kazmi, M. A., Neitz, M., Neitz, J., Sakmar, T. P., Yan, E. C., and Batista, V. S. (2013) Spectral tuning of ultraviolet cone pigments: an interhelical lock mechanism. *Journal of the American Chemical Society* **135**, 19064-19067

136. Sakmar, T. P., Menon, S. T., Marin, E. P., and Awad, E. S. (2002) Rhodopsin: insights from recent structural studies. *Annual review of biophysics and biomolecular structure* **31**, 443-484

137. Chen, M. H., Kuemmel, C., Birge, R. R., and Knox, B. E. (2012) Rapid release of retinal from a cone visual pigment following photoactivation. *Biochemistry* **51**, 4117-4125

138. Robinson, P. R., Cohen, G. B., Zhukovsky, E. A., and Oprian, D. D. (1992) Constitutively active mutants of rhodopsin. *Neuron* **9**, 719-725

139. Janz, J. M., and Farrens, D. L. (2003) Assessing structural elements that influence Schiff base stability: mutants E113Q and D190N destabilize rhodopsin through different mechanisms. *Vision research* **43**, 2991-3002

140. Janz, J. M., Fay, J. F., and Farrens, D. L. (2003) Stability of dark state rhodopsin is mediated by a conserved ion pair in intradiscal loop E-2. *The Journal of biological chemistry* **278**, 16982-16991

141. Singhal, A., Ostermaier, M. K., Vishnivetskiy, S. A., Panneels, V., Homan, K. T., Tesmer, J. J., Veprintsev, D., Deupi, X., Gurevich, V. V., Schertler, G. F., and Standfuss, J. (2013) Insights into congenital stationary night blindness based on the structure of G90D rhodopsin. *EMBO reports* **14**, 520-526

142. Gross, A. K., Rao, V. R., and Oprian, D. D. (2003) Characterization of rhodopsin congenital night blindness mutant T94I. *Biochemistry* **42**, 2009-2015

143. Gross, A. K., Xie, G., and Oprian, D. D. (2003) Slow binding of retinal to rhodopsin mutants G90D and T94D. *Biochemistry* **42**, 2002-2008

144. Rao, V. R., Cohen, G. B., and Oprian, D. D. (1994) Rhodopsin mutation G90D and a molecular mechanism for congenital night blindness. *Nature* **367**, 639-642

145. Toledo, D., Ramon, E., Aguila, M., Cordomi, A., Perez, J. J., Mendes, H. F., Cheetham, M. E., and Garriga, P. (2011) Molecular mechanisms of disease for mutations at Gly-90 in rhodopsin. *The Journal of biological chemistry* **286**, 39993-40001

146. Dizhoor, A. M., Woodruff, M. L., Olshevskaya, E. V., Cilluffo, M. C., Cornwall, M. C., Sieving, P. A., and Fain, G. L. (2008) Night blindness and the mechanism of constitutive signaling of mutant G90D rhodopsin. *The Journal of neuroscience : the official journal of the Society for Neuroscience* **28**, 11662-11672

147. Park, P. S. (2014) Constitutively active rhodopsin and retinal disease. *Advances in pharmacology* **70**, 1-36

148. Schafer, C. T., and Farrens, D. L. (2015) Conformational selection and equilibrium governs the ability of retinals to bind opsin. *J Biol Chem* **290**, 4304-4318

149. Sato, K., Morizumi, T., Yamashita, T., and Shichida, Y. (2010) Direct observation of the pH-dependent equilibrium between metarhodopsins I and II and the pH-independent interaction of metarhodopsin II with transducin C-terminal peptide. *Biochemistry* **49**, 736-741

150. Park, J. H., Morizumi, T., Li, Y., Hong, J. E., Pai, E. F., Hofmann, K. P., Choe, H. W., and Ernst, O. P. (2013) Opsin, a structural model for olfactory receptors? *Angewandte Chemie* **52**, 11021-11024

151. Hildebrand, P. W., Scheerer, P., Park, J. H., Choe, H. W., Piechnick, R., Ernst, O. P., Hofmann, K. P., and Heck, M. (2009) A ligand channel through the G protein coupled receptor opsin. *PloS one* **4**, e4382

152. Piechnick, R., Ritter, E., Hildebrand, P. W., Ernst, O. P., Scheerer, P., Hofmann, K. P., and Heck, M. (2012) Effect of channel mutations on the uptake and release of the retinal ligand in opsin. *Proceedings of the National Academy of Sciences of the United States of America* **109**, 5247-5252

153. Standfuss, J., Edwards, P. C., D'Antona, A., Fransen, M., Xie, G., Oprian, D. D., and Schertler, G. F. (2011) The structural basis of agonist-induced activation in constitutively active rhodopsin. *Nature* **471**, 656-660

154. Deupi, X., Edwards, P., Singhal, A., Nickle, B., Oprian, D., Schertler, G., and Standfuss, J. (2012) Stabilized G protein binding site in the structure of constitutively active metarhodopsin-II. *Proceedings of the National Academy of Sciences of the United States of America* **109**, 119-124

155. Schadel, S. A., Heck, M., Maretzki, D., Filipek, S., Teller, D. C., Palczewski, K., and Hofmann, K. P. (2003) Ligand channeling within a G-protein-coupled receptor. The entry and exit of retinals in native opsin. *The Journal of biological chemistry* **278**, 24896-24903

156. Heck, M., Schadel, S. A., Maretzki, D., and Hofmann, K. P. (2003) Secondary binding sites of retinoids in opsin: characterization and role in regeneration. *Vision research* **43**, 3003-3010

157. Mustafi, D., and Palczewski, K. (2009) Topology of class A G protein-coupled receptors: insights gained from crystal structures of rhodopsins, adrenergic and adenosine receptors. *Molecular pharmacology* **75**, 1-12

158. Mertz, B., Feng, J., Corcoran, C., and Neeley, B. (2015) Explaining the mobility of retinal in activated rhodopsin and opsin. *Photochemical & photobiological sciences : Official journal of the European Photochemistry Association and the European Society for Photobiology* **14**, 1952-1964

159. Wang, T., and Duan, Y. (2011) Retinal release from opsin in molecular dynamics simulations. *Journal of molecular recognition : JMR* **24**, 350-358

160. Leff, P. (1995) The two-state model of receptor activation. *Trends in pharmacological sciences* **16**, 89-97

161. Kefalov, V. J., Crouch, R. K., and Cornwall, M. C. (2001) Role of noncovalent binding of 11-cis-retinal to opsin in dark adaptation of rod and cone photoreceptors. *Neuron* **29**, 749-755

162. Brunette, A. M., Sinha, A., David, L. L., and Farrens, D. L. (2016) Evidence that the Rhodopsin Kinase (GRK1) N-terminus and the Transducin Galpha C-terminus interact with the Same "Hydrophobic Patch" on Rhodopsin TM5. *Biochemistry*

163. Hargrave, P. A. (2001) Rhodopsin structure, function, and topography the Friedenwald lecture. *Investigative ophthalmology & visual science* **42**, 3-9

164. Kiser, P. D., Golczak, M., and Palczewski, K. (2014) Chemistry of the retinoid (visual) cycle. *Chemical reviews* **114**, 194-232

165. Veleri, S., Lazar, C. H., Chang, B., Sieving, P. A., Banin, E., and Swaroop, A. (2015) Biology and therapy of inherited retinal degenerative disease: insights from mouse models. *Disease models & mechanisms* **8**, 109-129

166. Lamb, T. D., and Pugh, E. N., Jr. (2006) Phototransduction, dark adaptation, and rhodopsin regeneration the proctor lecture. *Investigative ophthalmology & visual science* **47**, 5137-5152

167. Cohen, G. B., Yang, T., Robinson, P. R., and Oprian, D. D. (1993) Constitutive activation of opsin: influence of charge at position 134 and size at position 296. *Biochemistry* **32**, 6111-6115

168. Tsukamoto, H., and Farrens, D. L. (2013) A constitutively activating mutation alters the dynamics and energetics of a key conformational change in a ligand-free G protein-coupled receptor. *The Journal of biological chemistry* **288**, 28207-28216

169. Hofmann, K. P., Scheerer, P., Hildebrand, P. W., Choe, H. W., Park, J. H., Heck, M., and Ernst, O. P. (2009) A G protein-coupled receptor at work: the rhodopsin model. *Trends in biochemical sciences* **34**, 540-552

170. Li, J., Edwards, P. C., Burghammer, M., Villa, C., and Schertler, G. F. (2004) Structure of bovine rhodopsin in a trigonal crystal form. *Journal of molecular biology* **343**, 1409-1438

171. Srinivasan, S., Ramon, E., Cordomi, A., and Garriga, P. (2014) Binding specificity of retinal analogs to photoactivated visual pigments suggest mechanism for fine-tuning GPCR-ligand interactions. *Chemistry & biology* **21**, 369-378

172. Pettersen, E. F., Goddard, T. D., Huang, C. C., Couch, G. S., Greenblatt, D. M., Meng, E. C., and Ferrin, T. E. (2004) UCSF Chimera--a visualization system for exploratory research and analysis. *Journal of computational chemistry* **25**, 1605-1612

173. Matsumoto, H., and Yoshizawa, T. (2008) Rhodopsin regeneration is accelerated via noncovalent 11-cis retinal-opsin complex--a role of retinal binding pocket of opsin. *Photochemistry and photobiology* **84**, 985-989

174. Liu, J., Liu, M. Y., Nguyen, J. B., Bhagat, A., Mooney, V., and Yan, E. C. (2011) Thermal properties of rhodopsin: insight into the molecular mechanism of dim-light vision. *The Journal of biological chemistry* **286**, 27622-27629

175. Tian, H., Naganathan, S., Kazmi, M. A., Schwartz, T. W., Sakmar, T. P., and Huber, T. (2014) Bioorthogonal fluorescent labeling of functional g-protein-coupled receptors. *Chembiochem : a European journal of chemical biology* **15**, 1820-1829

176. Jastrzebska, B., Orban, T., Golczak, M., Engel, A., and Palczewski, K. (2013) Asymmetry of the rhodopsin dimer in complex with transducin. *Faseb J* **27**, 1572-1584

177. Han, M., Smith, S. O., and Sakmar, T. P. (1998) Constitutive activation of opsin by mutation of methionine 257 on transmembrane helix 6. *Biochemistry* **37**, 8253-8261

178. Martin, E. L., Rens-Domiano, S., Schatz, P. J., and Hamm, H. E. (1996) Potent peptide analogues of a G protein receptor-binding region obtained with a combinatorial library. *The Journal of biological chemistry* **271**, 361-366

179. Imamoto, Y., Seki, I., Yamashita, T., and Shichida, Y. (2013) Efficiencies of activation of transducin by cone and rod visual pigments. *Biochemistry* **52**, 3010-3018

180. Ferretti, L., Karnik, S. S., Khorana, H. G., Nassal, M., and Oprian, D. D. (1986) Total synthesis of a gene for bovine rhodopsin. *Proceedings of the National Academy of Sciences of the United States of America* **83**, 599-603

181. Dunham, T. D., and Farrens, D. L. (1999) Conformational changes in rhodopsin. Movement of helix f detected by site-specific chemical labeling and fluorescence spectroscopy. *The Journal of biological chemistry* **274**, 1683-1690

182. Xie, G., Gross, A. K., and Oprian, D. D. (2003) An opsin mutant with increased thermal stability. *Biochemistry* **42**, 1995-2001

183. Resek, J. F., Farahbakhsh, Z. T., Hubbell, W. L., and Khorana, H. G. (1993) Formation of the meta II photointermediate is accompanied by conformational changes in the cytoplasmic surface of rhodopsin. *Biochemistry* **32**, 12025-12032

184. Jager, S., Palczewski, K., and Hofmann, K. P. (1996) Opsin/all-trans-retinal complex activates transducin by different mechanisms than photolyzed rhodopsin. *Biochemistry* **35**, 2901-2908

185. Sugihara, M., Suwa, M., and Bondar, A. N. (2014) Dynamics of bovine opsin bound to G-protein fragments. *Journal of structural biology*

186. Hofmann, K. P., Pulvermuller, A., Buczylko, J., Van Hooser, P., and Palczewski, K. (1992) The role of arrestin and retinoids in the regeneration pathway of rhodopsin. *The Journal of biological chemistry* **267**, 15701-15706

187. Palczewski, K., Jager, S., Buczylko, J., Crouch, R. K., Bredberg, D. L., Hofmann, K. P., Asson-Batres, M. A., and Saari, J. C. (1994) Rod outer segment retinol

dehydrogenase: substrate specificity and role in phototransduction. *Biochemistry* **33**, 13741-13750

188. Surya, A., and Knox, B. E. (1998) Enhancement of opsin activity by all-trans-retinal. *Experimental eye research* **66**, 599-603

189. Buczylko, J., Saari, J. C., Crouch, R. K., and Palczewski, K. (1996) Mechanisms of opsin activation. *The Journal of biological chemistry* **271**, 20621-20630

190. Brueggemann, L. I., and Sullivan, J. M. (2001) All-trans-retinal forms a visible-absorbing pigment with human rod opsin. *Biochemistry* **40**, 4446-4453

191. Sommer, M. E., Smith, W. C., and Farrens, D. L. (2006) Dynamics of arrestin-rhodopsin interactions: acidic phospholipids enable binding of arrestin to purified rhodopsin in detergent. *The Journal of biological chemistry* **281**, 9407-9417

192. Feuerstein, S. E., Pulvermuller, A., Hartmann, R., Granzin, J., Stoldt, M., Henklein, P., Ernst, O. P., Heck, M., Willbold, D., and Koenig, B. W. (2009) Helix formation in arrestin accompanies recognition of photoactivated rhodopsin. *Biochemistry* **48**, 10733-10742

193. Ostermaier, M. K., Peterhans, C., Jaussi, R., Deupi, X., and Standfuss, J. (2014) Functional map of arrestin-1 at single amino acid resolution. *Proceedings of the National Academy of Sciences of the United States of America* **111**, 1825-1830

194. Szczepek, M., Beyriere, F., Hofmann, K. P., Elgeti, M., Kazmin, R., Rose, A., Bartl, F. J., von Stetten, D., Heck, M., Sommer, M. E., Hildebrand, P. W., and Scheerer, P. (2014) Crystal structure of a common GPCR-binding interface for G protein and arrestin. *Nature communications* **5**, 4801

195. Jastrzebska, B., Palczewski, K., and Golczak, M. (2011) Role of bulk water in hydrolysis of the rhodopsin chromophore. *The Journal of biological chemistry* **286**, 18930-18937

196. Saari, J. C., Garwin, G. G., Van Hooser, J. P., and Palczewski, K. (1998) Reduction of all-trans-retinal limits regeneration of visual pigment in mice. *Vision research* **38**, 1325-1333

197. Lee, K. A., Nawrot, M., Garwin, G. G., Saari, J. C., and Hurley, J. B. (2010) Relationships among visual cycle retinoids, rhodopsin phosphorylation, and phototransduction in mouse eyes during light and dark adaptation. *Biochemistry* **49**, 2454-2463

198. Yao, X., Parnot, C., Deupi, X., Ratnala, V. R., Swaminath, G., Farrens, D., and Kobilka, B. (2006) Coupling ligand structure to specific conformational switches in the beta2-adrenoceptor. *Nature chemical biology* **2**, 417-422

199. Kobilka, B. K., and Deupi, X. (2007) Conformational complexity of G-protein-coupled receptors. *Trends in pharmacological sciences* **28**, 397-406

200. Deupi, X., and Kobilka, B. K. (2010) Energy landscapes as a tool to integrate GPCR structure, dynamics, and function. *Physiology* **25**, 293-303

201. Brown, M. F., Salgado, G. F., and Struts, A. V. (2010) Retinal dynamics during light activation of rhodopsin revealed by solid-state NMR spectroscopy. *Biochimica et biophysica acta* **1798**, 177-193

202. Hunyady, L., Vauquelin, G., and Vanderheyden, P. (2003) Agonist induction and conformational selection during activation of a G-protein-coupled receptor. *Trends in pharmacological sciences* **24**, 81-86

203. Tsukamoto, H., Szundi, I., Lewis, J. W., Farrens, D. L., and Kliger, D. S. (2011) Rhodopsin in nanodiscs has native membrane-like photointermediates. *Biochemistry* **50**, 5086-5091

204. Maeda, A., Okano, K., Park, P. S., Lem, J., Crouch, R. K., Maeda, T., and Palczewski, K. (2010) Palmitoylation stabilizes unliganded rod opsin. *Proceedings of the National Academy of Sciences of the United States of America* **107**, 8428-8433

205. Sachs, K., Maretzki, D., Meyer, C. K., and Hofmann, K. P. (2000) Diffusible ligand all-trans-retinal activates opsin via a palmitoylation-dependent mechanism. *The Journal of biological chemistry* **275**, 6189-6194

206. Tsukamoto, H., Terakita, A., and Shichida, Y. (2010) A pivot between helices V and VI near the retinal-binding site is necessary for activation in rhodopsins. *The Journal of biological chemistry* **285**, 7351-7357

207. Sommer, M. E., and Farrens, D. L. (2006) Arrestin can act as a regulator of rhodopsin photochemistry. *Vision research* **46**, 4532-4546

208. Van Eps, N., Anderson, L. L., Kisselev, O. G., Baranski, T. J., Hubbell, W. L., and Marshall, G. R. (2010) Electron paramagnetic resonance studies of functionally active, nitroxide spin-labeled peptide analogues of the C-terminus of a G-protein alpha subunit. *Biochemistry* **49**, 6877-6886

209. Piechnick, R., Heck, M., and Sommer, M. E. (2011) Alkylated hydroxylamine derivatives eliminate peripheral retinylidene Schiff bases but cannot enter the retinal binding pocket of light-activated rhodopsin. *Biochemistry* **50**, 7168-7176

210. Zhuang, T., Chen, Q., Cho, M. K., Vishnivetskiy, S. A., Iverson, T. M., Gurevich, V. V., and Sanders, C. R. (2013) Involvement of distinct arrestin-1 elements in binding to different functional forms of rhodopsin. *Proceedings of the National Academy of Sciences of the United States of America* **110**, 942-947

211. Blakeley, L. R., Chen, C., Chen, C. K., Chen, J., Crouch, R. K., Travis, G. H., and Koutalos, Y. (2011) Rod outer segment retinol formation is independent of Abca4, arrestin, rhodopsin kinase, and rhodopsin palmitylation. *Investigative ophthalmology & visual science* **52**, 3483-3491

212. Fay, J. F., and Farrens, D. L. (2012) A key agonist-induced conformational change in the cannabinoid receptor CB1 is blocked by the allosteric ligand Org 27569. *The Journal of biological chemistry* **287**, 33873-33882

213. Ghanouni, P., Gryczynski, Z., Steenhuis, J. J., Lee, T. W., Farrens, D. L., Lakowicz, J. R., and Kobilka, B. K. (2001) Functionally different agonists induce

distinct conformations in the G protein coupling domain of the beta 2 adrenergic receptor. *The Journal of biological chemistry* **276**, 24433-24436

214. Swaminath, G., Xiang, Y., Lee, T. W., Steenhuis, J., Parnot, C., and Kobilka, B. K. (2004) Sequential binding of agonists to the beta2 adrenoceptor. Kinetic evidence for intermediate conformational states. *The Journal of biological chemistry* **279**, 686-691

215. Dundas, J., Ouyang, Z., Tseng, J., Binkowski, A., Turpaz, Y., and Liang, J. (2006) CASTp: computed atlas of surface topography of proteins with structural and topographical mapping of functionally annotated residues. *Nucleic acids research* **34**, W116-118

216. Kim, Y. J., Hofmann, K. P., Ernst, O. P., Scheerer, P., Choe, H. W., and Sommer, M. E. (2013) Crystal structure of pre-activated arrestin p44. *Nature* **497**, 142-146

217. Jones Brunette, A. M., and Farrens, D. L. (2014) Distance mapping in proteins using fluorescence spectroscopy: tyrosine, like tryptophan, quenches bimane fluorescence in a distance-dependent manner. *Biochemistry* **53**, 6290-6301

218. Farrens, D. L. (2010) What site-directed labeling studies tell us about the mechanism of rhodopsin activation and G-protein binding. *Photochemical & photobiological sciences : Official journal of the European Photochemistry Association and the European Society for Photobiology* **9**, 1466-1474

219. Tsukamoto, H., Farrens, D. L., Koyanagi, M., and Terakita, A. (2009) The magnitude of the light-induced conformational change in different rhodopsins correlates with their ability to activate G proteins. *The Journal of biological chemistry* **284**, 20676-20683

220. Fay, J. F., and Farrens, D. L. (2015) Structural dynamics and energetics underlying allosteric inactivation of the cannabinoid receptor CB1. *Proceedings of the National Academy of Sciences of the United States of America* **112**, 8469-8474

221. Kefalov, V. J. (2012) Rod and cone visual pigments and phototransduction through pharmacological, genetic, and physiological approaches. *The Journal of biological chemistry* **287**, 1635-1641

222. Shichida, Y., and Imai, H. (1998) Visual pigment: G-protein-coupled receptor for light signals. *Cellular and molecular life sciences : CMLS* **54**, 1299-1315

223. Tesmer, J. J. (2016) Hitchhiking on the heptahelical highway: structure and function of 7TM receptor complexes. *Nature reviews. Molecular cell biology*

224. Shukla, A. K., Singh, G., and Ghosh, E. (2014) Emerging structural insights into biased GPCR signaling. *Trends in biochemical sciences* **39**, 594-602

225. Eichel, K., Jullie, D., and von Zastrow, M. (2016) beta-Arrestin drives MAP kinase signalling from clathrin-coated structures after GPCR dissociation. *Nature cell biology* **18**, 303-310

226. Dratz, E. A., Furstenau, J. E., Lambert, C. G., Thireault, D. L., Rarick, H., Schepers, T., Pakhlevaniants, S., and Hamm, H. E. (1993) NMR structure of a receptor-bound G-protein peptide. *Nature* **363**, 276-281.

227. Pulvermuller, A., Schroder, K., Fischer, T., and Hofmann, K. P. (2000) Interactions of metarhodopsin II. Arrestin peptides compete with arrestin and transducin. *J Biol Chem* **275**, 37679-37685.

228. Mansoor, S. E., Dewitt, M. A., and Farrens, D. L. (2010) Distance mapping in proteins using fluorescence spectroscopy: the tryptophan-induced quenching (TrIQ) method. *Biochemistry* **49**, 9722-9731

229. Mansoor, S. E., and Farrens, D. L. (2004) High-throughput protein structural analysis using site-directed fluorescence labeling and the bimane derivative (2-pyridyl)dithiobimane. *Biochemistry* **43**, 9426-9438

230. Mansoor, S. E., Palczewski, K., and Farrens, D. L. (2006) Rhodopsin self-associates in asolectin liposomes. *Proceedings of the National Academy of Sciences of the United States of America* **103**, 3060-3065

231. Elgeti, M., Kazmin, R., Heck, M., Morizumi, T., Ritter, E., Scheerer, P., Ernst, O. P., Siebert, F., Hofmann, K. P., and Bartl, F. J. (2011) Conserved Tyr223(5.58) plays different roles in the activation and G-protein interaction of rhodopsin. *Journal of the American Chemical Society* **133**, 7159-7165

232. Goncalves, J. A., South, K., Ahuja, S., Zaitseva, E., Opefi, C. A., Eilers, M., Vogel, R., Reeves, P. J., and Smith, S. O. (2010) Highly conserved tyrosine stabilizes the active state of rhodopsin. *Proceedings of the National Academy of Sciences of the United States of America* **107**, 19861-19866

233. Isayama, T., McCabe England, S. L., Crouch, R. K., Zimmerman, A. L., and Makino, C. L. (2009) Beta-ionone activates and bleaches visual pigment in salamander photoreceptors. *Visual neuroscience* **26**, 267-274

234. Isayama, T., Chen, Y., Kono, M., Degrip, W. J., Ma, J. X., Crouch, R. K., and Makino, C. L. (2006) Differences in the pharmacological activation of visual opsins. *Visual neuroscience* **23**, 899-908

235. Kefalov, V. J., Carter Cornwall, M., and Crouch, R. K. (1999) Occupancy of the chromophore binding site of opsin activates visual transduction in rod photoreceptors. *The Journal of general physiology* **113**, 491-503

236. Han, M., Groesbeek, M., Sakmar, T. P., and Smith, S. O. (1997) The C9 methyl group of retinal interacts with glycine-121 in rhodopsin. *Proceedings of the National Academy of Sciences of the United States of America* **94**, 13442-13447

237. Matsumoto, H., and Yoshizawa, T. (1975) Existence of a beta-ionone ring-binding site in the rhodopsin molecule. *Nature* **258**, 523-526

238. Daemen, F. J. (1978) The chomophore binding space of opsin. *Nature* **276**, 847-848

239. Steen, A., Thiele, S., Guo, D., Hansen, L. S., Frimurer, T. M., and Rosenkilde, M. M. (2013) Biased and constitutive signaling in the CC-chemokine receptor CCR5

by manipulating the interface between transmembrane helices 6 and 7. *The Journal of biological chemistry* **288**, 12511-12521

240. Ye, L., Van Eps, N., Zimmer, M., Ernst, O. P., and Scott Prosser, R. (2016) Activation of the A adenosine G-protein-coupled receptor by conformational selection. *Nature*

241. Kefalov, V. J., Estevez, M. E., Kono, M., Goletz, P. W., Crouch, R. K., Cornwall, M. C., and Yau, K. W. (2005) Breaking the covalent bond--a pigment property that contributes to desensitization in cones. *Neuron* **46**, 879-890

242. Matsumoto, H., Tokunaga, F., and Yoshizawa, T. (1975) Accessibility of the iodopsin chromophore. *Biochimica et biophysica acta* **404**, 300-308

243. Crescitelli, F. (1988) The gecko visual pigment: the chromophore dark exchange reaction. *Experimental eye research* **46**, 239-248

244. Mahalingam, M., and Vogel, R. (2006) The all-trans-15-syn-retinal chromophore of metarhodopsin III is a partial agonist and not an inverse agonist. *Biochemistry* **45**, 15624-15632

245. Kroeze, W. K., Sassano, M. F., Huang, X. P., Lansu, K., McCorvy, J. D., Giguere, P. M., Sciaky, N., and Roth, B. L. (2015) PRESTO-Tango as an open-source resource for interrogation of the druggable human GPCRome. *Nature structural & molecular biology* **22**, 362-369

246. Mansoor, S. E., McHaourab, H. S., and Farrens, D. L. (2002) Mapping proximity within proteins using fluorescence spectroscopy. A study of T4 lysozyme showing that tryptophan residues quench bimane fluorescence. *Biochemistry* **41**, 2475-2484

247. Phillips, J. C., Braun, R., Wang, W., Gumbart, J., Tajkhorshid, E., Villa, E., Chipot, C., Skeel, R. D., Kale, L., and Schulten, K. (2005) Scalable molecular dynamics with NAMD. *Journal of computational chemistry* **26**, 1781-1802

248. Nicholson, H., Anderson, D. E., Dao-pin, S., and Matthews, B. W. (1991) Analysis of the interaction between charged side chains and the alpha-helix dipole using designed thermostable mutants of phage T4 lysozyme. *Biochemistry* **30**, 9816-9828

249. Humphrey, W., Dalke, A., and Schulten, K. (1996) VMD: visual molecular dynamics. *Journal of molecular graphics* **14**, 33-38, 27-38

250. Zoete, V., Cuendet, M. A., Grosdidier, A., and Michielin, O. (2011) SwissParam: a fast force field generation tool for small organic molecules. *Journal of computational chemistry* **32**, 2359-2368

Appendix Chapter 1: Sampling transient molecular states with molecular dynamics simulations

This appendix covers my efforts to observe transient interactions and conformations using extremely simple and basic molecular dynamic simulations. Two such efforts will be detailed. The first involves computational simulations based on previous work in our lab by Drs. Steve Mansoor and Amber Brunette calibrating the tryptophan-induced quenching (TrIQ) technique for distance mapping in proteins (217,246). The goal of these simulations was to observe how the bimane probe and the quenching tryptophan might interact. These simulations were performed by a summer intern in the Farrens lab, Brianna McIntosh, and were conducted under my direction.

The second set of simulations sought to observe the transient opening of the binding pocket of an inactive opsin proposed in Chapter 2, Figure 2.7. These simulations were setup and performed by the author of this dissertation. All simulations were run using NAMD2 on Dr. Chapman's cluster (247). It should be noted that this work represents only a first pass at simulating these conditions and should not be over-interpreted. The results of these simulations are presented below.

A1.1: Simulating tryptophan-induced quenching with lysozyme

The TrIQ technique is a useful tool for monitoring protein movements (Chapter 3), protein-protein interactions (Chapter 4) (29), and distance measurements (228). However, it is unclear how the bimane probe and the Trp are interacting. Analysis of the "components of fluorescence" gives some insight, as the quenching can be broken into either static or dynamic quenching fractions. These quenched populations are differentiated by differences in their observed fluorescent lifetime. A dynamically quenched probe (one in which quenching occurs during the excited state of the fluorophore) displays a shorter lifetime than an unquenched control, indicating the probe exits the excited state before productive fluorescent emission can occur. In contrast, static quenching only displays a loss of total emission and no difference in the fluorescent lifetime. We have interpreted the static quenching results as reflecting a precomplex between the probe and Trp that either prevents excitation or quenches the fluorescence within the time resolution of our instrument. These different quenching modes are reviewed in (217,228). As those prior studies do not provide atomic-level information about the molecular interactions underlying dynamic or static quenching, we conducted molecular dynamics simulations to better understand the interactions.

A1.1.1: Simulation setup

The simulation cells were produced using two separate software packages. First, the T4 lysozyme structure (1L63 (248)) was modified in YASARA (http://www.yasara.com) to incorporate the quenching Trp and a cysteine for labeling

with bimane. The bimane molecule was built in silico in YASARA and attached to the cysteine. The molecule was then transferred to VMD (249), where it was solvated and setup in a spherical simulation cell.

Topology and parameter files for simulating bimane were generated by submitting the bimane structure file to the SwissParam webserver (250). The simulations were run using NAMD2. The solvated protein cell was then relaxed for 0.5ns before production runs were performed for 15ns. Data was analyzed in VMD and graphics generated in Chimera.

A1.1.2: Results

Based on the previous work from our lab, three probe/quencher pairs were chosen for simulation. The closest of these sites, 116W132B, had a Cα-Cα (distance between Cα carbons) of only 7.5Å, the other two pairs, 116W128B and 116W123B, were a little over 10Å. These pairs were chosen they exhibit substantial quenching (Figure A1.1), with the 7.5Å distance almost entirely showing static quenching, suggesting it might display some sort of complex (217). Snapshots of from these simulations are displayed in Figure A1.2. Although all three pairs showed some steady-state quenching, only 116W132B displayed any sort of complex with the bimane and Trp stacking. Interestingly, the other two pairs did not show substantially more flexibility, but rather remained further apart (Figure A1.3).

A1.2: Simulating inactive opsin in a POPC bilayer

The conformational selection model proposed in Chapter Two predicted a new state, inactive Ops with an open binding pocket, to allow 11-cis retinal (11CR) to enter the protein (148). We speculate that this open inactive conformation (open Ops) is in equilibrium with the closed Ops state from the crystal structures. To test this idea, I set up a simulation cell around an 11CR-bound rhodopsin structure with the retinal removed in a POPC bilayer and ran simulations to observe if either Hole A (TM1-TM7) or Hole B (TM5-TM6) can transiently open, a key requirement for this hypothesis.

A1.2.1: Simulation setup

The opsin structure (1GZM (170)) was oriented along the z-axis and the retinal ligand was removed using Chimera (172). The protein was then placed into a POPC membrane and solvated in VMD. The system was then minimized in 0.5ns increments using NAMD2, first by allowing the lipid tails to relax, then everything but the protein, and finally the entire system.

A1.2.2: Results

The membrane-opsin simulation cell (Figure A1.4) was run twice for 75ns each at 20°C. Both simulations showed an opening of the binding pocket (discussed below) and TM6, a hallmark of the active state, remained in the inactive position (Figure A1.5).

Over the course of each run, both simulations showed an opening of both proposed holes. The gating phenylalanies for both holes—F293 for Hole A and F208 for Hole B—show a rotameric shift from their position between the transmembrane helices,

as shown in the 11CR-bound structure (3), into the membrane space. Thereby adopting positions similar to that of the active structures (6) (Figure: A1.5). These observations support, but do not prove, the existence of an open, yet inactive, Ops conformation predicted in Chapter Two.

A1.3: Summary

In this appendix, I have covered efforts to observe transient interactions at the molecular level using molecular dynamics simulations. Two such situations were modeled. First, we observed the interactions underlying how the fluorescent probe interacts with the quenching Trp during TrIQ assays. These simulations showed complex formation for a probe/quencher pair with a Cα-Cα distance of 7.5Å. Further distances did not show such an interaction. Our second set of simulations attempted to investigate the features of the apoprotein opsin, in particular whether the binding pocket opens transiently for the inactive opsin, as our model in Chapter 2 predicts. To our knowledge, the accessibility of the inactive opsin binding pocket has not yet been reported.

In silico recapitulation of TrIQ experiments with T4 lysozyme appears to confirm our hypothesis that static quenching of fluorescence is caused by a pre-complex between the probe and quencher. The other two sites modeled here displayed large components of dynamic quenching in spectroscopic experiments and therefore would not be expected to form stable complexes. This interpretation is reflected in our simulations, as the bimane probe and the tryptophan quencher stay far apart through the duration of the simulations. Interestingly, none of the pairs showed any substantial changes in position, which might

indicate that our simulations were too short to observe transient interactions that might arise between the further apart pairs.

Simulations starting with the inactive apoprotein reveal that the bulky residues around both Hole A and Hole B can adopt an active-like rotameric state, which exposes the binding pocket to the membrane. In comparison, the cytoplasmic face continued to reflect the inactive structure, suggesting this might be the open Ops conformation that we predicted. These results are well in line with previous ligand-binding simulations that have modeled retinal mobility through the proposed ligand channel (151,158). These studies suggested that the retinals bind through Hole A and then exit through Hole B. The movement of the second phenylalanine around Hole B (F273) might support this idea, as the residue appears to partially obstruct the TM5-TM6 opening. This might allow facilitate "trapping" a retinal that had entered through Hole A to form a Schiff base before it can escape, which would fit with our previous interpretations presented and discussed in Chapter Two.

The simulations presented here obviously have to be taken with a grain of salt, as many of the quantum interactions are simplified by these software packages in favor of faster computation times. That said, this work does provide evidence for the transient states that are expected during TrIQ experiments and in the inactive opsin protein. In the future, to corroborate these preliminary results, the simplest pursuit should be to obtain atomic level structural information through either crystallography, electron microscopy, or NMR, in addition to increasing the sampling of the simulations and steering the molecular dynamics to better capture these potential transient molecular states.

Figure A1.1: Experimental data rationalizing the choice of bimane-tryptophan pairs used for the simulations presented here

The bimane-tryptophan pairs used for these simulations were chosen based on previous work by Drs. Amber Brunette and Steve Mansoor. Data from Dr. Brunette's 2014 publication is presented in this figure (217). Steady-state quenching ratios, the ratio of the fluorescence from an unquenched control to the quenched fluorescence, are shown as a function of Cα-Cα distances in the first panel. Larger ratios indicate more quenching. The middle panel presents the ratios of the fluorescent lifetimes across the same distances. In the case of the lifetime, higher ratios are indicative of dynamic quenching. The final panel displays the calculated components of fluorescence—the relative fraction of unquenched, dynamically quenched, and statically quenched fluorescence—for each of these pairs. The three pairs chosen for this study correspond to the 7.5, 10.1, and 10.7Å distances.

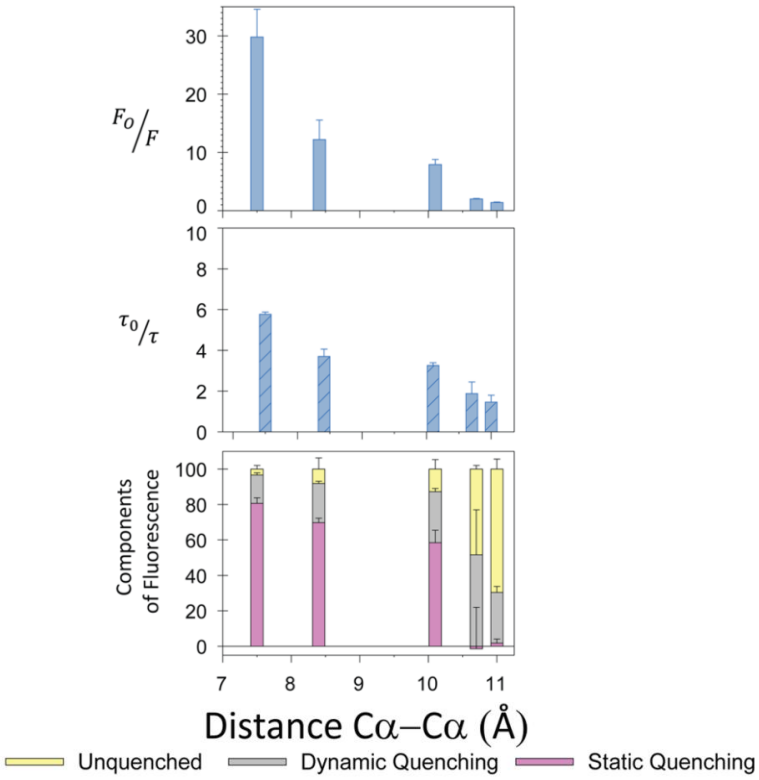
F_0/F
30
20
10
0
τ_0/τ
10
8
6
4
2
0
Components of Fluorescence
100
80
60
40
20
0
7
8
9
10
11
Distance Cα–Cα (Å)
Unquenched
Dynamic Quenching
Static Quenching

Figure A1.2: Simulation of the probe quencher pairs on T4 lysozyme

Bimane/tryptophan probes were chosen to match previous fluorescence experiments previously carried out in our lab. T4 lysozyme was mutated and modified in silico to incorporate a tryptophan residue at position 116 and a bimane attached to a cysteine at the three labeling sites (132, 128, and 123). Data from Brunette and Farrens (217) is presented above cartoons of the structures displaying both the Trp (purple) and the bimane (green). Note that the closest pair (116W132B) appears to form a complex between the engineered elements.

Label Site	N132C	E128C	Q123C
Cα–Cα (Å)	7.5	10.1	10.7

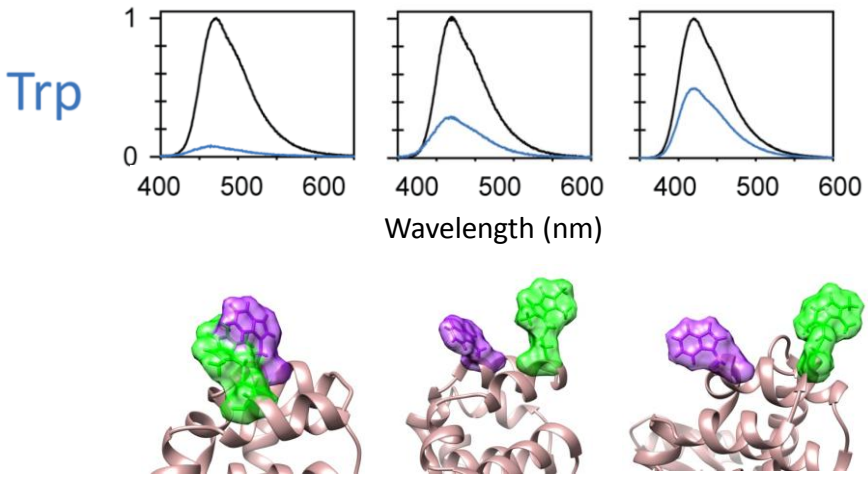

Figure A1.3: Distance calculations between the Trp and bimane across the three simulations

Analyzing the simulation data reveals that the distance between the quenching Trp and the fluorescence probe bimane does not show substantial change over the course of the short simulation for any of the labeling positions tested. The arrows pointing to the ball and stick representations of Trp and bimane indicate which atoms were used to measure the distances.

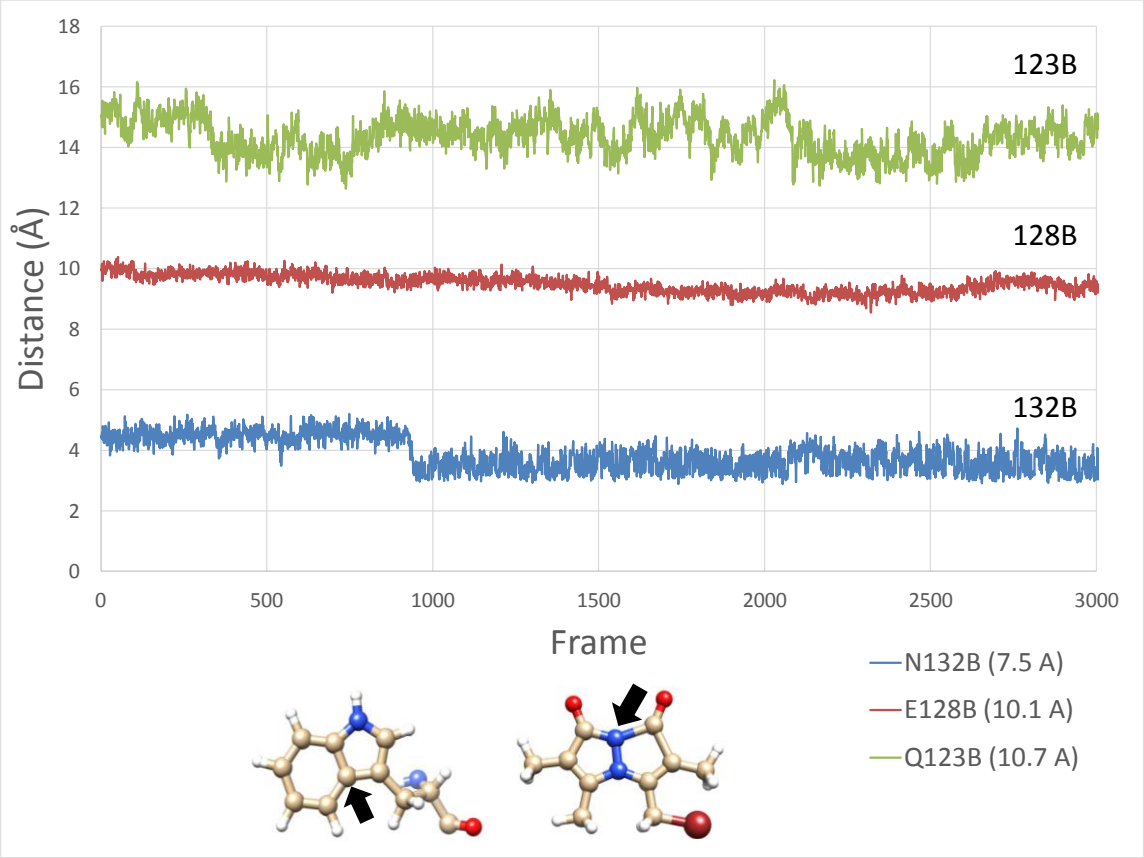
18
16
14
12
10
8
6
4
2
0
Distance (Å)
0
500
1000
1500
2000
2500
3000
Frame
123B
128B
132B
N132B (7.5 A)
E128B (10.1 A)
Q123B (10.7 A)

Figure A1.4: Simulation cell of opsin in a POPC bilayer

The initial simulation cell used to model the dynamics of inactive opsin in a POPC bilayer. The inactive rhodopsin structure, 1GZM, was first stripped of the 11CR in Chimera and oriented along to z-axis, this last step was important so that the protein sits in the membrane properly. The rest of the simulation cell was constructed in VMD. Note that the solvent extends further above and below the bilayer, fully covering the protein; however the excess waters and ions are not modeled in this figure.

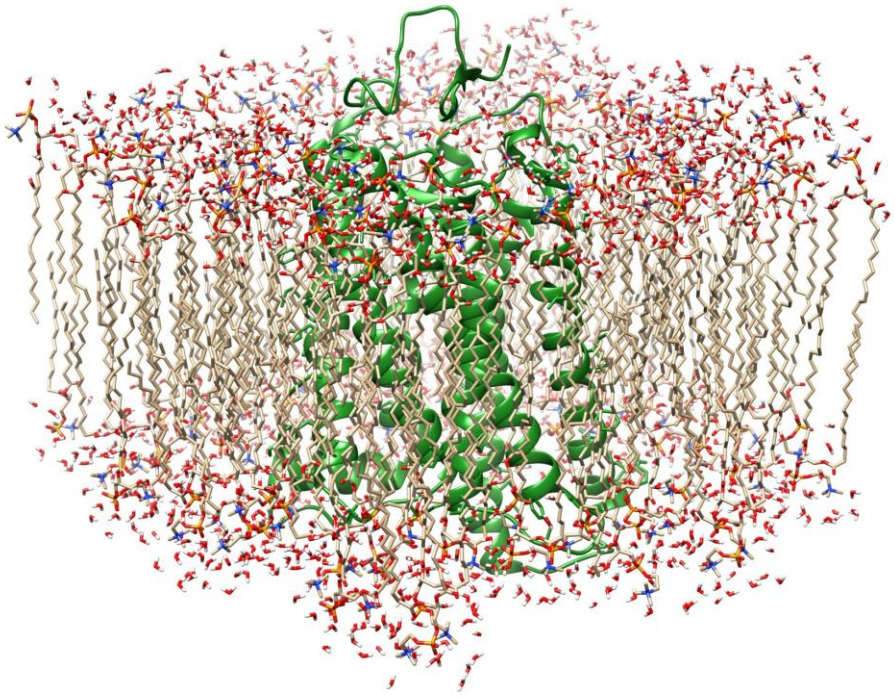

Figure A1.5: TM6 of the simulated opsin remains in the inactive conformation during the experiment

Comparing a snap shot of the simulated opsin (green) with both the inactive Ops (gray, 1GZM) and active Ops* (blue, 3PXO) conformations reveal that the cytoplasmic cleft closely resembles the inactive state (left) rather than the active (right).

Ops
Ops*
Simulated
Ops

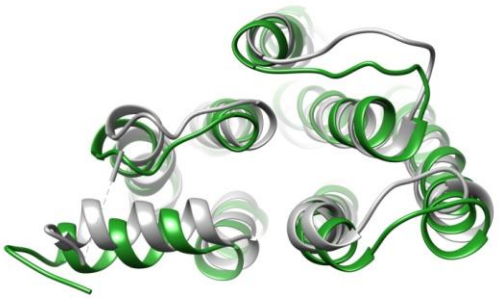

TM6

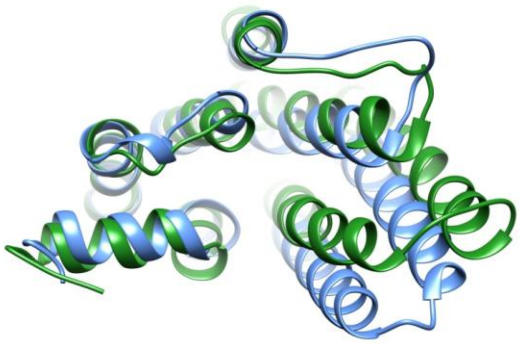

TM6

Figure A1.6: Comparison of the simulated opsin with Ops and Ops* of the residues flanking Hole A and B

Since the simulated opsin remained inactive over the course of the simulation, we next analyzed if Hole A or B had opened. Both Hole A and Hole B appear to adopt a conformation similar to Ops*, suggesting an opening of the binding pocket. The simulated protein is depicted in green here and compared with the inactive Ops (gray, 1GZM) on the left and with the active Ops* (blue, 3PXO) on the right. RMSDs across the frames of the simulations are shown on the right, with the two gating phenylalanines, F208 and F293, displaying substantial movements associated with rotameric shifts opening the holes.

Ops
Ops*
Simulated
Ops

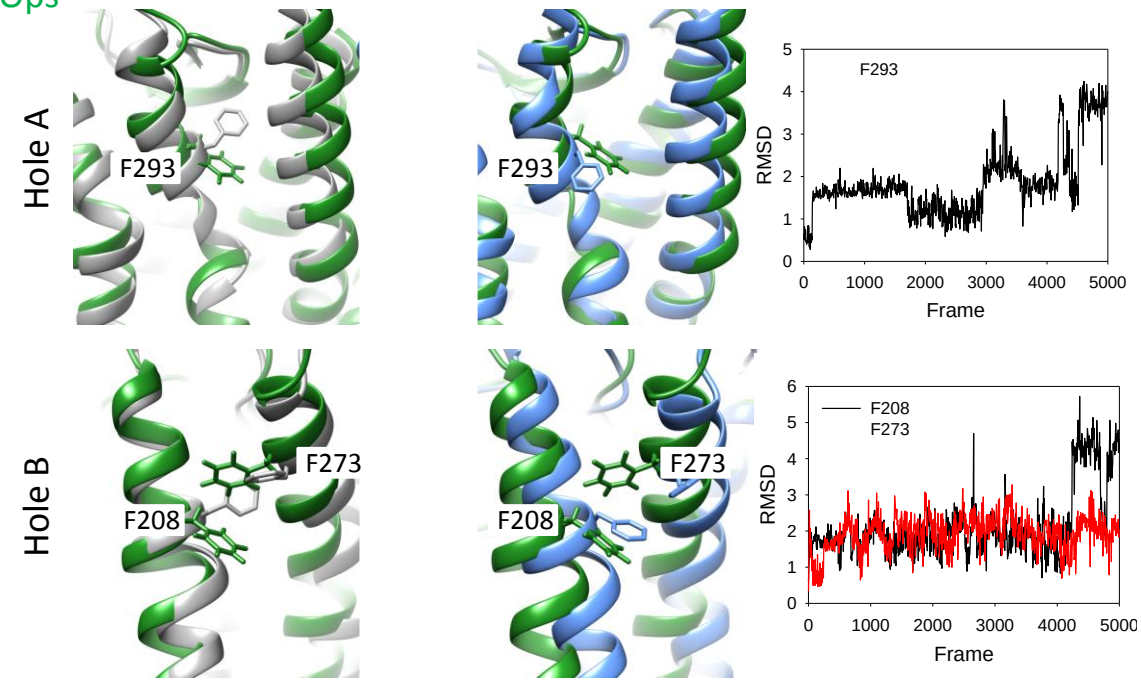

Appendix Chapter 2: Kinetic modeling of the transient activation hypothesis confirms its incompatibility with our results in Chapter Two

In Chapter Two of this dissertation, I tested the hypothesis presented by Heck and colleagues that both the inverse agonist 11CR and the agonist ATR require an active-state receptor conformation to enter the binding pocket (152). This appendix covers my efforts to compare simulations of this transient activation model, using the kinetics modeling software Cellware (http://www.bii.a-star.edu.sg/achievements/applications/cellware/), with our experimental binding data. In short, simulations showed that the transient activation hypothesis could not explain our retinal binding results. These *in silico* experiments are presented and discussed below.

A2.1: Background

As stated above, the transient activation hypothesis (TAH) for retinal binding (Figure A2.1) presents that both 11CR and ATR enter and exit the binding pocket when the receptor is in an active conformation. This would suggest that an increase in the relative population of active receptors would result in more rapid binding of both retinals. In Chapter Two, I tested this postulate by measuring the rates of retinals binding to opsins with increasing relative active populations. Our results testing ATR binding support that branch of the TAH, with the more active opsin samples accelerating agonist uptake. However, 11CR binding was slowed by the increased Ops* population. This would

suggest that the TAH does not accurately describe 11CR binding to opsin. To confirm this, I conducted *in silico* binding experiments mirroring our experimental conditions and focused on the 11CR branch of the transient activation model.

A2.2: Results

As only our 11CR binding results deviated from the TAH, I set up a binding simulation in the Cellware software focusing exclusively on 11CR arm of the model. This simplified version can be found in Figure A2.2 and simply reflects the inactive opsin transitioning to the active form before 11CR binds. Formation of the Schiff base locks the non-covalent Ops*/11CR complex into the inactive, dark-state rhodopsin. As dark-state rhodopsin is relatively stable, this reaction was modeled as nonreversible.

Kinetic parameters were fit to match our experimental data with WT opsin, where the proteins are predominantly in the inactive conformation. Once the binding constants and Schiff base formation rates were adjusted to reflect our data, I changed the isomerization constant governing the proportional population of Ops* to Ops, assuming that the other constants would not change. Bringing this ratio closer to an equal representation of the two states, as might be expected for M257Y-CAM, begins to show a deviation between the experiments and the modeled binding. Theoretically, if TAH is correct, then the binding of 11CR should be faster with the shift in the isomerization constant. Yet, our data showed that the binding was measurably slower. Drastically shifting the Ops*:Ops ratio to the Ops* state, as in the case with the M257Y-CAM incubated with Gt peptide, further exacerbated the difference between the experimental and theoretical results.

A2.3: Summary

In this appendix, I have presented *in silico* experiments attempting to use the transient activation hypothesis to describe our 11CR binding data. Whereas, ATR clearly shows accelerated binding when more Ops* is present, the increased activeness has an inhibitory effect on 11CR binding. Modeling the TAH confirms that the model predicts a greater Ops* population equates to faster binding of 11CR. Therefore, this model could not be reconciled with our experimental data. Thus, we proposed to replace this hypothesis with a conformational selection model. This is discussed in greater detail in Chapter Two.

Figure A2.1: Transient activation model for retinals binding to opsin

The standing hypothesis proposes that retinals bind to opsin through a transient activation of the protein. Key to this model is that both 11CR and ATR bind through a similar active-like state. This figure was adapted from (152) and taken from (148).

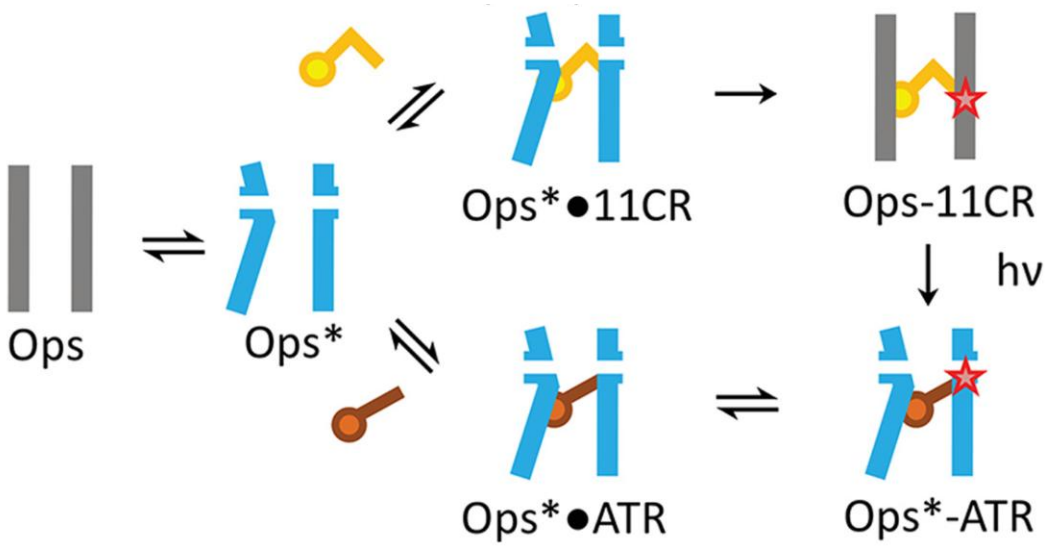
Ops
Ops*
Ops*●11CR
Ops-11CR
hν
Ops*●ATR
Ops*-ATR

Figure A2.2: *In silico* modeling of the transient activation hypothesis confirms that this model cannot reconcile our experimental 11CR binding data

The 11CR-binding arm of the transient activation hypothesis (TAH) was simulated in the Cellware software (top). The solid reaction nodes denote reversible reactions, whereas the empty node leading to the dark-state, 11CR-bound rhodopsin is modeled as irreversible. The kinetic parameters were then adjusted to match our experimental time-course data for the incredibly inactive WT receptor. Then, while keeping all other parameters constant, the ratio of Ops to Ops* was changed along with the receptor's isomerization constant to reflect the proposed ratios of M257Y-CAM and M257Y-CAM with Gt peptide. Whereas our data show the rate of 11CR binding decreases as the receptors become more active, the theoretical modeling of the transient activation hypothesis predicts the opposite. Therefore, we can definitively state that the TAH is irreconcilable with our experimental data and had to be replaced with the conformational selection model presented in Chapter Two.

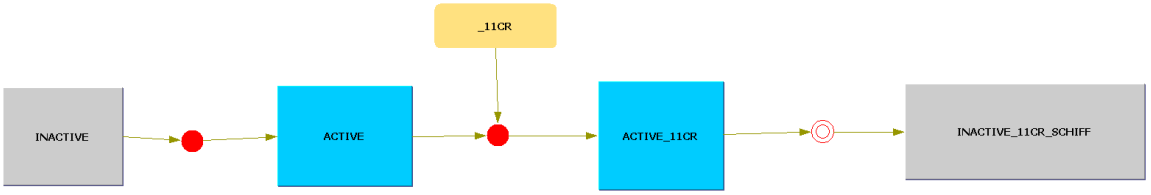
_11CR
INACTIVE
ACTIVE
ACTIVE_11CR
INACTIVE_11CR_SCHIFF

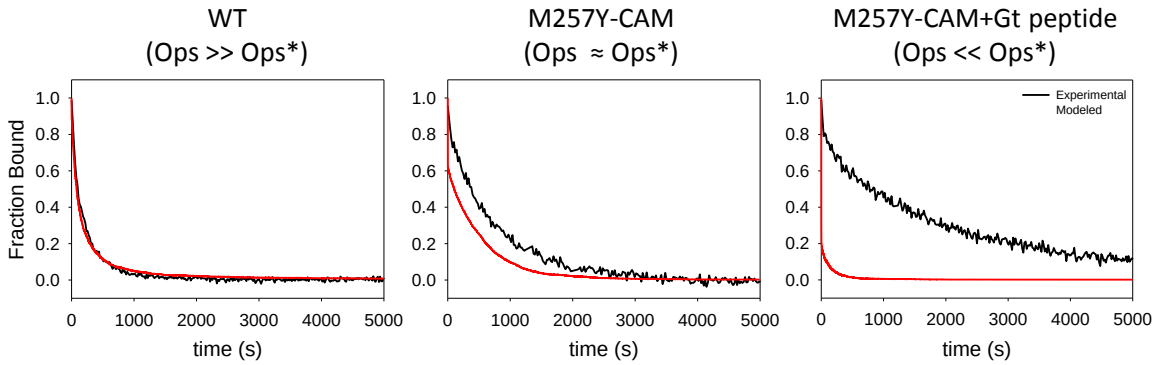
WT
(Ops >> Ops*)
M257Y-CAM
(Ops ≈ Ops*)
M257Y-CAM+Gt peptide
(Ops << Ops*)
Fraction Bound
1.0
0.8
0.6
0.4
0.2
0.0
0
1000
2000
3000
4000
5000
time (s)
Experimental
Modeled

Appendix Chapter 3: Instrument improvements for improved fluorescent time-course experiments

At the onset of my dissertation project, the steady-state fluorometers available in the Farrens lab all used a standard xenon arc lamp light sources for sample excitation. Although these lamps have been effective data generation in the past, I noticed that, while performing retinal release assays, the light sources required an extended warm-up period before assays could be performed. Therefore, I upgraded the excitation sources for one of the fluorometers to LEDs. I purchased two such LEDs from OceanOptics that had maximal wavelengths corresponding to tryptophan (295nm) and the fluorescent probe bimane (405nm) excitation. The LEDs proved to greater stability in optical output compared to the arc lamps and were ready for use immediately, without any warm-up, thereby increasing the throughput of experiments. Additionally, the OceanOptics LED system can be turned on and off through 5V TTL signal, which, conveniently, is the same signal used to operate the excitation shutter in the standard arc lamp set up, therefore, I was able to hijack this system to control the LEDs with the existing software. An added benefit of the shutter control is that the fluorometer would turn off the LEDs after data collection. With this new system, I was able to produce the high quality fluorescence data presented in my dissertation.

Figure A3.1: Setup and testing of the LED augmented fluorometer

The xenon arc lamp from a standard PTI Quantamaster steady-state fluorometer was replaced with OceanOptics LLS-LED systems with maximal wavelengths set to 295 and 405nm. A simple setup schematic is shown in the top left. The light from the LEDs was channeled to the sample compartment through a bifurcated fiber optic cable and focused on the sample cuvette with a collimator. The fluorescent emission was then collected with by separate PMTs and filtered to the respective wavelengths for tryptophan (330nm) and bimane (460nm). The LEDs themselves are pictured in the top right. A spectrum depicting the scattering from the two LEDs used simultaneously and matched in intensity. Finally, the lower right time-course of retinal release from WT rhodopsin from a traditional xenon lamp source (black) and using the 295nm LED (red). Note that the retinal release rates are the same for both instruments, yet the LED data has less noise.

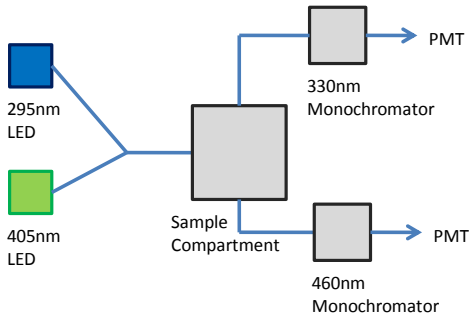

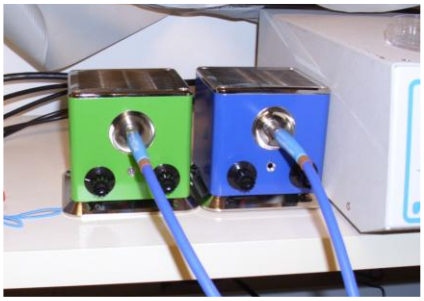

Matched LED Scatter